The Comparative Study between the Adsorptive Capacity of Activated Carbon Obtained from the Enhanced Hydrothermal Polymerization Process with Conventional Activated Carbons in the Removal of Micropollutants of Concern

By

Vimbai Susan Kasonde
KSNVIM001

Supervised by:
Prof David S Ikumi

Dissertation Submitted in Fulfillment of the Requirements
For the Degree of
Master of Science in Engineering - Water Quality Engineering

Department of Civil Engineering
University of Cape Town, Private Bag Rondebosch, 7700
South Africa 7700

Declaration

I, Vimbai Susan Kasonde know the meaning of plagiarism and declare that all the work in the document, save for that which is properly acknowledged, is my own. This thesis/dissertation has been submitted to the Turnitin module (or equivalent similarity and originality checking software) and I confirm that my supervisor has seen my report and any concerns revealed by such have been resolved with my supervisor.

Signed: Signed by candidate Date: 24/07/2023

Abstract

Adsorption is one of the most widely used techniques employed for the tertiary treatment of wastewater to remove micropollutants. One of the most popular adsorbents used towards adsorption is activated carbon. However, due to the high cost of the conventional commercial activated carbon (produced from coal, which is a finite resource), it is important to find alternative precursors that are readily available, low cost, and can potentially produce activated carbon which is effective in the adsorption process. Sludge from wastewater treatment plants is one alternative which has been investigated and found desirable due to its high organic content. It is an unavoidable by-product of water treatment facilities that is becoming difficult to manage due to stricter disposal laws. The use of sludge as a precursor for activated carbon production serves to address the issue of an alternative, relatively low-cost adsorbent and the sludge disposal dilemma. Hence the sludge, which is an otherwise waste product is converted into a useful resource to aid in the reduction of the pollution of water which is a scarce commodity. In this study, hydrochar derived from primary sludge combined with waste activated sludge was used to produce activated carbon through pyrolysis. The hydrochar derived activated carbon (HC-AC) was characterized along with a commercial granular activated carbon (GAC) and a green alien wood activated carbon (AW-AC). The three carbons were later used in batch adsorption tests to determine the optimum conditions needed for each carbon to achieve maximum removal of methylene blue dye and lead (II) ions in aqueous solution by varying parameters such as pH, adsorbent dosage, initial concentration of the adsorbate, and contact time. Results from these tests were compared at the optimum conditions for each adsorbent and it was found that for methylene blue dye adsorption the percentage removal was in the order HC-AC (99.28%) > GAC (99.13%) > AW-AC (98.73%). The percentage removal

of lead (II) ions was in the order HC-AC (99.33%) > GAC (97.25%) > AW-AC (96.92%), showing that at optimum conditions, HC-AC performed slightly better than the other adsorbents in the removal of the pollutants.

Keywords:

Sludge management

Adsorption

Hydrochar

Enhanced hydrothermal polymerization

Table of Contents

List of Figures

List of Tables

Acknowledgement

I would firstly like to thank God for the ability to do this project and take on this study. Thank you to my parents and my sister Kumbirai, for their continuous support and prayers during this project. Thank you to Dr. Eustina Musvoto, Prof. Leslie Petrik, and the University of the Western Cape team. Lastly, a big thank you to Prof. David Ikumi and the team at University of Cape Town for their guidance throughout this project.

Abbreviations

AC Activated Carbon

ASTM American Society for Testing and Materials

AW-AC Alien Wood- Activated Carbon

AWWA American Water Works Association

BET Brunauer-Emmet-Teller

EDS Energy Dispersive X-Ray Spectroscopy

EHTP Enhanced Hydrothermal Polymerization

FT-IR Fourier Transform Infrared

ICP-OES Inductively Coupled Plasma - Optical Emission Spectroscopy

TGA Thermogravimetric Analysis

GAC Granular Activated Carbon

HC-AC Hydrochar Derived Activated Carbon

HCL Hydrochloric Acid

HNO_3 Nitric Acid

MB Methylene Blue

MBN Methylene Blue Number

NaOH Sodium Hydroxide

PAC Powdered Activated Carbon

PB Lead

SEM Scanning Electron Microscopy

WHO World Health Organization

UV-VIS Ultraviolet- Visible Spectroscopy

WWTP Wastewater Treatment Plant

Nomenclature

$\boldsymbol{C_0}$ initial concentration in aqueous solution (mol L^{-1})

$\boldsymbol{C_t}$ concentration in solution at any time *t* (mol L^{-1})

$\mathbf{C_e}$ equilibrium concentration of the adsorbate (mg/L)

$\mathbf{K_f}$ Freundlich constant

$\mathbf{k_1}$ adsorption rate constant for first-order kinetic equation (min^{-1})

$\mathbf{k_2}$ adsorption rate constant second-order kinetic equation (g/mg min)

$\boldsymbol{W}$ weight of adsorbent (mg)

$\mathbf{q_e}$ equilibrium concentration of metals ions on adsorbent (mg/g)

$\boldsymbol{q_t}$ the amount of metals ions adsorbed at any time, *t* (mg/g)

$\mathbf{q_{max}}$ Langmuir monolayer capacity of the adsorbent (mg/g)

$\boldsymbol{R^2}$ linear regression coefficient

t time (min)

V volume of solution (mL)

Chapter 1 Introduction

1.1 Background

The industrial revolution has seen a plethora of persistent hazardous pollutants being released into the hydrological environment which sees further decrease in the availability of water for potable use (Dichiara, Weinstein and Rogers, 2015; Gude, 2017). It has become increasingly important to identify economically viable and environmentally friendly methods of removing these micropollutants from the final effluents from wastewater treatment plants. Doing this not only creates a pathway for the implementation of water reuse, aids in averting the water crisis, but also works to protect human and environmental health against the long term adverse effects related to the accumulation of micropollutants. The known threats to human health, include damage to the central nervous system and resulting physiological disorders (Danish and Ahmad, 2018; Alghamdi *et al.*, 2019).

Examples of conventional micropollutants removal techniques include; coagulation–flocculation, chemical precipitation, ion exchange, adsorption, membrane filtration, reverse osmosis, ozonation, and electrochemical treatments (Fu and Wang, 2011; Ali, 2012; Piaskowski, Świderska-Dąbrowska and Zarzycki, 2018; Ahmad *et al.*, 2021). Most of these existing technologies are expensive and energy intensive, placing them out of reach for most water utilities in low and middle-income countries (LMICs), with limited financial resources. Of the above mentioned methods, adsorption presents many advantages such as; the ability to remove or minimize various organic and inorganic pollutants at exceedingly low concentrations, high availability and low

cost of adsorption media, reversibility of the process leading to multiple reuse, and flexibility of design (Fu and Wang, 2011; Dichiara, Weinstein and Rogers, 2015).

The use of biomass wastes such as; coconut shells, bamboo, wood waste, rice husk, bagasse, corn cob and sludge to produce adsorbents to remove micropollutants from wastewater effluent via adsorption reduces the cost associated with the production of adsorbents form finite fossil fuels, promotes a circular flow of materials, generates new income streams, and sequestrates carbon (Li *et al.*, 2020).

1.2 Research Problem Statement

Most sludge based activated carbons used for the removal of pollutants are prepared by either chemical or physical activation as this has been proven to increase the surface area. However, it would be interesting to evaluate the performance of activated carbon, generated from the pyrolysis of hydrochar (without further activation) that is produced from processing a combination of primary sludge (PS) and waste activated sludge (WAS), for the removal of wastewater pollutants. Investigations on the performance of this sludge (PS and WAS) derived activated carbon could include comparing its characteristics and adsorptive capacity with commercially available granular activated carbons.

Results from this study will;

1. Provide Municipalities and other wastewater treatment facilities with an alternative method to manage the large volumes of sludge produced annually and a tertiary treatment method for final effluent reclamation and reuse.

2. Provide a valuable South African case study that evaluates the application of activated derived from hydrochar produced from PS and WAS as a tool to transitioning to a circular economy within the South African water sector.

1.3 Research Question and Hypothesis

The research question of this study is whether the activated carbon derived from hydrochar, obtained from processing municipal sludge (PS and WAS), exhibits effective removal of micropollutants of concern from the final effluent when compared to commercially available granular activated carbon (GAC) and other locally available green adsorption media .

It is hypothesized that the lower costing hydrochar generated from the processing of municipal sludge will exhibit similar removal of micropollutants as GAC.

1.4 Research Objectives

The overarching purpose of this study is to determine the effectiveness of the activated carbon derived using hydrochar from processing sludge produced from the Enhanced Hydrothermal Polymerization (EHTP) reactor in removing micropollutants of concern (e.g., heavy metals) from aqueous solution. The hydrochar derived activated carbon will be compared with conventional, commercially available coal based granular activated carbon and locally available green adsorption media, namely alien wood activated carbon.

The specific objectives of this study are as follows:

1. To prepare activated carbon from hydrochar (which was processed from wastewater treatment plant (WWTP) generated sludge) by pyrolysis and to characterize the activated carbon (AC) together with the commercially available granular activated carbon (GAC) as well as a locally available green activated carbon produced from alien wood (AW-AC). The characteristics of the AC prepared from hydrochar and the other two activated carbons shall be compared.
2. To observe the effective removal of methylene blue and lead (II) ions from aqueous solution by batch adsorption using the activated carbons (i.e., the one prepared from sludge, GAC, and AW-AC) under optimum conditions (i.e., pH, adsorbent dosage, initial solute concentration, and contact time).

1.5 Scope of Research

The scope of this study was mainly in line with the production of activated carbon from processing sludge hydrochar, characterizing it along with commercially available granular activated carbon and green activated carbon, and comparing the adsorptive performance of the hydrochar derived activated carbon and other adsorbents in the removal of methylene blue and lead (II) ions in aqueous phase using batch laboratory scale tests under several experimental parameters (pH, adsorbent dosage, solution concentration and contact time). This study is limited to laboratory work and analysis. No major modeling using complex software was done.

1.6 Dissertation Outline

This dissertation comprises of 5 chapters. Chapter 1 introduces the study by outlining the background, research problem statement, research questions and hypothesis, research objectives and the scope. Chapter 2 contains the review of literature focusing on activated carbon and its derivation from sludge, the adsorption technique and the kinetics and isotherm studies used to explain it, as well as the principles behind the analytical techniques employed in this study. Chapter 3 describes the detailed methods used to address the objectives set out in Chapter 1. Chapter 4 shows and discusses the results of the experimental work outlined in Chapter 3. Lastly, Chapter 5 gives a conclusion of the main findings followed by recommendations for further studies. A visual outline of the thesis is shown in Figure 1.1.

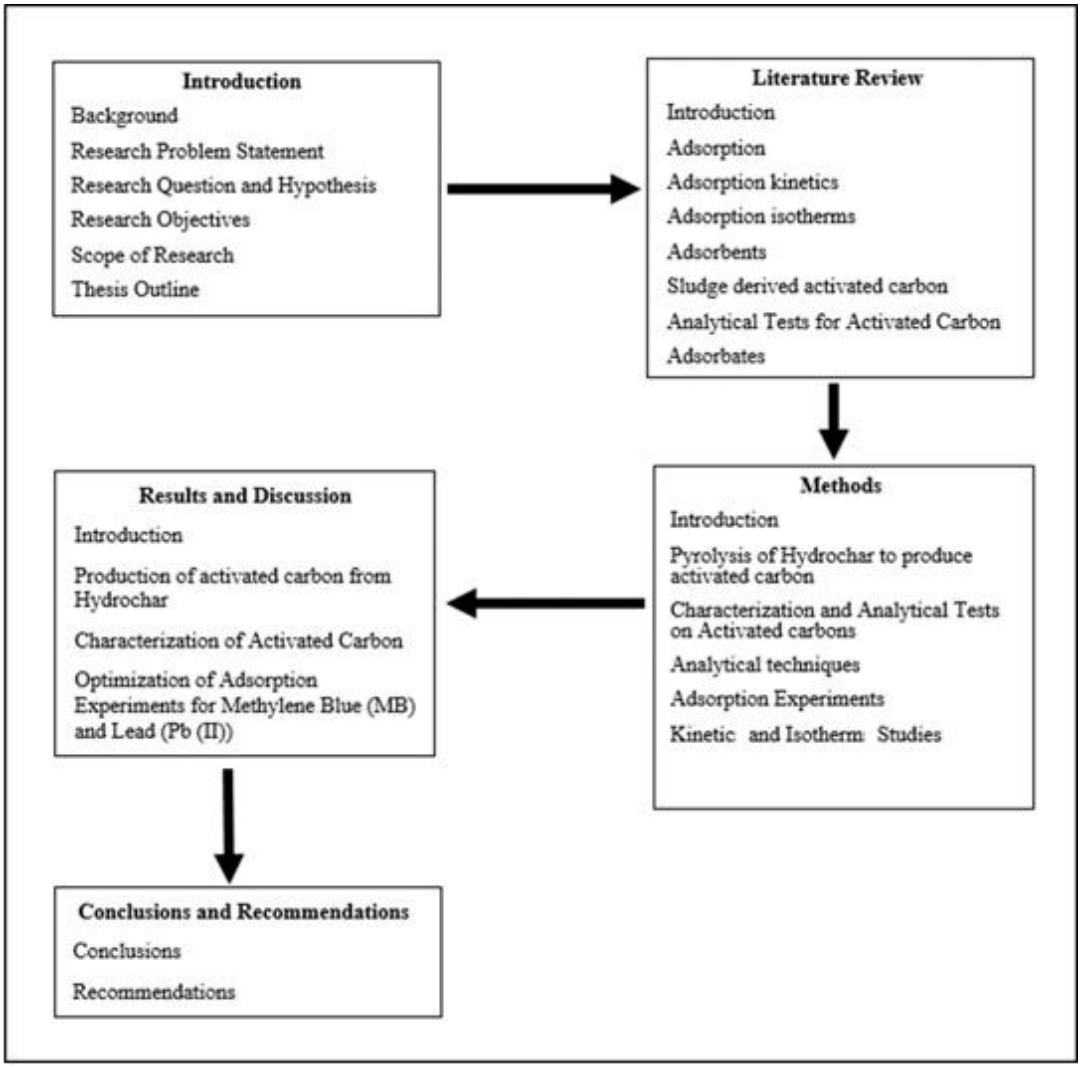

Figure 1.1 Schematic representation of the thesis

Chapter 2 Literature Review

2.1 Introduction

The large-scale use of water by various industries is one of the greatest sources of water pollution. The removal of pollutants from wastewater effluent is limited to a few physicochemical and/or biological techniques due to technological and economic reasons (Crini and Lichtfouse, 2019). (Saravanan *et al.*, 2021) classified water treatment technologies into three major categories: physical, chemical, and biological methods. The advantages and disadvantages of some of these technologies are displayed in Table 2.1.

Table 2.1 Different pollution control methodologies and their advantages and disadvantages (Saravanan et al., 2021)

No	Physical Methods	Advantages	Disadvantages
1	Sedimentation	1. No energy requirement 2. Excellent reproducibility	1. Selective process 2. Lacks precision
2	Degasification	1. Mitigates the chemicals required for further process	1.Limited capacity for the pollutant removal
3	Filtration	1. Autoclaving can be done in some cases	1. Time consuming process, 2. Clogging of filters may occur
	Chemical Methods	**Advantages**	**Disadvantages**
1	Flocculation and Coagulation	1. Used for fine particle removal 2. Removes metals, color and turbidity	1. Multiple process step 2. Toxic if improperly used 3. High sludge production 4. Operational cost is high
2	Ozonation	1. No chemical necessity 2. Elimination of vast variety of microbes, organic and inorganic compounds 3. No need to alter pH and temperature 4. Stronger germicidal activity	1. Less solubility of ozone requires special mixing techniques, 2. Relatively expensive than other methods, 3. In ozone generation, toxicity issues and fire hazards may occur.
3	Chemical Precipitation	1. Easy process control 2. Low operational cost 3. Effective over a wide temperature range	1. Production of large quantity of sludge 2. Difficulty in the disposal of sludge

		4. Controllable pH	
4	Adsorption	1. Low operational cost 2. Relatively high efficiency 3. Design simplicity 4. Non-toxic process 5. Regenerative process	1. Low selectivity of adsorbent 2. Disposal problems
5	Ion exchange	1. Possible to regenerate resin 2. Zero hardness can be achieved 3. Rapid separation process 4. Small area requirement	1. Pre-treatment is required in most of the effluents 2. Ionic competition 3. Fouling of matrix
	Biological Methods	**Advantages**	**Disadvantages**
1	Bioremediation	1. Natural process 2. On-site treatment 3. Cost effective process 4. Complete destruction	1. Slow process 2. Heavy metals are not expelled 3. Bioremediation site must have soil with high penetrability 4. Considerable gaps exist in the comprehension of microbial environment
2	Aerobic Treatment	1. Simplicity of activity 2. Limits creation of odor 3. Decreases pathogens and fats. 4. A more prominent number of microbe types can be utilized for processing.	1. Cost expensive 2. Maintenance problem

3	Anaerobic Treatment	1. Produces renewable energy 2. Less environmental pollution	1. High capital cost 2. Odor nuisance
4	Oxidation ponds	1. Extremely high concentration 2. Symbiosis relation exists	1. Odor problem 2. Needs more space
5	Activated sludge	1. Giving a decent profit for beginning venture 2. Doesn’t require more space 3. Easy operation 4. Moderately effective	1. Storm surge 2. High operational cost 3. Sludge disposal problem

2.2 Adsorption

The process of adsorption describes the mechanism by which a material called the adsorbate (in a gaseous or liquid bulk) binds on the surface of a solid material known as an adsorbent (El-Dairi *et al.*, 2014). It has been reported as the most widely applied alternative technique for the removal of pollutants in wastewater treatment technologies (Chung *et al.*, 2015; Aljamali, Khdur and Alfatlawi, 2021; Chowdhury *et al.*, 2022). Because of its relatively straightforward design, ease of operation, affordability, energy efficiency, and insensitivity to toxic pollutants, adsorption is preferred to alternative methods of treatment (Yagub *et al.*, 2014; Tan and Hameed, 2017). A limitation associated with the adsorption process is the sourcing of suitable precursors to make adsorbents that achieve removal acceptable at commercial levels (Ali, 2012). Adsorption has been found to effectively remove both organic and inorganic pollutants (Chung *et al.*, 2015), especially emerging contaminants that are stubborn to removal by conventional biological wastewater treatment technologies (Yagub *et al.*, 2014). (Tan and Hameed, 2017) generally categorized water pollutants found in literature into six groups: (i) heavy metals, (ii) phenolics, (iii) dyes, (iv) pesticides, (v) pharmaceuticals and personal care products (PPCPs), and (vi) others (hydrocarbons, inorganic anions, etc.). Various solid adsorbents such as activated carbons, zeolites, clay, mesoporous silica, polymeric resin, and metal-organic frameworks have been employed in adsorption studies (Tan and Hameed, 2017), but due to the high costs associated with regeneration or reuse of most adsorbents, the use of cheaper alternative adsorbents such as agricultural solid wastes, biomass solid waste based activated carbon adsorbents, and Industrial by-products has been investigated (Yagub *et al.*, 2014; Chung *et al.*,

2015) .The mechanism of adsorption has been reported as comprising of three stages:

1. Diffusion of molecules from the bulk phase towards the interface space (external diffusion).
2. Diffusion of molecules inside the pores (internal diffusion); diffusion of molecules on the surface phase (surface diffusion).
3. Adsorption of the adsorbate on the active sites of the adsorbent (Tan and Hameed, 2017; Wang and Guo, 2020; Musah *et al.*, 2022).

The adsorption process is generally divided into two classes, namely physisorption (physical adsorption) and chemisorption (chemical adsorption).

Physisorption is as a result of the attraction of weak forces (Van der Waals' forces) between the adsorbate and the adsorbent. Due to the weak nature of this paring this type of adsorption is usually reversible. **Chemisorption** is a result of the formation of strong chemical bonds between the adsorbate and adsorbent involving the exchange of electrons (Yagub *et al.*, 2014; Sazali, Harun and Sazali, 2020; Musah *et al.*, 2022). The removal efficiency of pollutants by way of adsorption is dependent on factors such as the surface area, the presence of surface functional groups on the adsorbent, and the dosage of the adsorbent present in solution (Li *et al.*, 2002). It is also influenced by parameter such as the pH, initial solute concentration, temperature, and contact time (Yagub *et al.*, 2014).

2.3 Adsorption Kinetics

The main purpose of the study of adsorption kinetics is to describe the rate of solute uptake and the retention of the solute from the aqueous phase to the solid phase interface (adsorbent) at given parameters (Batool *et al.*, 2018; Tejada-Tovar *et al.*, 2022). The kinetics can also be used to evaluate the performance of the adsorbent (Wang and Guo, 2020). The design of adsorption systems largely relies on the rates calculated from the kinetic studies of adsorption (Yagub *et al.*, 2014). Of the mathematical models developed to describe the kinetics of the adsorption of dyes, metal ions and other compounds in aqueous solution over the years, the pseudo-first-order and pseudo-second-order kinetic models have been the most widely applied and compared (Qiu *et al.*, 2009; Simonin, 2016; Tan and Hameed, 2017) and will be discussed briefly.

2.3.1 Pseudo-First-Order and Pseudo-Second-Order Kinetic Models

The pseudo-first-order (PFO) kinetics, first proposed by Lagergren in 1988 (Ho and McKay, 1999b), and the pseudo-second-order (PSO) kinetics (Ho and McKay, 1999a) have been extensively compared in literature with most studies reporting the superiority of the PSO equation to that of the PFO when it comes to fitting data from adsorption experiments (Tseng, Wu and Juang, 2010; Yagub *et al.*, 2014; Tan and Hameed, 2017). This effect is possibly as a result of treating the experimental data with the linearized equations of the PFO and PSO, which give the plots log (q_e-q_t) versus time (t), and t/q_t versus time (t) respectively, where q_e is the removal capacity at equilibrium; q_t is the removal capacity at time t, and t is the time. The correlation coefficient of the PSO is likely to be higher and closer to one as both the x and y axis of the PSO plot contain the

variable t (Tseng, Wu and Juang, 2010). The PFO describes the adsorption rate of the solute onto the adsorbent based on the adsorption capacity (Qiu *et al.*, 2009; Yagub, Sen and Ang, 2012). The model assumes that the rate of adsorption is proportional to the difference between the maximum capacity at equilibrium and the capacity at any time i.e. (q_e-q_t) (Ho and McKay, 1999a). Its linearized integral form and the plot used to derive its constants (k_1 and q_e) are displayed in Table 2.2. The PSO is used to calculate the initial rate of sorption (Yagub, Sen and Ang, 2012; Yagub *et al.*, 2014), and is especially applicable on small amounts of initial concentration (Batool *et al.*, 2018), whereas the PFO is favored at high initial concentration (Mokhena *et al.*, 2016). The PSO assumes that the rate of uptake is second order with respect to the surface sites that are available on the adsorbent (Tan and Hameed, 2017; Hubbe, Azizian and Douven, 2019), and that the rate limiting step may be chemical adsorption (Qiu *et al.*, 2009). The linearized integral form of the model and the plot used to derive its constants k_2 and q_e are depicted in Table 2.2.

Table 2.2 Kinetics adsorption models *(Tejada-Tovar* et al.*, 2022)*

Model	Integrated equation	Plot	Parameters
Pseudo-first- order	$Log(q_e - q_t) = Logq_e - \frac{k_1}{2.303}t$	$Log(q_e - q_t) vs\ t$	q_t = adsorption capacity at any time t (mg/g)
			q_e = adsorption capacity at equilibrium (mg/g)
			k_1 = Lagergren's constant (min^{-1})
			t = time (min)
Pseudo-second-order	$\frac{t}{q_t} = \frac{1}{k_2 q_e^2} + \frac{1}{q_e}\ t$	$\frac{t}{q_t}\ vs\ t$	k_2 = pseudo-second order constant (g/ mg min)

It has been observed that the q_e value obtained from the PFO equations is usually farther away from the value obtained experimentally when compared to that obtained by the PSO equations which is often less but closer, and that the wide applicability of the PSO over the PFO steams more from a mathematical basis than it does from a physical one. The added advantage of using the PSO is that the q_e value is not required for fitting the experimental data (Musah *et al.*, 2022).

2.4 Adsorption Isotherms

Adsorption isotherms are mathematical models that are crucial to comprehending the mechanism of adsorption by illustrating the interaction between the adsorbate and the surface of the adsorbent as well as providing information regarding the adsorption capacity at given operating conditions (Yagub *et al.*, 2014; Musah *et al.*, 2022; Tejada-Tovar *et al.*, 2022). A number

of isotherms including Elovich, Freundlich, Langmuir, Redlich–Peterson, and Temkin have been published in literature (Batool et al., 2018). The Langmuir (1918) and Freundlich (1906) are the two most widely employed isotherms (Yagub, Sen and Ang, 2012).

2.4.1 Langmuir and Freundlich Isotherms

Langmuir Isotherm:

The Langmuir isotherm is based on the basic assumption that the adsorption process occurs at specific homogeneous sites on the adsorbent surface (Yagub, Sen and Ang, 2012; Chung *et al.*, 2015; Tejada-Tovar *et al.*, 2022). The isotherm also assumes:

- That each adsorbent has fixed adsorption sites on its surface, and that at specific parameters, a portion of these sites may be occupied by adsorbate.
- That only one entry can be accommodated on each site of adsorption on the adsorbent surface.
- That there is no interaction between adsorbates occupying different adsorption sites.
- That each adsorption site has the same heat of adsorption and is unaffected by the percentage of sites occupied by the adsorbate.

Based on the aforementioned assumptions, the Langmuir adsorption isotherm is valid only for monolayer adsorption (Musah *et al.*, 2022). Four linear forms of the Langmuir are usually presented in literature. The linear equations presented in Table 2.3 have been used to express the Langmuir isotherm and the plots also displayed alongside these equations have been used to deduce the Langmuir constants K_L and q_{max} (Y., 2006; Osmari *et al.*, 2013). From these

same plots, the separation factor, R_L which indicates the nature of the isotherm can also be determined using the following equation: $R_L = \frac{1}{1+K_L C_i}$ where K_L is the Langmuir constant and C_i is the initial concentration of the adsorbate. If the R_L value falls between 0 and 1, i.e. $0 < R_L < 1$, then the isotherm is deemed favorable (Chung *et al.*, 2015; Musah *et al.*, 2022; Tejada-Tovar *et al.*, 2022).

Freundlich Isotherm:

The Freundlich isotherm is an empirical model occasionally employed as a tool for data description due to the mathematical simplicity of its equation and its aptitude for characterizing non-linear adsorption processes across a range of adsorbate concentrations (Chung *et al.*, 2015; Musah *et al.*, 2022). Unlike the Langmuir model that assumes that the adsorption process occurs at specific homogeneous sites with the same heat of adsorption, the Freundlich isotherm assumes a heterogeneous adsorption surface with unequal available sites with different adsorption energies (Yagub, Sen and Ang, 2012). It is typically used to quantify the relationship between the amount of adsorbate removed per unit weight of adsorbent and the adsorbate concentration still present in solution at equilibrium (Musah *et al.*, 2022). The isotherm is formulated as per the equation in Table 2.3 and its constants K_F and n can be formulated from the plot of Log q_e vs Log C_e (Yagub, Sen and Ang, 2012; Batool *et al.*, 2018; Musah *et al.*, 2022). If the K_F value falls within the range of 1-20, and the n value is above 1, then adsorption is considered promising, and the data fits the model well (Batool *et al.*, 2018). The value of the linear regression coefficient R^2 is used to determine which model best fits the adsorption data (Yagub *et al.*, 2014).

Table 2.3 Adsorption isotherm models

Model	equation	Plot	Parameters	Ref
Langmuir 1	$\frac{1}{q_e} = \left(\frac{1}{K_L . q_{max}}\right) . \frac{1}{C_e} + \frac{1}{q_{max}}$	$\frac{1}{q_e} vs \frac{1}{C_e}$	**q_e** = the solute mass adsorbed per unit adsorbent mass at equilibrium (mg/g) **q_{max}** = maximum adsorption capacity (mg/g) **C_e** = adsorbate concentration at equilibrium (mg/L) **K_L** = Langmuir constant related to the affinity of the adsorbent for the adsorbate	(Osmari *et al.*, 2013)
Langmuir 2	$q_e = q_m - \frac{1}{K_L}\frac{q_e}{C_e}$	$q_e \, vs \frac{q_e}{C_e}$		
Langmuir 3	$\frac{q_e}{C_e} = q_m K_L - K_L q_e$	$\frac{q_e}{C_e} \, vs \, q_e$		
Langmuir 4	$\frac{C_e}{q_e} = \frac{1}{q_m K_L} + C_i$	$\frac{C_e}{q_e} vs \, C_e$		
Freundlich	$Log \, q_e = \frac{1}{n} Log C_e + Log K_F$	$Log \, q_e \, vs \, Log C_e$	**K_F** = Freundlich constant, related to the adsorption capacity of the adsorbent (mg/g) **n** = adsorption intensity of the adsorbent according to its heterogeneity	(Tejada-Tovar *et al.*, 2022)

2.5 Adsorbents

An adsorbent is a solid substance (in rare cases a liquid) used to remove molecules or ions from liquid or gas bulks as they stick to its surface (El-Dairi *et al.*, 2014; Crini *et al.*, 2019). As adsorption is a surface process, a good adsorbent is generally characterized by possessing a porous structure which is an indicator of high surface area (Gupta *et al.*, 2009; El-Dairi *et al.*, 2014). Other properties of importance when considering the suitability of an adsorbent include: low cost, high adsorption capacity, appropriate pore distribution and diameter, as well as the presence of suitable surface functional groups (Mariana *et al.*, 2021)). As pointed out by (Dąbrowski, 2001), the range of application of adsorbents in industry and laboratory practices is broad hence there are a variety of adsorbents as can be seen in Table 2.4.

Table 2.4 Basic types of adsorbents *(Dąbrowski, 2001)*

Carbon adsorbents	Mineral adsorbents	Other adsorbents
Active carbons	Silica gels	Synthetic polymers
Activated carbon fibers	Activated alumina	Composite adsorbents:
Molecular carbon sieves	Oxides of metals	Complex mineral carbons, X-elutrilithe; X=Zn, Ca
Fullerenes	Hydroxides of metals	
	Zeolites	
Mesocarbon microbeads		
Heterofullerenes	Clay minerals	Mixed sorbents
Carbonaceous nanomaterials	Pillared clays	
	Porous clay hetero structures	
	PCHs	
	Inorganic nanomaterials	

2.5.1 Activated Carbon

The term ‘activated carbon’, is broad and encompasses carbonized materials exhibiting a high surface area, porosity, as well as surface reactivity (Cuhadaroglu and Uygun, 2008; Bhatnagar *et al.*, 2013; Heidarinejad *et al.*, 2020). Due to popularity in its applications in water and wastewater treatment, the demand of activated carbon is ever increasing, this has seen an increase in the cost of the adsorbent due the finite nature of the precursors of conventional commercial activated, such as coal (Tan, Ahmad and Hameed, 2008). This compels the need for the exploration of alternative sources of adsorbents, which possess physiochemical properties similar to those of the existing highly efficient commercial activated carbon such as; high specific area and porosity, thermal stability, adsorptive capacity, and chemical composition, while at the same time being cost effective, and having a relatively renewable precursor (Danish and Ahmad, 2018). Materials such as; coconut shells, bamboo, wood waste, rice husk, bagasse, corn cob and other waste agricultural biomass have been commonly reported in literature as suitable precursors of activated carbon (El Qada, Allen and Walker, 2006; Chan *et al.*, 2012; Bernard, Jimoh and Odigure, 2013; Boonpoke *et al.*, 2013; Yahya, Al-Qodah and Ngah, 2015; Danish and Ahmad, 2018). One other precursor researchers have looked into is sludge (Otero *et al.*, 2003; De Filippis *et al.*, 2013; Filho *et al.*, 2020). It has been considered a favorable precursor of activated carbon owing to its high organic content (Li, Yue, Gao, Ma, *et al.*, 2011; Du *et al.*, 2019). The amount of sludge being produced yearly has become unmanageable as traditional methods of disposal such as ocean discharge, incineration, composting, and land application are being phased out due to concerns of environmental pollution, harm to human

and aquatic life, and high capital cost (Hadi *et al.*, 2015; Li *et al.*, 2016). The conversion of sludge to activated carbon is therefore a promising solution to managing the inescapable production of sludge by wastewater treatment plants (Du *et al.*, 2019; Almahbashi *et al.*, 2021; Lin *et al.*, 2021).

2.6 Sludge Derived Activated Carbon

Sludge is an unavoidable by-product of wastewater treatment plants that is proving difficult to manage because of the large quantities produced yearly and the strict disposal laws. The production of activated carbon from conventional precursors such as coal is expensive (Rozada *et al.*, 2003; Li, Yue, Gao, Ma, *et al.*, 2011). The production of activated carbon from sludge is an answer to both these problems. Sludge is favored as an activated carbon precursor due to its high organic content and its carbonaceous nature (Chen, Jeyaseelan and Graham, 2002; Li, Yue, Gao, Ma, *et al.*, 2011; Hadi *et al.*, 2015). The preparation of sludge derived activated carbon has been reported in literature as being via mostly carbonization and then further activation by physical means using carbon dioxide, steam or air (Li, Yue, Gao, Wang, *et al.*, 2011; Hadi *et al.*, 2015; Puccini *et al.*, 2017), chemical activation before carbonization using chemical agents such as sulfuric acid, zinc chloride, potassium hydroxide, and phosphoric acid (Hadi *et al.*, 2015) as this significantly enhances the surface area (Chen, Jeyaseelan and Graham, 2002; Zhang, Nriagu and Itoh, 2005), and as a result the adsorption capacity. These produced ACs have been characterized and reported as having surface areas ranging between 100-600mg^2/g (Zhang, Nriagu and Itoh, 2005; Li, Yue, Gao, Wang, *et al.*, 2011; Li *et al.*, 2016).

2.7 Analytical Tests for Activated Carbon

Analytical techniques such as scanning electron microscopy (SEM), Fourier-transform infrared (FTIR) spectroscopy, energy dispersive X-ray spectroscopy (EDS), Raman spectroscopy, thermogravimetric analysis (TGA), and Brunauer-Emmett-Teller (BET) are employed to determine the surface properties and thermal stability (TGA) of activated carbons. An overview of the techniques is given in sections 2.7.1 - 2.7.6.

2.7.1 Scanning Electron Microscopy (SEM)

Scanning electron microscopy is a surface imaging technique used to examine and analyze microstructure morphology, characterize chemical composition as well as providing information about surface topography, crystalline structure, and electrical behavior. As a result it is not only one of the most versatile techniques available but also one of the leading techniques for insitu analysis of microareas (K D Vernon-Parry, 2000; Zhou *et al.*, 2007; Zhao and Li, 2018). The scanning electron microscope provides the ability to visually detect pores, crevices and surface deposits (Novak *et al*., 2019). The advantages of SEM include; having a large depth field which ensures that most of the specimen surface is in focus, high magnification and resolution, strong stereoscopic vision, the ability to switch between different techniques allowing for a cross-correlation of information, no destruction of specimen during evaluation, and ease of preparation of specimen for evaluation (K D Vernon-Parry, 2000). A scanning electron microscope creates an image by projecting a focused beam of electrons to systematically scan across the surface of a specimen, causing the specimen and electrons to interact, leading to the production of numerous signals which are used to gather information regarding surface composition and topography (Zhou *et al.*, 2007).

2.7.2 Fourier- Transform Infrared (FTIR) Spectroscopy

Fourier transform infrared spectroscopy is a non-invasive analytical technique that uses infrared light to scan and obtain chemical properties of samples in situ. As a form of vibrational spectroscopy, the FT-IR spectrum displays the molecular structure as well as the molecular environment. This technique works by exposing the sample to infrared radiation, which is absorbed by the sample stimulating vibrational motion by the transfer of energy, thereby producing spectral bands which are characterized by amplitude and frequency. Infrared radiation with a wave number range of between 4000 and 400 cm^{-1} is emitted by a blackbody source, then an interferometer inside the spectrophotometer, measures the energy transmitted to the sample and then encodes the spectral signals and transmits them through the surface of the sample, where specific energy signals are absorbed. In time, the infrared beam passes through the detector, onto the processing computer for Fourier transformation of energy signals. (Sacksteder and Barry, 2001; Undavalli, Khandelwal and Fuels, 2021). The unique spectral absorption bands can be associated with fundamental vibrations which correspond to certain functional groups (Berthomieu and Hienerwadel, 2009). Of the infrared based dispersive spectroscopy instruments, FT-IR is one of the most preferred because of its heightened sensitivity, precision, accuracy, speed, non-invasiveness and ease of operation (Undavalli, Khandelwal and Fuels, 2021). The use of FT-IR spectroscopy covers a variety of applications such as the identification of unknown compounds and characterization of components in mixtures (e.g., liquids, solids, or films).

2.7.3 Energy Dispersive X-ray Spectroscopy (EDS)

The energy dispersive X-ray spectroscopy (EDS), which at times is referred to as EDX, is a technique that is used in conjunction with scanning electron microscopy and is widely applied for elemental analysis and chemical composition determination, associated with electron microscopy (Torres-Rivero *et al*., 2021). This technique is dependent on the characteristic X-rays emitted by a specimen. The investigated sample is irradiated by a stream of high energy charged particles (electrons or protons). An electron from a higher binding energy electron level falls into the core hole and an X-ray with the energy of the difference of the electron level binding energies is emitted, and a spectrum that depicts the peaks correlated to the elemental composition of the investigated sample is displayed (Colpan *et al*., 2018).

The elements in an investigated sample are determined by the energies of the X-rays emitted from the area being excited by the high energy electron beam. The rate at which the characteristic X-rays are determined can be used to take the measurement of the elements present in the sample. Though the EDS system is able to provide information regarding present chemical elements in the specimen it cannot identify the molecular structure. Applications of EDS are typically in quality control, material research, forensic science, and failure analysis (Bergström, 2015).

2.7.4 Raman Spectroscopy

Raman spectroscopy is a non-destructive spectroscopic technique used to analyze vibrational, rotational, and other low-frequency modes in a material system. It relies on a laser in the visible, near infrared, or near ultraviolet range to disperse Raman scattering of monochromatic light. The energy laser photons

are shifted up and down resulting in system excitations being absorbed or emitted by laser light. This shift in energy provides information about photon modes in the system (Bergström, 2015). Raman spectroscopy has become one of the most sensitive analytical techniques due to recent developments. Not only does it achieve very low detection limits, it also allows easy identification of specimen by giving vibrational information which can be treated as its fingerprint. It allows for the study of complex samples as its signals are often characteristic for analyzed compounds (Kudelski, 2008). Its non-destructive character, ability to deliver specific chemical identification and wide range of instrumental and sampling methodologies allows for its wide range of application including; chromatographic detection, environmental monitoring, and materials chemistry (Lyon *et al.*, 1998). The Raman Effect is the process by which most photons are elastically scattered when light is scattered from a molecule. The energy difference between the incident photon and the Raman scattered photon is equal to the energy of a vibration of the scattering molecule. The Raman spectrum is made up of a plot of intensity of scattered light versus the energy difference. Raman spectroscopy works by irradiating a spot on the sample being tested with a laser beam. The Raman effect then produces scattered radiation which includes information about the molecular vibrations and rotations, which depend on the particular atoms or ions that comprise the molecule (Bergström, 2015).

2.7.5 Thermogravimetric Analysis (TGA)

Thermogravimetric analysis is a quantitative chemical engineering experimental technique applied to derive mass changes and thermal stabilities of samples as a function of increasing temperature (Bottom, 2008). The

temperature in the furnace can be ramped up as high as 1600 °C depending on the information required about the sample, in addition the atmosphere in which the experiment is carried out can be reactive, inert or oxidizing (Saadatkhah *et al.*, 2020). The technique provides information to do with some physical and chemical phenomena such as:

- Decomposition or carbonization which is carried out in an inert environment and results in the formation of gaseous products.
- Oxidative degradation which occurs in an air or oxygen environment.
- Adsorption and desorption of gases and other volatile components.
- Vaporization of water.
- Solid-gas reactions where a products evolve or where hydrogen gas is purged causing a reduction reaction to occur (Bottom, 2008).

However, the technique cannot provide information for reactions in which mass remains unchanged, phase transitions or polymorphic transformations. The thermogravimetric analyzer is fitted with a precise microbalance coupled with a sample pan closed inside a temperature programed and controlled furnace. The mass changes of the sample under investigation are represented graphically by a thermogram which depicts the mass change versus temperature or time. The thermogram is unique for each sample and it provides information such as the thermal and oxidative stability, moisture and volatile content, decomposition kinetics, component composition, and sample lifetime. Thermograms generally consist of multiple stages or sections. At temperatures below 150 °C, volatile compounds, trapped gases and physiosorbed water are usually lost. Between 150 °C and 250 °C, a loss of mass occurs due to the loss of chemisorbed water and volatile decomposition products. Compounds begin to decompose above 250 °C,

and materials such as metals and non-volatile inorganic ashes remain above the end temperature. Metallic compounds gain mass and increase the oxidation state when an oxidizing environment is created (Saadatkhah *et al.*, 2020).

2.7.6 Brunauer-Emmett-Teller (BET)

The Brunauer–Emmett–Teller (BET) Method developed by Brunauer, Emmett and Teller in 1938, is an analytical technique used to measure the specific surface area of a material based on its multilayer adsorption of nonreactive gas molecules such as nitrogen at 77K or argon at 87K at a range of pressures (Brunauer, Emmett and Teller, 1938; Sinha *et al.*, 2019). During the procedure, known amounts of a non-corrosive gas are released into a cell containing the material to be analyzed in steps. A partial vacuum is then created to achieve saturation pressure after which no more adsorption takes place regardless of any increases in pressure. The pressure changes due to the adsorption process are monitored by pressure transducers. Adsorption layers are formed and then the sample is removed from the gaseous atmosphere and heated to release the adsorbed gaseous molecules so that they can be quantified. A BET isotherm is formed from the collected data and a linearized plot of the gas adsorbed as a function of relative pressure is displayed making it possible to determine the surface area of the material (Hwang and Barron, 2011).

2.8 Adsorbates

2.8.1 Methylene Blue

Methylene blue (MB) is a synthetic cationic dye which is an odorless dark green powder at room temperature and dissolves in aqueous solutions to form a deep blue color. It has a molecular formula: $C_{16}H_{18}N_3ClS$, a molecular weight of 319.85g/mol and a λmax of 663nm (Khan *et al.*, 2022). Its other names include basic blue 9, tetramethylthionine chloride and color index (CI) number 52015 (Raposo, De La Rubia and Borja, 2009). The chemical structure is given by the following figure.

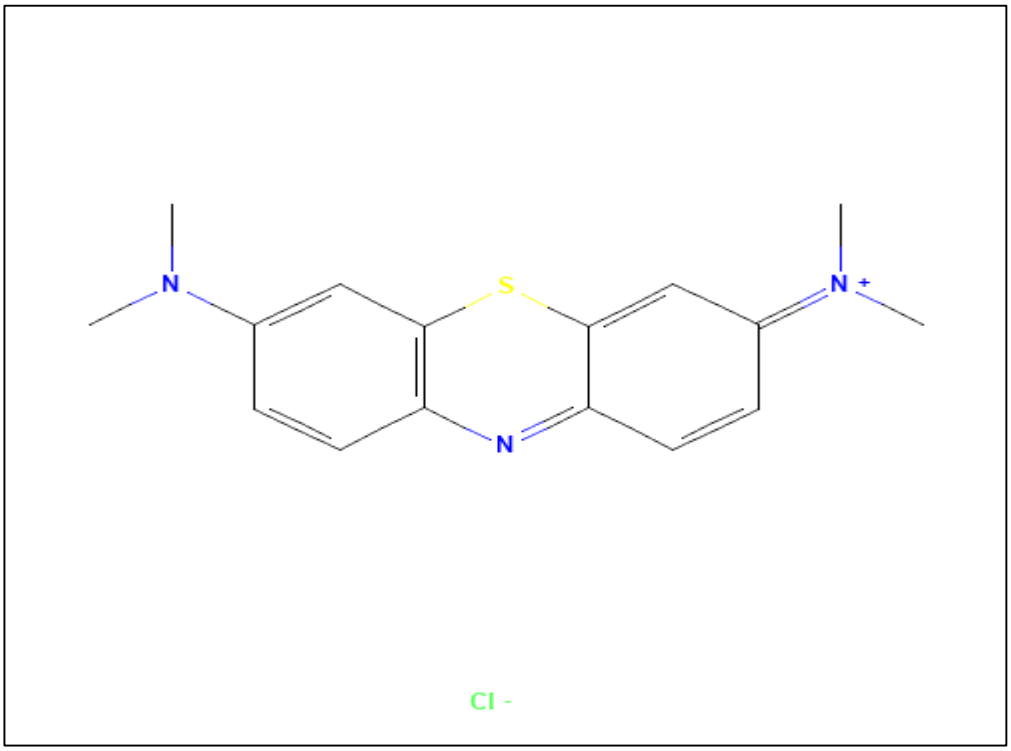

Figure 2.1 Chemical structure of methylene blue dye (Kim S et al., 2023)

Its applications spans the textile, pharmaceutical, paper, dyeing, printing, paint, medicine, and food industries (Khan *et al.*, 2022), and it has been used extensively an indicator of visible pollution and of the mesoporosity of adsorbents (Bestani *et al.*, 2008). The discharge of large volumes of the dye by the textile industry into natural water bodies poses health risks to humans and significant threats to the environment. Methylene blue dye is substantially toxic to humans above certain concentrations and is known to cause several sever health conditions such as respiratory distress, abdominal disorders, blindness, digestive and mental disorders, as well as mild risks such as nausea, diarrhea, vomiting, and eye irritation. In the environment its adverse effects include visual pollution, a reduction in the transmittance of sunlight and oxygen solubility which affects photosynthetic organisms as well as poisoning the food supply of some aquatic life (Khan *et al.*, 2022). Studies of methylene blue adsorption are performed widely to evaluate the mesoporosity of adsorbents and as model of visual pollution (Bestani *et al.*, 2008).

2.8.2 Lead

Lead (Pb) is a chemical element with an atomic number of 82. Its presence in the aqueous environment is due to its release from natural sources (mineral deposits) as well as untreated effluent from industrial activity(such as the manufacture of lead-acid batteries, solders and alloys) (Papanikolaou, Hatzidaki and Belivanis, 2005; Herschy, 2012). It is widely used due to its important physio-chemical properties such as resistance to corrosion, poor conductibility, and malleability. Consequently, it is a persistent poison that is not biodegradable and accumulates in the environment as well as the human body where it affects multiple body functions such as the neurodevelopment in children, fertility, as

well as cardiovascular function leading to death. Its main channels of entry into the human body are via the ingestion of food or water that are contaminated with lead (Herschy, 2012; Wani, Ara and Usmani, 2015). Due to its toxicity at low concentrations the World Health Organization and the South African National Standard (SANS) have set the guideline value for lead in drinking water at 10 μg/L (Herschy, 2012; SANS 241, 2015).

2.9 Closure

The literature study briefly introduces water treatment technologies along with their advantages and disadvantages. It discusses the implementation of the adsorption process in the removal of pollutants from aqueous solution as well as the kinetic and isotherm models used to determine the rate of the adsorption process and the mechanism of adsorption, respectively. It also looks at activated carbon as an adsorbent in the adsorption process and its derivation from sludge, as well as the analytical tests used to determine its surface properties and thermal stability. Lastly, it discusses the adsorbates (methylene blue and lead) which are to be focused on in the current study.

Chapter 3 Methods

3.1 Introduction

This chapter contains a brief summary of the preparation of the hydrochar and the experimental procedures of this dissertation which can be grouped into three main categories:

- Pyrolysis of hydrochar to produce activated carbon.
- Characterization and analytical tests on activated carbons.
- Application of activated carbons in the adsorption studies of methylene blue dye and lead (II) ions.

3.1.1 Preparation of Hydrochar

A combination of primary sludge and waste activated sludge was used to prepare hydrochar by the enhanced hydrothermal polymerization (EHTP) process which is an emerging technology for the conversion of biomass to hydrochar (Musvoto *et al.*, 2018). The sludge was obtained from a biological nutrient removal (BNR) activated sludge wastewater treatment plant in South Africa and the hydrochar was prepared in a pilot-scale plant installed at the treatment plant. The sludge processed in the EHTP reactor was taken from the underflow of the primary settling tank (primary sludge; PS) and the dissolved air flotation (DAF) thickeners (waste activated sludge; WAS) which are highlighted in Figure 3.1. A patented catalyst solution was mixed with a portion of the composite sludge and fed into the EHTP reactor which had a capacity of 60 liters. The reactor was sealed and purged with an inert gas (N_2) prior to heating. The contents of the reactor were then heated to a temperature of 190 ±

5° C at a dwelling time of 60 minutes. After the set time had elapsed, the reactor was cooled to room temperature and the contents of the reactor (hydrochar and supernatant) were poured into a container and then separated. The solid portion (hydrochar) was dried and stored.

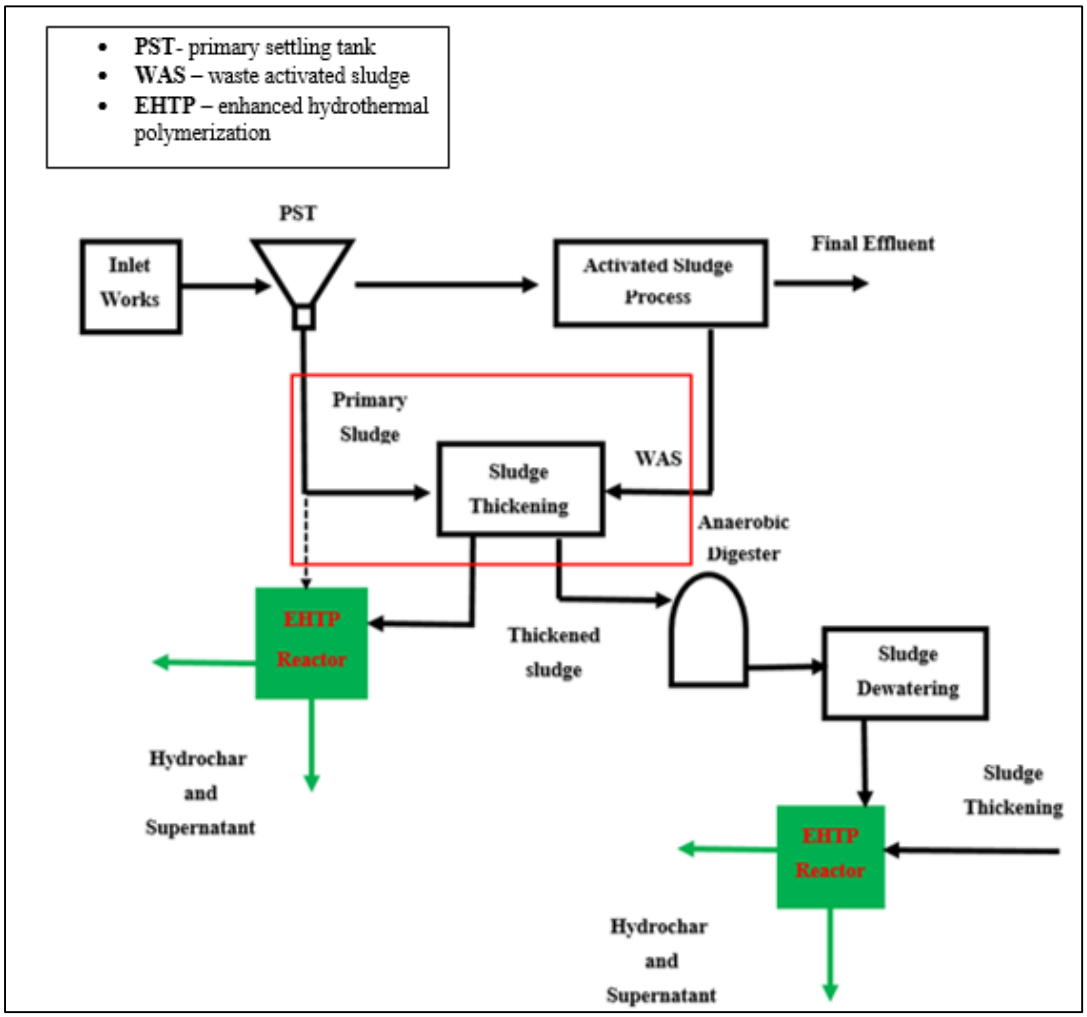

Figure 3.1 Schematic layout of incorporation of EHTP technology at a typical wastewater treatment plant (Musvoto *et al.*, 2018)

3.2 Pyrolysis of Hydrochar to Produce Activated Carbon

Prior to carbonization thermogravimetric analysis was carried out on the hydrochar to ascertain its chemical stability and the best temperature to use for pyrolysis. The pyrolysis method in this study was adapted from a procedure published in a work by (Saha *et al.*, 2019).

Procedure:

Hydrochar from the EHTP process was pyrolyzed in a Labofurn horizontal tubular furnace under inert conditions (nitrogen gas (N_2)). The hydrochar was pyrolyzed at three different temperatures; 175, 425 and 600 °C. Five to six grams of the hydrochar was weighed into two ceramic boats which were placed at the center of a quartz tube that was inserted into the horizontal tubular furnace. The tube had an airtight inlet cap and outlet nozzle connected to pipes to allow for the flow of N_2 throughout the pyrolysis process at a volumetric flow rate of 0.1 L/min, to prevent any unwanted combustion or gasification. The nitrogen gas was passed through the quartz tube for a minute before the furnace was turned on to ensure that the atmosphere was inert. The pyrolysis procedure was performed in two steps. In the first step, the furnace was heated from ambient temperature to 100 °C at a rate of 10 °C/min. The temperature was maintained at 100 °C for 1 min to stabilize the temperature and to ensure the removal of moisture from the hydrochar. In the second step, the furnace was heated from 100 °C to the set pyrolysis temperature at a rate of 20 °C/min, which was followed by a dwelling time of 60 min at the same temperature. Thereafter, the furnace was allowed to cool to room temperature by natural cooling.

Once at room temperature, the nitrogen flow was cut off and the pyrolyzed hydrochar was weighed to ascertain its loss of mass due to the pyrolysis process.

It was then transferred to a Fisherbrand™ centrifuge tube and stored in a desiccator until further analyses. The procedure was replicated until an amount of activated carbon sufficient to carry out the characterization and adsorption tests was produced. The set up for the pyrolysis procedure is shown in Figure 3.2 , and the materials and apparatus are shown in Table 3.1.

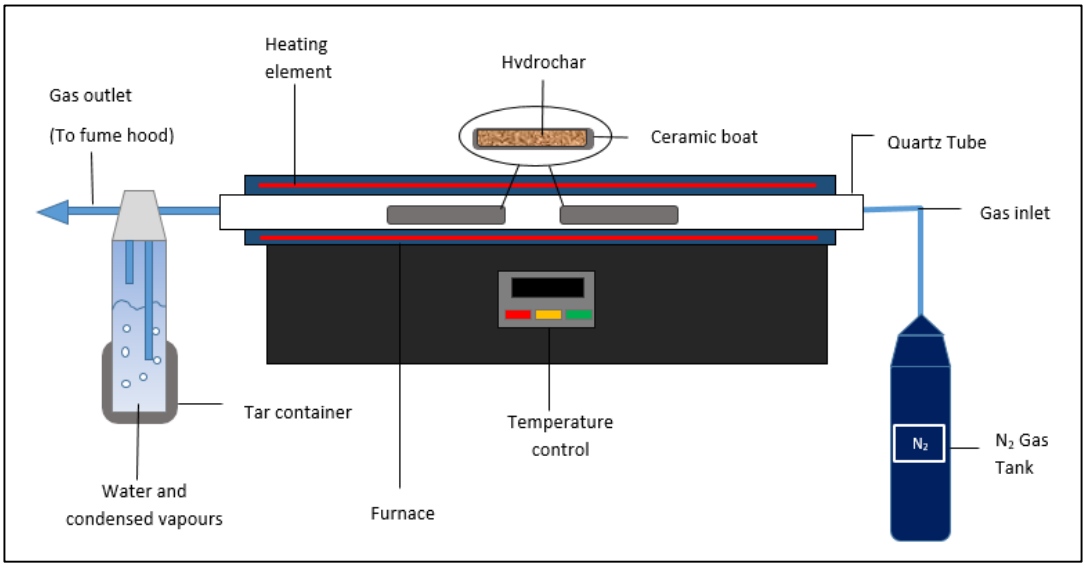

Figure 3.2 Schematic of horizontal tube furnace used for pyrolysis

Calculation:

The ceramic boats and hydrochar were weighed prior and post pyrolysis using an electronic balance. The percentage weight loss of the hydrochar and the percentage yield were then calculated from the weight measurements using Equations 3.1 and 3.2 respectively.

$$\%\, Weight\ loss = \frac{C - D}{C - B} \times 100 \tag{3.1}$$

$$\%\, Yield = \frac{Initial\ mass\ (g)}{Final\ mass\ (g)} \times 100 \tag{3.2}$$

Where:

B = weight of the empty ceramic boat, g.

C = weight of the ceramic boat plus hydrochar, g.

D = weight of ceramic boat plus the pyrolyzed hydrochar (now activated carbon), g.

Table 3.1 Materials and apparatus for the pyrolysis procedure

Materials and apparatus:
Hydrochar
Ceramic boat
Mettler Toledo® electronic balance accuracy ± 0.0001g
Kiln Contractors (Pty) Ltd Labofurn horizontal Tubular furnace
GlassChem quartz tube
Nitrogen gas
Flow meter
Centrifuge tubes(Fisherbrand™)

3.3 Characterization and Analytical Tests on Activated Carbons

Sample Preparation

Granular activated carbon (GAC), commercially referred to as ACARB 1000A was supplied by a commercial South African supplier. It was dried according to the method outlined in Section 3.3.1 and used as received from the supplier. Alien wood activated carbon (AW-AC) was produced by a small scale South African manufacturer through the pyrolysis of alien wood from forests in the south eastern part of South Africa. It was crushed and sieved and a representative sample with a particle size similar to the bulk of the GAC sample was dried and used in further experiments. Hydrochar received from the pilot scale EHTP reactor was pyrolyzed to derive activated carbon. The product of pyrolysis was termed hydrochar derived activated carbon (HC-AC). It was dried prior to further testing. The characterization tests carried out on the activated carbons are shown in Table 3.2 and the analytical tests are outlined in Section 3.4.

Table 3.2 Characterization tests conducted on the activated carbons

Properties
Moisture content (%)
Ash content (%)
Iodine number (mg/g)
Particle size (µm)
Attrition (%)
Bulk density (g/cm^3)
pH
Surface area (BET N_2) (m^2/g)

3.3.1 Moisture Content

The moisture content refers to the amount of water physically bound to an adsorbent under normal conditions. The activated carbon was heated in an air circulation oven at constant temperature to eliminate moisture and attain a constant weight. The method used in this study was adopted from (CEFIC, 1986).

Procedure:

A pre-dried ceramic crucible with a lid was weighed and tarred. The representative carbon sample was placed into the crucible and weighed. Deep crucibles were used such that the depth of the carbon in the crucible did not exceed 1.25 cm.

The oven was preheated to 150 ± 5 °C. The crucible containing the carbon sample as well as the lid were placed in the oven side by side. The oven was closed, and the sample was left to dry to constant weight for 3 hours. After the three hours, the oven was opened and the lid placed on the crucible quickly to avoid reintroducing any moisture back into the sample. The closed crucible containing the dried sample was then transferred to a desiccator to cool to ambient temperature and thereafter it was weighed to determine the dry weight. The procedure was replicated at least twice and the average value recorded. The materials and apparatus used for this procedure are given in Table 3.3.

Calculations:

The moisture content M_c is given in percentage form:

$$M_C = \frac{D - E}{D - B} \times 100 \quad (3.3)$$

Where:

B = weight of crucible with lid, g.

D = weight of crucible with lid plus original sample, g.

E = weight of crucible with lid plus dried sample, g.

Table 3.3 Materials and apparatus for the moisture content test

Materials and apparatus
Activated carbon: 1-2 g for **powdered** activated carbon 5-10 g for **granular** activated carbon
Mettler Toledo® electronic balance accuracy ± 0.0001g
Seamless ceramic crucible with a lid
Forced circulation oven set at 150 ± 5°C
Desiccator

3.3.2 Ash Content

The ash content refers to the non-combustible portion that remains after the carbonaceous matter is burnt off. The method used in this study was adapted from the method by (CEFIC, 1986).

Procedure:

After the moisture content procedure outlined in section 3.3.1 was completed, the crucible containing the dried activated carbon with its lid placed beside it was placed in a muffle furnace which was set at a temperature of 700 ± 25 °C, at a ramping rate of 20 °C/ min, and a dwelling time of seven hours. After the set time elapsed the crucible containing the sample was left to cool to 200 °C then the oven was opened and its lid was quickly placed on top to avoid loss of ash. The container was placed in a desiccator, left to cool to room temperature, and then weighed to the nearest 0.0001g. The procedure was replicated at least twice and the average value recorded. The materials and apparatus for this procedure are given in Table 3.4 .

Calculations:

The ash content (Ac) is given in percentage form:

$$A_c = \frac{F - G}{B - G} \times 100 \tag{3.4}$$

Where:

G = weight of crucible with lid, g.

B = weight of crucible with lid plus dried sample, g.

F = weight of crucible with lid plus ashed sample, g.

Table 3.4 Materials and apparatus for the ash content test

Materials and apparatus
Dried activated carbon
Kiln Contractors (Pty) Ltd Labofurn muffle furnace
Seamless ceramic crucible with a lid
Mettler Toledo® electronic balance accuracy ± 0.0001g
Desiccator

3.3.3 Iodine Test

The iodine test is a worldwide standard test used to determine the microporocity and adsorptive capacity of activated carbon. In this study, it was the first procedure to be carried out because it was the determining characteristic used to select which pyrolysis temperature would be best for producing activated carbon from hydrochar. The iodine number is defined as, "the X/M value at a residual iodine concentration (C) of 0.02 N " (ASTM D4607-94, 2006).

Procedure:

The iodine test was conducted as per the method detailed in the American Society for Testing and Materials (ASTM D4607-94, 2006) document. Sodium thiosulphate solution was prepared and then allowed to sit in an amber bottle for four days prior to use. The iodine solutions was prepared and stirred for four hours using a magnetic stirrer on medium speed to ensure that all the crystals had dissolved. The two solutions were then standardized prior to use to ascertain normality, and the starch indicator was made fresh daily. The activated carbon was pulverized to meet the particle size requirements for the test i.e. (<149μm), and then dried in accordance with the moisture content procedure (Section 3.3.1). Three different carbon dosages were estimated, weighed and then transferred to clean, dry, and heat resistant narrow necked Erlenmeyer flasks

equipped with ground glass stoppers. A 5 wt. % hydrochloric acid (HCL) solution was then pipetted into each flask. The flasks containing the acid and carbon mixtures were then swirled gently until the carbon was completely wetted. The stoppers were then loosened to vent the flasks. Thereafter, the flasks were placed on a hot plate in a fume hood and allowed to boil gently for 30 ± 2 seconds (s) to remove any sulfur which may interfere with the test results. The flasks were then removed from the hot plate and allowed to cool to room temperature.

Beakers with funnels lined with folded filter paper (Whatman® No. 2V or equivalent) were prepared and set aside for filtration. A 100 mL of 0.100 N standardized Iodine solution was pipetted into each of the cooled flasks and they were immediately plugged and shaken vigorously for 30 ± 1 (s). Thereafter, each mixture was poured into the prepared funnels with filter paper and filtered by gravity. Fifty milliliters of the resulting filtrates was pipetted to clean wide mouthed Erlenmeyer flasks. The above mentioned standardized 0.100 N Sodium thiosulphate was poured into a burette and used to titrate the filtrate until a pale yellow color was observed. Following this, 2 mL of freshly prepared starch solution indicator was added to the solution and the titration was continued drop wise until a colorless solution was achieved.

Calculations:

The concentration of the adsorbate in solution determines the carbons capacity for that adsorbate. Therefore, it is important that the concentrations of the iodine solution and resulting filtrates are known as this helps to select a fitting carbon dosage to produce final concentrations agreeing with the definition of the iodine number. The activity of the carbon dictated how much of the carbon was to be used in the determination of the iodine number. The procedure was replicated at

least twice and the average value recorded. For each carbon dosage used, two calculations were required; the iodine absorbed per gram of carbon (X/M), mg/g, and the residual iodine concentration (C), N.

To calculate the value of X/M, the following values needed to be derived first:

$$A = (N_2)(12693) \tag{3.5}$$

Where:

N_2 = iodine normality, N.

$$B = (N1)(126.93) \tag{3.6}$$

Where:

N1 = sodium thiosulfate normality, N.

$$DF = \frac{1 + H}{F} \tag{3.7}$$

Where:

DF = dilution factor.

I = iodine used, mL.

H = 5 % hydrochloric acid used, mL.

F = filtrate, mL.

The following equation was used to determine the value of X/M:

$$X/M = \frac{[A - (DF)(B)(S)]}{M} \tag{3.8}$$

Where:

X/M = iodine absorbed per gram of carbon, mg/g.

S = sodium thiosulfate used during titration, mL.

M = carbon used, g.

To calculate the residual iodine normality the following equation was used:

$$C = \frac{N_1 \,.\, S}{F} \tag{3.9}$$

Where:

C = residual filtrate normality, N.

N_1 = sodium thiosulfate normality, N.

F = filtrate used during titration, mL.

To estimate the carbon dosage the following equation was used:

$$M = \frac{[A - (DF)(C)(126.93)(F)}{E} \quad (3.10)$$

Where:

M = carbon dosage, g.

A = (N_2). (12693.0).

DF = dilution factor.

C = residual iodine normality, N.

F = filtrate used, mL.

E = estimated iodine number of carbon.

To find the residual iodine normality that is within the acceptable range for the iodine test .i.e. 0.0080-0.0334 N the correction factor sheet (Table 3.5) was used. The materials and apparatus for this test are displayed in Table 3.6.

Table 3.5 Residual filtrate normality correction factor sheet (Comm Rep, 1974)

Residual Filtrate Norma1ty C	0.0000	0.0001	0.0002	0.0003	0.0004	0.0005	0.0006	0.0007	0.0008	0.0009
0.0080	1.1625	1.1613	1.1600	1.1575	1.1550	1.1538	1.1513	1.1500	1.1475	1.1463
0.0090	1.1438	1.1425	1.1400	1.1375	1.1363	1.1350	1.1325	1.1300	1. 1288	1.1275
0.0100	1. 1250	1.1238	1.1225	1.1213	1.1200	1.1175	1.1163	1.1150	1.1138	1.1113
0.0110	1.1100	1.1088	1.1075	1.1063	1.1038	1.1025	1.1000	1.0988	1.0975	1.0963
0.0120	1.0950	1.0938	1.0925	1.0900	1.0888	1.0875	1.0863	1.0850	1.0838	1.0825
0.0130	1.0800	1.0788	1.0775	1.0763	1.0750	1.0738	1.0725	2.0713	1.0700	1.0688
0.0140	1.0675	1.0663	1.0650	1.0625	1.0613	1.0600	1.0588	1.0575	1.0563	1.0550
0.0150	1.0538	1.0525	1.0513	1.0500	1.0488	1.0475	1.0463	1.0450	1.0438	1.0425
0.0160	1.0413	1.0400	1.0388	1.0375	1.0375	1.0363	1.0350	1.0333	1.0325	1.0313
0.0170	1.0300	1.0288	1.0275	1.0263	1.0250	1.0245	1.0238	1.0225	1.0208	1.0200
0.0180	1.0200	1.0188	1.0175	1.0163	1.0150	1.0144	1.0138	1.0125	1.0125	1.0113
0.0190	1.0100	1.0088	1.0075	1.0075	1.0063	1.0050	1.0050	1.0038	1.0025	1.0025
0.0200	1.0013	1.0000	1.0000	0.9988	0.9975	0.9975	0.9963	0.9950	0.9950	0.9938
0.0210	0.9938	0.9925	0.9925	0.9913	0.9900	0.9900	0.9888	0.9875	0.9875	0.9863
0.0220	0.9863	0.9850	0.9850	0.9838	0.9825	0.9825	0.9813	0.9813	0.9800	0.9788
0.0230	0.9788	0.9775	0.9775	0.9763	0.9763	0.9750	0.9750	0.9738	0.9738	0.9725
0.0240	0.9725	0.9708	0.9700	09700	0.9688	0.9688	0.9675	0.9675	0.9663	0.9663
0.0250	0.9650	0.9650	0.9638	0.9638	0.9625	0.9625	0.9613	0.9613	0.9606	0.9600
0.0260	0.9600	0.9588	0.9588	0.9575	0.9575	0.9563	0.9563	0.9550	0.9550	0.9538
0.0270	0.9538	0.9525	0.9525	0.9519	0.9513	0.9513	0.9506	0.9500	0.9500	0.9488
0.0280	0.9488	0.9475	0.9475	0.9463	0.9463	0.9463	0.9450	0.9450	0.9438	0.9438
0.0290	0.9425	0.9425	0.9425	0.9413	0.9413	09400	0.9400	0.9394	0.9388	0.9388
0.0300	0.9375	0.9375	0.9375	0.9363	0.9363	09363	0.9363	0.9350	0.9350	0.9346
0.0310	0.9333	0.9333	0.9325	0.9325	0.9325	0.9319	0.9313	0.9213	0.9300	0.9300
0.0320	0.9300	0.9294	0.9288	0.9288	0.9280	0.9275	0.9275	0.9275	0.9270	0.9270
0.0330	0.9263	0.9263	0.9257	0.9250	0.9250					

Table 3.6 Materials and apparatus for the iodine test

Materials and apparatus:
Activated carbon
Grinder
Kingtest Sieve (149 μm)
Mettler Toledo® electronic balance accuracy ± 0.0001g
Narrow necked, 250 mL Erlenmeyer flasks with ground glass stoppers (Pyrex®)
Wide mouthed, 250 mL Erlenmeyer flasks
Hot-plate
Amber bottles for storage of iodine and sodium thiosulphate solutions
0.10 N standardized sodium thiosulphate solution
0.10 N standardized iodine solution
Starch solution
Folded filter paper, Whatman® 2v. 18 cm Ø
Glass funnels, 100 mm top inside diameter
Assorted size beakers
Volumetric type pipettes (5, 10, 25, 50, and 100 mL capacity)
Volumetric flasks, 1 L
Graduated cylinders

3.3.4 Particle Size Distribution

The method used to determine the particle size distribution of the activated carbons was adapted from the American Water Works Association (AWWA B604-74)(Comm Rep, 1974). The sieve sizes used for the analysis of the powdered carbon, HC-AC, were smaller than those used for the analysis of GAC and AW-AC due to the aperture of the sieves used for the latter mentioned carbons being too big and letting all the powder fall through. The sieve range

used for GAC and AW-AC was from 425 to 2360 μm, while the sieves used for HC-AC ranged from 45 to 150 μm.

Procedure:

Sieves to be used were preweighed then assembled on a bottom receiver pan in ascending order of the sieve openings. The sample was mixed by passing it through a riffle twice, then 100g ± 5 g was transferred to the top sieve and the sieve cover was placed on top. The assembly of sieves was placed on a sieve shaker and the sieve shaker cover was tightened. The sieve assembly was left to shake for 3 minutes ± 3 (s). After the set time elapsed, the sieve assembly was removed, and the individual sieves and the carbon retained on them were weighed on a tarred balance. The weights of the carbon retained on the individual sieves were to be added and if the amount deviated by more than 2g from the test sample weight, the analysis was to be repeated. The materials and apparatus of the procedure are displayed in Table 3.7.

Calculation:

$$\% R = \frac{(Sieve\ fraction\ weight)}{(Sum\ of\ sieve\ fraction\ weights)} \times 100 \qquad (3.11)$$

Where:

% R = the percentage of carbon retained on sieve.

Sieve fraction weight = the carbon retained on each sieve, g.

Sum of sieve fraction weights = the sum of the carbon retained on each sieve, g.

Table 3.7 Materials and apparatus for particle size distribution test

Materials and apparatus:
Activated carbon Sample splitter- similar to Jones Riffle Kingtest electric sieve shaker Kingtest sieves: (425-2360 μm) for granular carbon, (45-150 μm) for powdered carbon Mettler PE3000 top loader balance, with a sensitivity of 0.1 g Soft brass-wire brush

3.3.5 Attrition Analysis

The attrition test, also known as the abrasion test, is a measure of the resistance to abrasion of activated carbons (especially granular activated carbons) after being abraded by action of a magnetic stirrer in a fabricated abrasion unit for 24 hours (Comm Rep, 1974).

The method used in this study was reported by (Toles *et al.*, 2000). The attrition test was only performed on GAC and AW-AC as the particles of HC-AC were generally in powdered form (fine in nature) and it would be difficult to determine loss due to attrition accurately.

Procedure:

An acetate buffer of pH 4.8, was prepared by making a solution comprising of 0.07 M sodium acetate and 0.03 M acetic acid. A gram of the activated carbon was then weighed using an electronic balance and transferred into a 250 mL Erlenmeyer flask, thereafter a measuring cylinder was used to transfer 100 mL of the prepared acetate buffer into the flask with the carbon. An 8*22 mm magnetic stirring bar was added to the flask and parafilm was placed at the mouth of the flask to prevent spillage. The flask was placed on a magnetic stirrer at medium high speed and left stirring for 24 hours at room temperature.

After the 24 hour period the mixture was filtered through a 300 μm sieve. The mixture was washed with 200 mL of distilled water. The carbon retained on the sieve was quantitatively transferred to a preweighed ceramic pan using a spatula. The pan was placed in an oven set at 105 ± 5 °C for 2 hours to dry the carbon.

After the 2 hour period, the pan and its contents were placed in a desiccator to cool, then the final weight was measured using an electronic balance. The materials and apparatus for the procedure are displayed in Table 3.8. The procedure was replicated at least twice, and the average value was recorded.

Calculation:

$$\% \, Attrition = \frac{initial\ weight - \ final\ weight}{initial\ weight} \times 100 \qquad (3.12)$$

Where:

Initial weight = weight of carbon measured for the test, g.

Final weight = dry weight (ceramic pan + activated carbon) - weight of the empty ceramic pan, g.

Table 3.8 Materials and apparatus for the attrition test

Materials and apparatus:
Activated carbon
Mettler Toledo® electronic balance accuracy ± 0.0001g
Mettler Toledo® pH meter
250 mL volumetric flasks
0.07 M sodium acetate–0.03M acetic acid buffer of pH 4.8
8*22 mm magnetic stirrer bar
100 mL measuring cylinder
Distilled water
Mesh sieve 45 mesh (300 um)
Ceramic pan
Forced circulation oven set at 105 ± 5 °C

3.3.6 Bulk Density

The method used in this study was adapted from the method by the American Society for Testing and Materials (ASTM D2854 - 96, 2000) . The bulk density, which is also referred to as the apparent density can be defined as the mass to volume ratio of an activated carbon sample in air. This includes the pore system and the spaces among the particles. This parameter is useful for the estimation of the packing volume which is an essential feature when designing vessels to hold the material. Its unit of expression is g/mL (ASTM D2854 - 96, 2000).

Procedure:

A graduated 100 mL cylinder containing a glass funnel (100 mm top inside diameter) was placed on an electronic balance and tarred. A dried sample of activated carbon was passed through the glass funnel and allowed to fall freely into the graduated cylinder until it reached at least 50 % capacity of the cylinder.

The unsettled volume of the carbon was read, and its weight noted down. The procedure was replicated at least twice, and the average value was recorded. The materials and apparatus used in this procedure are shown in Table 3.9.

Calculation:

$$D_b = \frac{m}{V_o} \tag{3.13}$$

Where:

D_b = bulk density, g/mL.

m = mass of activated carbon, g.

V_o = volume occupied by activated carbon, mL.

Table 3.9 Materials and apparatus for the bulk density test

Materials and apparatus:
Activated carbon
Glass funnel, 100 mm top inside diameter
100 mL graduated cylinder
UWE (ADW-SA 1353) Electronic balance ± 0.001g

3.3.7 pH

The term pH relates to the intensity of the acidity or basicity of a material. The method adopted in this study was published by (Singh *et al.*, 2017).

Procedure:

Carbon was ground to less than 2 mm and air dried using the method in 3.3.1. Thereafter, 1 gram of the carbon was weighed into a 100 mL Erlenmeyer flask and 10 mL of deionized water was pipetted into the flask. The mouth of the flask was closed with parafilm, and the contents were shaken well by hand and then placed on an orbital shaker for one hour at ambient temperature. After the hour elapsed, the suspension was left to stand for 30 minutes. The pH meter was calibrated, and the pH of the suspension was measured. The pH value was recorded after stabilization of the meter reading. The pH measurements were replicated at least twice, and the average value was recorded. The materials and apparatus for the procedure are shown in Table 3.10.

Table 3.10 Materials and apparatus for the pH test

Materials and apparatus:
Activated carbon
Mettler Toledo® seven compact pH/ion meter with glass–calomel electrodes
Deionized water
100 mL centrifuge tubes or bottles
10 mL pipette
Standard buffers (pH 4, 7 and 10)
MRC orbital shaker

3.3.8 Brunauer-Emmett-Teller (BET) Surface Area Analysis

The carbon was dried as per the moisture content procedure detailed in 3.3.1. Thereafter, an empty glass round bottom cell with a glass rod and glass cap was weighed and the value was recorded, between 0.10 and 0.12 g of the activated carbon was measured and placed at the bottom of the empty cell then the rod and cap were added. The cell containing the sample was then submitted for testing and the surface area of the sample was obtained using the Micromeritics ASAP 2020 surface area analyzer. The surface area is measured in m^2/g.

3.4 Analytical Techniques

Analytical techniques such as scanning electron microscopy (SEM), Fourier-transform infrared spectroscopy (FTIR), energy dispersive X-ray spectroscopy (EDS), Raman spectroscopy, thermogravimetric analysis (TGA), and Brunauer-Emmett-Teller (BET) are employed to determine the surface properties and thermal stability of activated carbons. An overview of the techniques is given in sections 3.4.1 - 3.4.3.

3.4.1 Fourier-transform Infrared (FTIR) Spectroscopy

Fourier transform infrared (FTIR) spectroscopy experiments were performed on a FT-IR-Perkin Elmer 2 in a 400 to 4000 cm^{-1} wavelength interval, with 10 scans per sample.

A mortar and pestle were cleaned using acetone and set aside. A substantial amount of potassium bromide (KBr) was added to a clean crucible and dried in the oven for an hour at 100 °C and placed in a desiccator. Thereafter, the KBr was transferred to the mortar and ground to a fine powder. An amount of the

ground KBr was then transferred to a stainless steel metal disk with a cutout hole which was placed on top of another solid stainless disk to prevent loss of the sample a third stainless steel disk with an impression was placed on top of the other two, forming a sandwich which was then carefully placed onto a hand press. The handle of the press was pumped to press the disks together so that a pellet could be formed. The press was left for a few seconds and then the pressure was released. The disk with a cutout hole was carefully removed to reveal a transparent pellet. The disk was inserted into the machines sample holder and the background was run and the absorbance data was obtained in the wave number range of 400-4000 cm^{-1} with a scan rate of 0.2 cm s^{-1}.

A carbon sample was dried to remove moisture in accordance with the method outlined in Section 3.3.1. The carbon was placed in a clean mortar and ground to a fine powder, the carbon was homogeneously mixed with the KBr at a ratio of 1:100 mg, respectively. The mixture was compressed in the hand press following the steps used before running the background using KBr, and the spectrum was recorded in the same spectral range as the background.

The major functional groups of activated carbons based on the assignment of wave numbers from FTIR analysis are summarized in Table 3.11, and were used to assign the peaks on the three activated carbons (GAC, AW-AC, and HC-AC).

Table 3.11 Assignments of Functional Groups on Carbon Surfaces (Shen, Li and Liu, 2012)

Group or functionality	Assignment regions (cm^{-1})	Group or functionality	Assignment regions (cm^{-1})
C-O in ethers (stretching)	1000-1300	Carboxylic anhydrides	980-1300, 1740-1880
Alcohols	1049-1276, 3200-3640	C-H (stretching)	2600-3000
–C-OH (stretching)	1000-1220	N-H, C=N	1560-1570
O-H	1160-1200, 2500-3620	Cyclic amides	646,1461, 1546,1685
Carbonates; carboxyl-carbonates	1100-1500, 1590-1600	C-N aromatic ring	1000, 1250, 1355
–C-C aromatic (stretching)	1585-1600	C-N	1190
Quinones	1550-1680	C=C=N	2070-2040
Carboxylic acids	1120-1200, 1665-1760, 2500-3300	N-O-	1300-1000
Lactones	1160-1370, 1675-1790		

3.4.2 Scanning Electron Microscopy (SEM), Energy Dispersive Spectroscopy (EDS) and Raman Spectroscopy

A small amount of the sample was put on an aluminum stub covered with carbon tape. The stub was then carbon coated in an evaporation coater and the sample was examined in the scanning electron microscope. The elemental analysis was carried out in the Nova NanoSEM using an Oxford X-Max detector and Inca software. The images were taken with the Tescan MiraSEM. Raman spectra were collected using the 532 nm laser and 100x objective.

3.4.3 Thermogravimetric Analysis (TGA)

The Discovery SDT 650 was used to carry out the thermogravimetric analysis. The sample was placed in a 90 μL alumina pan and heated from room temperature up to 700 °C at 3 °V/min in an N_2 environment and kept at 700 °C for 15 minutes.

3.5 Adsorption Experiments

Batch experiments were performed to ascertain and compare the adsorptive capacity of the three activated carbons (GAC, AW-AC and HC-AC) for the removal of cationic dyes and heavy metals from aqueous solution. This was done by varying one factor at a time while the rest remained fixed, so as to investigate the effect of each factor independently on the adsorption process, and to find the optimal working conditions for each adsorbent. The three adsorbents were used in batch studies to assess their performance in the removal of the following micropollutants from solution:

- Methylene blue ($C_{16}H_{18}ClN_3S$)
- Lead ($Pb(NO_3)_2$)

Overall, the experiments were carried out at a room temperature of 23 ± 1 °C. Reagents used were of analytical grade, and the stock solutions were prepared using high-purity Milli-Q water. The stock solutions were further diluted with deionized water to obtain the working concentrations in the adsorption studies.

The pH of the working solutions was adjusted to the desired value using drops of prepared 0.1 M hydrochloric acid (HCL) and sodium hydroxide (NaOH) solutions. The adsorbent and solution mixtures were filtered through 0.45μm syringe filters (Whatman®), and the filtrates obtained were analyzed to determine the residual concentrations of the working solutions. Ultraviolet-

visible spectroscopy (Equipment product classification: GBC UV-VIS 920) was used to determine the concentration of the methylene blue dye stock and filtrate solutions. The spectrophotometer was set at a wavelength of 663nm. Inductively coupled plasma optical emission spectroscopy (Equipment product classification: Varian 710 ICP-OES) was used to determine the concentration of lead (II) ions in the stock and filtrate solutions.

The concentration of the adsorbate adsorbed was considered as being the difference between the initial and final concentration of the working solutions. At least two replicates were run in parallel for each experiment and the average values were used for further calculations.

Preparation of Solutions:

Hydrochloric Acid (HCL) - The stock solution of hydrochloric acid was calculated to be 12.178 M based on a density of 1.2 g/mL, a formula weight of 36.46 g/mol, and a concentration of 37 % w/w. To make the 0.1 M solution, 0.821 mL of the stock solution was pipetted and slowly added to 25 mL of deionized water in a beaker. The solution was then quantitatively transferred to a volumetric flask and the final volume of solution was adjusted to 100 mL with deionized water.

Sodium Hydroxide (NaOH) - The stock solution of sodium hydroxide was calculated to be 18.938 M based on a density of 1.515 g/mL, a formula weight of 40 g/mol, and a concentration of 50 % w/w. To make the 0.01 M solution, 0.528 mL of the stock solution was pipetted and slowly added to 25 mL of deionized water in a beaker then quantitatively transferred to a volumetric flask and the final volume of solution was adjusted to 100 mL with deionized water.

Methylene blue ($C_{16}H_{18}ClN_3S$) – To make a 1000 mg/L methylene blue solution, 1g of methylene blue was weighed and dissolved in 100 mL of deionized water in a beaker then quantitatively transferred to a volumetric flask and the final volume of solution was adjusted to 1 L with deionized water. A magnetic stirrer was added, and the solution was stirred for 4 hours to make sure that the methylene blue was fully dissolved. The flask was covered with foil to ensure that no photodegradation of the dye took place. Stirring and further tests were carried out in a dark room with a torch.

Lead in the form of ($Pb(NO_3)_2$) – The molar mass of $Pb(NO_3)_2$ is 331.2 g/mol and the molar mass of lead (Pb) is 207.19 g/mol. That is to say 331.2 g of $Pb(NO_3)_2$ contains 207.19 g of lead. To make a 1000 mg/L lead solution, 1.6 g of lead nitrate was weighed and dissolved in 100 mL of deionized water in a beaker then quantitatively transferred to a volumetric flask and the final volume of solution was adjusted to 1 L with deionized water.

Procedure:

A typical adsorption experiment was carried out as follows: a volume of solution adjusted to the working pH was added to a conical flask containing the adsorbent .The mixture was placed on an MRC rotary shaker set at 150 rpm for a prescribed period of time. Thereafter, the mixture was filtered through a 0.45 μm syringe filter and analyzed to obtain the residual concentration of the adsorbate left in solution.

- For methylene blue: the absorbance before and after adsorption was measured using an Ultraviolet visible spectrophotometer (GBC UV-VIS 920) at a wavelength of 663nm. A narrow width quarts cuvette with dark walls was used

for analysis of the samples. The resultant concentration was calculated using the equation obtained from the calibration curve.

- For Lead: the concentration was measured using inductively coupled plasma atomic emission spectroscopy (Varian 710 ICP-OES), which employs the use of a torch and has a nebulizer to generate an argon plasma. The instrument was calibrated with a blank and 1, 5, 10, and 100 ppm LGC 1586 spectra scan multi element standard. The samples were analyzed three times and the average reading was taken using a 10 % deviation
  - The percentage removal and removal capacity were obtained using the following equations.

Calculations:

$$\% \, Removal = \frac{C_0 - C_t}{C_0} \times 100 \tag{3.14}$$

$$q_t = \frac{(C_0 - C_t)V}{W} \tag{3.15}$$

Where:

Co = the initial solution concentration, mg/L,

Ct = the solution concentration at time t, mg/L,

V = volume in mL, and

W = weight of the adsorbent, mg.

3.5.1 Methylene Blue Adsorption Experiments

Step 1: Effect of Time and Initial Concentration

The procedures for the kinetic experiments were essentially identical to those of the equilibrium tests. Methylene blue solutions with varied initial concentrations were prepared from the stock solution using the dilution calculator ($C_1V_1 = C_2V_2$). The batch adsorption experiments were carried out in a series of 200 mL conical flasks, each with 100 mL methylene blue solutions with varied initial concentrations (2.5, 5, and 7.5 mg/L) at a pH of 6.5. Equal masses of the adsorbent (0.2g) were added to the individual flasks placed on the orbital shaker and the methylene blue solutions were added. The flasks containing the mixtures were closed with parafilm, covered with foil paper and placed on an orbital shaker set at 150 rpm. At predetermined time intervals, 2 mL of solution was withdrawn from the mixture using a syringe with a needle to minimize the removal of the adsorbent from the flask. The retrieved samples were filtered using a 0.45 μm syringe filter and analyzed using the UV-VIS spectrophotometer. Samples were withdrawn and tested until there was not much significant difference in the results signifying equilibrium. The concentration which showed the highest removal capacity was chosen as the optimum concentration and was maintained in the following experiments. The time at which equilibrium was observed was the time the following investigative tests were carried out. Parameters for this test are displayed in Table 3.12.

Table 3.12 Parameters for the methylene blue contact time and initial concentration test

		Adsorbents		
		GAC	**AW-AC**	**HC-AC**
Fixed parameters	Carbon dosage (g)	0.2	0.2	0.2
	pH	6.5	6.5	6.5
	Volume (mL)	100	100	100
Varied parameters	Concentration (mg/L)	2.5-5-7.5	2.5-5-7.5	2.5-5-7.5
	Time (min)	5-370	5-370	5-370

Step 2: Effect of pH

The determination of the optimum pH for the adsorption process was investigated as follows: 30 mL solutions of the optimized methylene blue concentration determined in step 1 were added to 100 mL conical flasks containing a fixed amount of adsorbent (0.06g). The pH of the solutions was varied between 2 and 11 using the prepared 0.1 M HCL and NaOH solutions. The flasks containing the mixtures were closed with parafilm, covered with foil paper and placed on an orbital shaker and agitated at a rate of 150 rpm until the equilibrium time had been reached. Once the equilibrium time was reached a sample was retrieved from each flask using a syringe and the sample was filtered using a 0.45 μm syringe filter and analyzed using the UV-VIS spectrophotometer. The percentage removal was calculated using Equation 3.14 and the optimum pH was chosen and maintained in the following experiments. Parameters for this test are displayed in Table 3.13.

Table 3.13 Parameters for the methylene blue pH test

		Adsorbents		
		GAC	**AW-AC**	**HC-AC**
Fixed parameters	Carbon dosage (g)	0.06	0.06	0.06
	Concentration (mg/L)	optimum	optimum	optimum
	Volume (mL)	30	30	30
	Time (min)	equilibrium	equilibrium	equilibrium
Varied parameters	pH	2-3-4-…11	2-3-4-…11	2-3-4-…11

Step 3: Effect of Adsorbent Dosage

The optimum dosage of the adsorbents was determined by fixing the following parameters: contact time, initial adsorbate concentration, pH, and the volume of solution (as can be seen in Table 3.14) and varying the amount of adsorbent in each flask. The adsorbent dosage was varied within a range of 0.03 g and 0.3 g. The flasks were covered in parafilm and covered with foil. After the equilibrium time was reached, samples were withdrawn from the mixtures in each flask using a syringe and the samples were filtered using a 0.45 μm syringe filter and analyzed using the UV-VIS spectrophotometer. The percentage removal was calculated using Equation 3.14 and the optimum adsorbent dosage was chosen and maintained in the following experiments.

Table 3.14 Parameters for the methylene blue dosage test

		Adsorbents		
		GAC	**AW-AC**	**HC-AC**
Fixed parameters	pH	optimum	optimum	optimum
	Concentration (mg/L)	optimum	optimum	optimum
	Volume (mL)	30	30	30
	Time (min)	equilibrium	equilibrium	equilibrium
Varied parameters	Adsorption dosage (g)	0.03-0.3	0.03-0.3	0.03-0.3

3.5.2 Lead Adsorption Experiments

Working concentrations were prepared for the adsorption tests by diluting the prepared stock solution containing the lead (II) ions with deionized water. The concentrations of the solutions were obtained by ICP-OES.

Step 1: Effect of pH

The determination of the optimum pH for the adsorption process was investigated as follows: a fixed amount of adsorbent (0.06g) was added to 100 mL conical flasks containing 30 mL solutions with a concentration of 5.3 mg/L. The pH of the solutions was varied between 2 and 8 using the prepared 0.1 M HCL and NaOH solutions. The flasks containing the mixtures were covered with parafilm and placed on an orbital shaker and agitated at a rate of 150 rpm for 120 minutes. Once the 120 minutes had elapsed, a sample was retrieved from each flask using a syringe and the sample was filtered using a 0.45 μm syringe filter and analyzed using ICP-OES. The removal percentages were calculated

using Equation 3.14, and the optimum pH value was chosen and maintained in the following experiments. The parameters for this test are displayed in Table 3.15.

Table 3.15 Parameters for the lead pH test

		Adsorbents		
		GAC	**AW-AC**	**HC-AC**
Fixed parameters	Adsorbent dosage (g)	0.06	0.06	0.06
	Concentration (mg/L)	5.3	5.3	5.3
	Volume (ml)	30	30	30
	Time (min)	120	120	120
Varied parameters	pH	2-3-4-5-6-7-8	2-3-4-5-6-7-8	2-3-4-5-6-7-8

Step 2: Effect of Adsorbent Dosage

The optimum dosage of the adsorbents was determined by fixing the following parameters; contact time, initial adsorbate concentration, pH, and the volume of solution as can be seen in Table 3.16. The amount of adsorbent in each flask was varied within a range of 0.03 g and 0.3 g. The flasks were closed with parafilm and agitated at 150 rpm for 120 minutes. Once the 120 minutes had elapsed, a sample was retrieved from each flask using a syringe and the sample was filtered using a 0.45 μm syringe filter and analyzed using ICP-OES. The percentage removal was calculated using Equation 3.14 and the optimum adsorbent dosage was chosen and maintained in the following experiments.

Table 3.16 Parameters for the lead adsorbent dosage test

		Adsorbents		
		GAC	**AW-AC**	**HC-AC**
Fixed parameters	pH	optimum	optimum	optimum
	Concentration (mg/L)	5.3	5.3	5.3
	Volume (ml)	30	30	30
	Time (min)	120	120	120
Varied parameters	Adsorbent dosage (g)	0.03-0.3	0.03-0.3	0.03-0.3

Step 3: Effect of Initial Concentration

The optimum concentration was investigated as follows; a series of 100 mL conical flasks was set up, each contained 30 mL lead solutions with varied initial concentrations ranging from 1.9-14.3 mg/L at the optimum pH detemined in step 1. Equal masses of the optimum dosage of the adsorbent were added to the individual flasks containing the lead solutions. The flasks containing the mixtures were closed using parafilm and placed on an orbital shaker set at 150 rpm. Once a period of 120 minutes had elapsed, samples were withdrawn from the mixture using a syringe. The retrived samples were filtered using a 0.45 μm syringe filter and analyzed using ICP-OES. The concentration which exhibited the highest percentage removal as calculated using Equation 3.14 was chosen as the optimum and was adopted in the equilibrium studies that were carried out in the following test. Parameters used in this test are displayed in Table 3.17.

Table 3.17 Parameters for the lead initial concentration test

		Adsorbents		
		GAC	**AW-AC**	**HC-AC**
Fixed parameters	pH	optimum	optimum	optimum
	Adsorbent dosage (g)	optimum	optimum	optimum
	Volume (mL)	30	30	30
	Time (min)	120	120	120
Varied parameters	Concentration (mg/L)	1.9-14.3	1.9-14.3	1.9-14.3

Step 4: Effect of Contact Time

The batch adsorption experiments were carried out in a series of 200 mL conical flasks. Each flask contained a mixture consisting of 100 mL of solution containing the lead (II) ions at the optimum concentration determined in step 3 and equal masses of the optimum adsorbent dosage determined in step 2. The solution pH was adjusted to the optimum value determined in step 1 .The solutions were added to the flasks which were already on the orbital shaker and obtained the adsorbent. The mixtures were closed using parafilm. The orbital shaker was set at 150 rpm. At predetermined intervals, 5 mL of sample was withdrawn from the mixture using syringe with a needle to minimize the removal of the adsorbent from the flask. The retrieved samples were filtered using a 0.45 μm syringe filter and analyzed using ICP-OES. Samples were withdrawn and tested until there was not much significant difference in the results signifying equilibrium. The percentage removal of each adsorbent was calculated using Equation 3.14.

3.6 Kinetics and Isotherms Studies

Kinetic studies were carried out as per the equations for the pseudo-first order and pseudo-second order equations presented in Table 2.2 of the literature review section. The Freundlich and Langmuir isotherms were used to analyze the experimental data using the equations found in Table 2.3 of the literature review section.

3.7 Closure

The experimental methodology for this study, from the preparation of the hydrochar derived activated carbon, the characterization of activated carbons, and the adsorption of methylene blue dye and lead (II) ions onto the activated carbons was discussed in this chapter. Results obtained from the experimental methodology are reported and discussed in Chapter 4.

Chapter 4 Results and Discussions

4.1 Introduction

The significance of this chapter is to explore how the various characteristics of the activated carbons, aqueous solutions, as well as other external factors affect the adsorption capacity of the activated carbons when removing pollutants from aqueous solution, and therefore, determine the optimum conditions for the adsorption of micropollutants in their aqueous phase onto the activated carbons.

The results in this study have been divided into 3 sections:

Section 1: production of activated carbon from hydrochar.

Section 2: characterization of activated carbons.

Section 3: optimization of adsorption experiments for methylene blue dye and lead (II) ions, and kinetic and isotherm studies.

4.2 Production of Activated Carbon from Hydrochar

4.2.1 Thermogravimetric Analysis

Thermogravimetric analysis was carried out on the hydrochar produced from primary sludge combined with waste activated sludge (HC-PS-WAS) (the precursor of the hydrochar derived activated carbon (HC-AC)) to ascertain its thermal stability and to determine the optimum temperature to pryolyze at to attain a substantial carbon yield. Figure 4.1 depicts the thermogram of HC-PS-WAS.

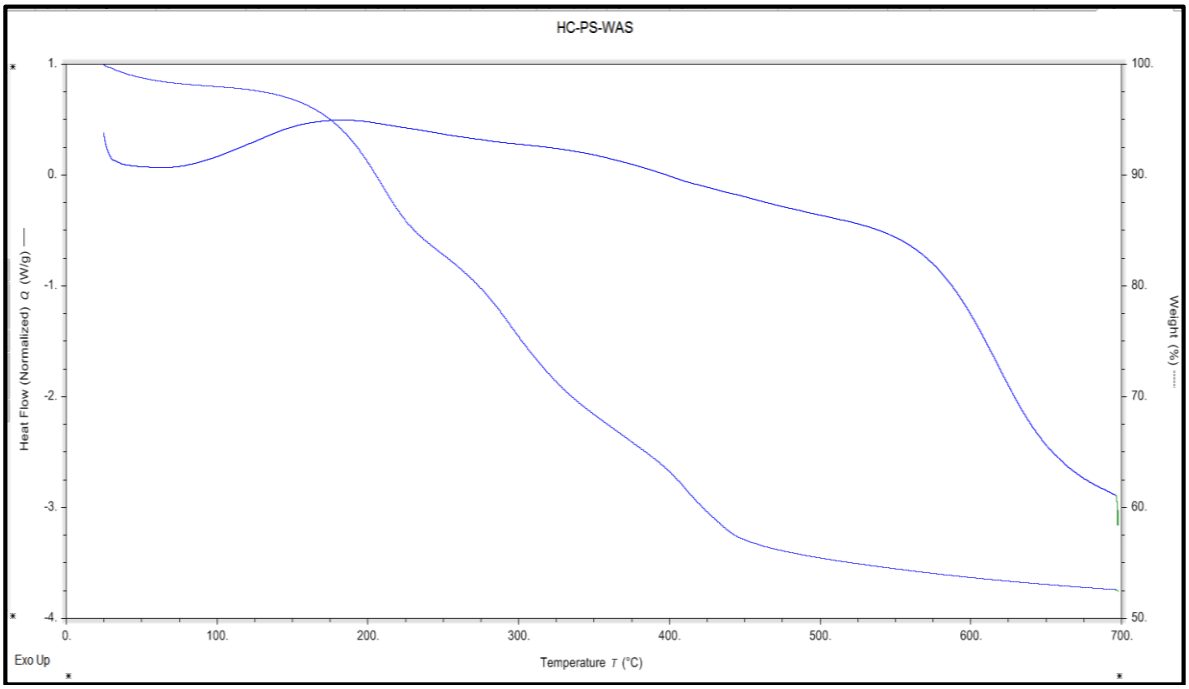

Figure 4.1 Thermogram of HC-PS-WAS

Three distinct steps can be observed from the temporal derivative mass curve in Figure 4.1, the first from 25 – 175 °C, a steep drop from 200 – 450 °C, followed by a moderate decline from 450 °C with the plot becoming constant towards 700 °C. The initial step between 25 °C and 175 °C shows a weight loss of about 6.5 % and can be ascribed to the release of moisture and volatile matter, the sharp decline and drastic weight loss of about 41 % between 200 °C and 450 °C is attributed to the decomposition of proteins and low molecular weight polymers. The third and last step, showed loss in weight of about 2.5 % that continued to 700 °C. It resulted from further decomposition of the char and formation of ash (De Filippis *et al.*, 2013).

4.2.2 Pyrolysis

From the TGA curve in Figure 4.1 three temperatures were chosen and investigated for the production of activated carbon. The calculations for the percentage weight loss and yield results were calculated using Equations 3.1 and 3.2, and the results obtained are displayed in Table 4.1.

Table 4.1 Percentage weight loss and yield

Pyrolysis temperature (°C)	175	425	600
Weight loss (%)	7.04	43.35	50.81
Yield (%)	91.08	56.65	49.19

Figure 4.2 shows; a) the hydrochar before annealing, b) the annealed product at 175 °C, c) the annealed product at 425 °C, and d) the annealed product at 600°C.

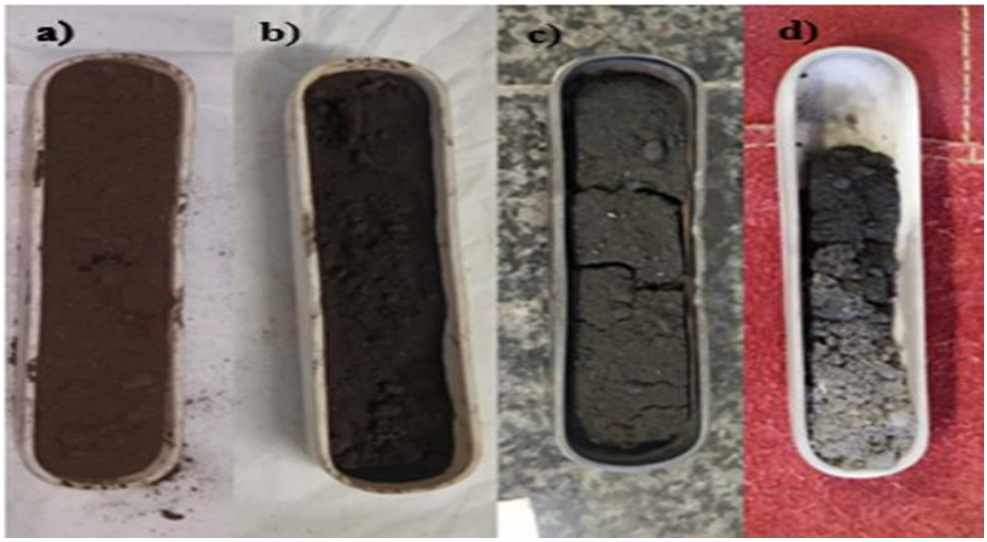

Figure 4.2 (a) HC-PS-WAS, (b) HC-AC (175°C), (c) HC-AC (425°C), (d) HC-AC (600°C)

Of the three temperatures, the pyrolyzed product at 600 °C had the lowest carbon yield (49.19%) and it showed signs of ashing, as a result it was excluded from any further investigation. Though the pyrolyzed product at 175 °C had a high carbon yield (91.1%) when compared to that at 425 °C (56.7%), the product resulting from pyrolysis at 425 °C was chosen as the best and the one to be used for the adsorption tests as it had a higher BET surface area and iodine number (97.20 mg^2/g and 110.66 mg/g) when compared to that at 175 °C (88 mg^2/g and 73.50 mg/g). The pyrolyzed product at 425 °C is referred to as hydrochar derived activated carbon (HC-AC) going forward.

4.3 Characterization of Activated Carbon

Prior to the adsorption studies, characterization tests were carried out on the three activated carbons (GAC, AW-AC and HC-AC) to determine; moisture content, ash content, surface area, bulk density, particle size, pH, chemical composition, surface morphology, iodine number, functional groups, and particle size as per the methods outlined in the experimental details. Results attained from these tests are briefly discussed and depicted in Table 4.2 and Figure 4.3-Figure 4.6.

Table 4.2 Properties of adsorbents

Properties	GAC	AW-AC	HC-AC
Moisture content (%)	3.78	7.86	3.36
Iodine number (mg/g)	1198.48	265.53	110.66
Surface area (BET N_2) (m^2/g)	1050[a]	108.78	97.20
Particle size (µm)	850-1180	850-1180	75-150
Attrition (%)	32	60	-
Bulk density (g/cm^3)	0.48	0.38	0.31
Ash content (%)	2.4	2.7	62.8
pH	5.1	7	2.6

[a] value from supplier, - test not conducted

4.3.1 Moisture Content (%):

Of the three activated carbons GAC and HC-AC had the lowest moisture content (3.8 and 3.4 %, respectively). The AW-AC had the highest moisture content (7.86 %), which is characteristic of activated carbons produced from lignocellulosic materials (Gad, El-Mouhty and Aly, 2009; Hoon and Cheok, 2013; Waji, 2018). Having a high moisture content has been linked with a reduction of the adsorptive capacity in activated carbons (Jeyakumar and Chandrasekaran, 2014; Zulkania, Hanum and Sri Rezki, 2018; Jawing *et al.*, 2021). The moisture content of the three activated carbons is less than 8 %, which is ideal for an activated carbon as stated in the requirements by the American Water Works Association (AWWA) (Comm Rep, 1974).

4.3.2 Iodine Number

The iodine number is a procedure used to measure the microporocity of activated carbon and to indicate the surface area with good precision, it is also used as a measure of the activation level of an adsorbent (Saka, 2012). The American Society for Testing and Materials (ASTM D4607-94, 2006) procedure defines it as the amount of iodine adsorbed in milligrams per gram of carbon at a residual iodine concentration of 0.02 N. The iodine number values obtained for the three adsorbents are shown in Table 4.2. The iodine numbers obtained for GAC, AW-AC and HC-AC were, 1198.4, 265.53, and 110.66 mg/g respectively. The iodine number of GAC is within the range of 500-1200mg/g which is indicative of a high degree of activation (Saka, 2012). Applying the same measure, it can be said that AW-AC and HC-AC have a low level of activation. Though the relationship between the iodine number and the surface area cannot be generalized as per the American Society for Testing and Materials (ASTM D4607-94, 2006) procedure, the results obtained support the BET results which show that the surface area of the adsorbents is in the order of GAC > AW-AC > HC-AC.

4.3.3 Ash Content and Surface Area

When compared with HC-AC which has a high ash content (62.8 %) and a low surface area (97 m^2/g), GAC and AW-AC have significantly lower ash contents, (2.4 % and 2.7 %, respectively) and higher surface areas (1050 and 108.76 m^2/g, respectively). The link between high ash content and low surface area has been vastly discussed in literature and has been mainly attributed to the blockage of pores by the ash (Abdul Halim Abdullah, Anuar Kassim, Zulkarnain Zainal, Mohd Zobir Hussien, Dzulkefly Kuang, 2001; Hoon and Cheok, 2013; Ntuli and

Hapazari, 2013; RShashankVRaman, 2015; Sajjadi, Chen and Egiebor, 2019; Bernardo *et al.*, 2020; Jawing *et al.*, 2021; Mkungunugwa *et al.*, 2021). The high ash content values for HC-AC in this study are fairly comparable to values reported in literature for sludge derived adsorbents (Rengaraj *et al.*, 2002; Smith *et al.*, 2009; Pedroza *et al.*, 2014; Almahbashi *et al.*, 2021). (Mkungunugwa *et al.*, 2021) also reported a correlation between high ash content and low carbon content which is supported by the EDS spectra results shown in Figure 4.5.

4.3.4 pH

The pH of the adsorbents was carried out and it was found that AW-AC had the highest pH value of 7, followed by GAC with a pH of 5.1 and lastly HC-AC with a low pH of 2.6. Most activated carbons found in literature have alkaline pH values as a result of washing with deionized water after activation and carbonization to neutralize the pH (Hameed, Din and Ahmad, 2007; Ebrahimian Pirbazari *et al.*, 2014). The extremely low pH value of HC-AC could be attributed to the fact that it was not washed after carbonization. The presence of the sharp peak at 1102 cm^{-1} on the FT-IR spectrum of HC-AC as shown in Figure 4.6 is indicative of an oxygen containing acidic surface functional group (carboxyl group) (Shen, Li and Liu, 2012) which could have contributed to the low pH value obtained (Chen, Jeyaseelan and Graham, 2002).

4.3.5 Bulk Density

The bulk density is an important parameter of activated carbon which is used to determine the volume capacity of a carbon, a high density is generally associated with a carbons ability to hold more adsorbate per unit volume during adsorption (Asuquo *et al.*, 2017; Ravichandran *et al.*, 2018). The bulk density

values of GAC, AW-AC, and HC-AC are 0.48, 0.38 and 0.31 g/cm3, respectively. The American Water Work Association (AWWA, 1991) has set a lower limit of 0.25 g/mL for activated carbon to be of practical use (Qureshi *et al.*, 2008; Yakout *et al.*, 2015; Ravichandran *et al.*, 2018) and all three carbons have bulk density values above this meaning it is acceptable to use them for the treatment of wastewater. The bulk density of a carbon is highly dependent on its precursor and the treatment method used (Chowdhury, 2013). Adsorbents derived from woody biomass have been reported as having higher bulk densities when compared to urban and industrial solid wastes such as sludge (Tomczyk, 2020). However, having a bulk density below 1.2 g/cm^3 has been reported as being indicative of an adsorbents small particle size which improves its adsorption capacity (Moyo *et al.*, 2013; Guyo and Moyo, 2017).

4.3.6 Attrition

Resistance to attrition is among the parameters of importance considered when selecting granular adsorbents for wastewater treatment (Dąbrowski, 2001) as it gives useful information regarding the carbons mechanical strength and ability to resist disintegration during transportation, normal handling, and regeneration (Ravichandran *et al.*, 2018). Due to the nature of the particles of granular carbons and their applications, there is a high possibility of intraparticle abrasion (Toles *et al.*, 2000) which could lead to the formation of fine particles associated with low attrition resistance (high losses) which can result in the blockage of systems (Asuquo *et al.*, 2017). The attrition test was only performed on GAC and AW-AC as the particles of HC-AC are generally in powdered form (fine in nature) and it would be difficult to determine loss on attrition accurately. From the results in Table 4.2 it can be seen that GAC exhibits lower loss due to attrition

(32%) when compared to AW-AC (60%). The result of AW-AC is characteristic of carbons derived from high cellulose biomass which has a tendency to be brittle (Jjagwe *et al.*, 2021), thus having a higher attrition value. This supports the notion that the precursor of a carbon has a direct effect on the carbons attrition resistance (Ravichandran *et al.*, 2018). The results from this study also support the report by (Toles *et al.*, 2000) that there is a link between density and attrition, stating that carbons with a lower density tend to exhibit higher attrition. This is the case with AW-AC which has a lower bulk density (0.38 g/cm^3) than GAC (0.48 g/cm^3) and a higher attrition value of 60 % when compared to the 32 % recorded for GAC.

4.3.7 Particle Size

The particle size of the adsorbents was found by using the sieves method as per the procedure outlined in Section 3.3.4. Sieves with openings ranging from 425 to 2360 μm were used to determine which sieves would have the largest retention of GAC when 100 g was placed on the top sieve. It was found that 91.6 % of the carbon was retained on the 850 and 1180 μm sieves collectively therefore, this portion was used for all tests. The carbon AW-AC was received in large chunks of varying sizes, for better handling and comparison it was crushed to form granules and the particles retained on the sieves 850 and 1180 μm were used for testing. The particle size of HC-AC was determined using sieves ranging from 45 to 150 μm, 99.8 % of the carbon was retained on the 75 and 150 μm sieves collectively and this portion was used for testing.

4.3.8 Scanning Electron Microscopy (SEM)

The scanning electron micrographs of the three carbons GAC, AW-AC, and HC-AC depicted in Figure 4.3 were carried out at three different magnifications, 500, 5kX, and 50kX at a scale of 1, 10, and 100 μm. The micrographs of GAC show a rough surface with numerous crevices and pores present for possible dye and metal adsorption. High surface roughness and macro porosity (>50nm) are important factors for adsorption and can be attributed for GACs' high surface area, making it a good adsorbent (Mansour et al., 2020). The surface of AW-AC is composed of well-developed tunnel shaped pores characteristic of wood based activated carbons (Yorgun and Yildiz, 2015). That being said the micrographs also shows a substantial amount of breakage of these tunnels which may affect its adsorptive capacity. The hydrochar derived carbon, HC-AC is characterized by a rough, uneven, fibrous surface with a wide variety of loose pores of different sizes that resemble canals. Similar micrographs were reported in studies dealing with sludge derived activated carbons (Li, Yue, Gao, Ma, et al., 2011; Pradhan, 2011; Oumabady et al., 2021).

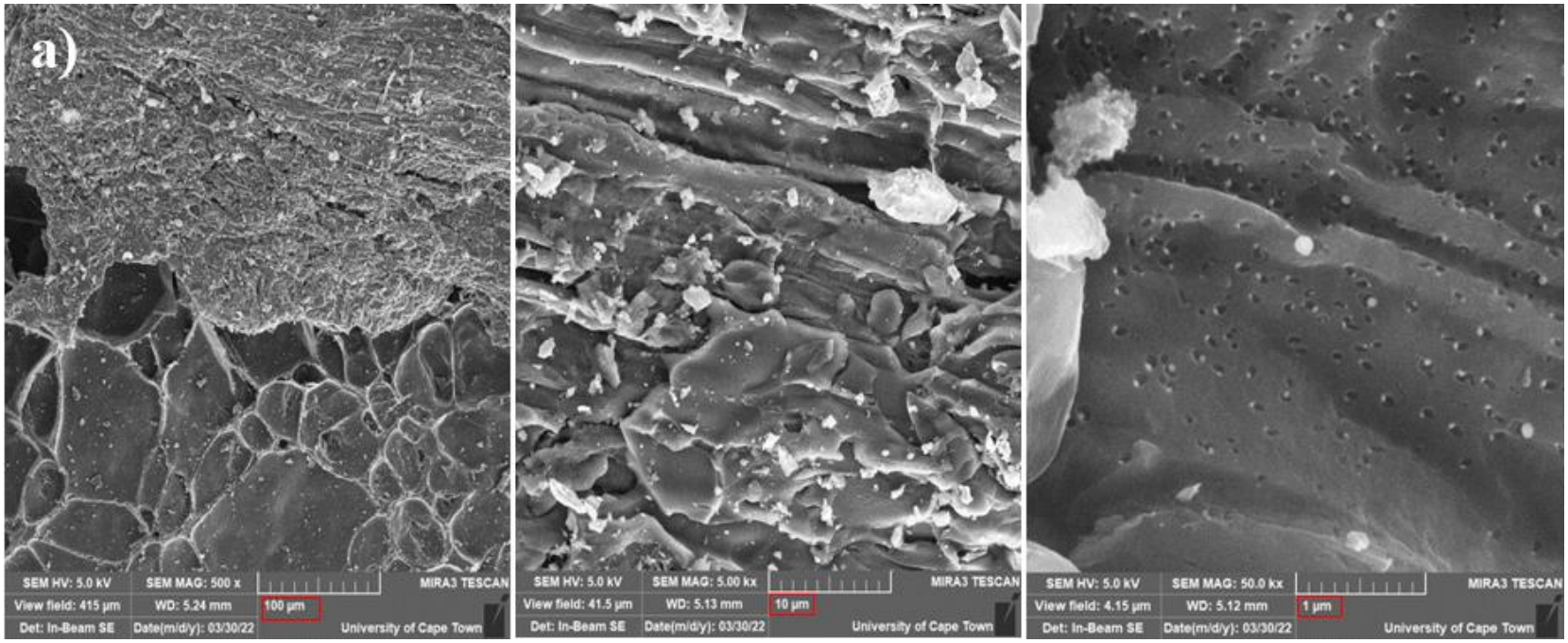
a)
SEM HV: 5.0 kV
SEM MAG: 500 x
MIRA3 TESCAN
View field: 415 µm
WD: 5.24 mm
100 µm
Det: In-Beam SE
Date(m/d/y): 03/30/22
University of Cape Town
SEM HV: 5.0 kV
SEM MAG: 5.00 kx
MIRA3 TESCAN
View field: 41.5 µm
WD: 5.13 mm
10 µm
Det: In-Beam SE
Date(m/d/y): 03/30/22
University of Cape Town
SEM HV: 5.0 kV
SEM MAG: 50.0 kx
MIRA3 TESCAN
View field: 4.15 µm
WD: 5.12 mm
1 µm
Det: In-Beam SE
Date(m/d/y): 03/30/22
University of Cape Town

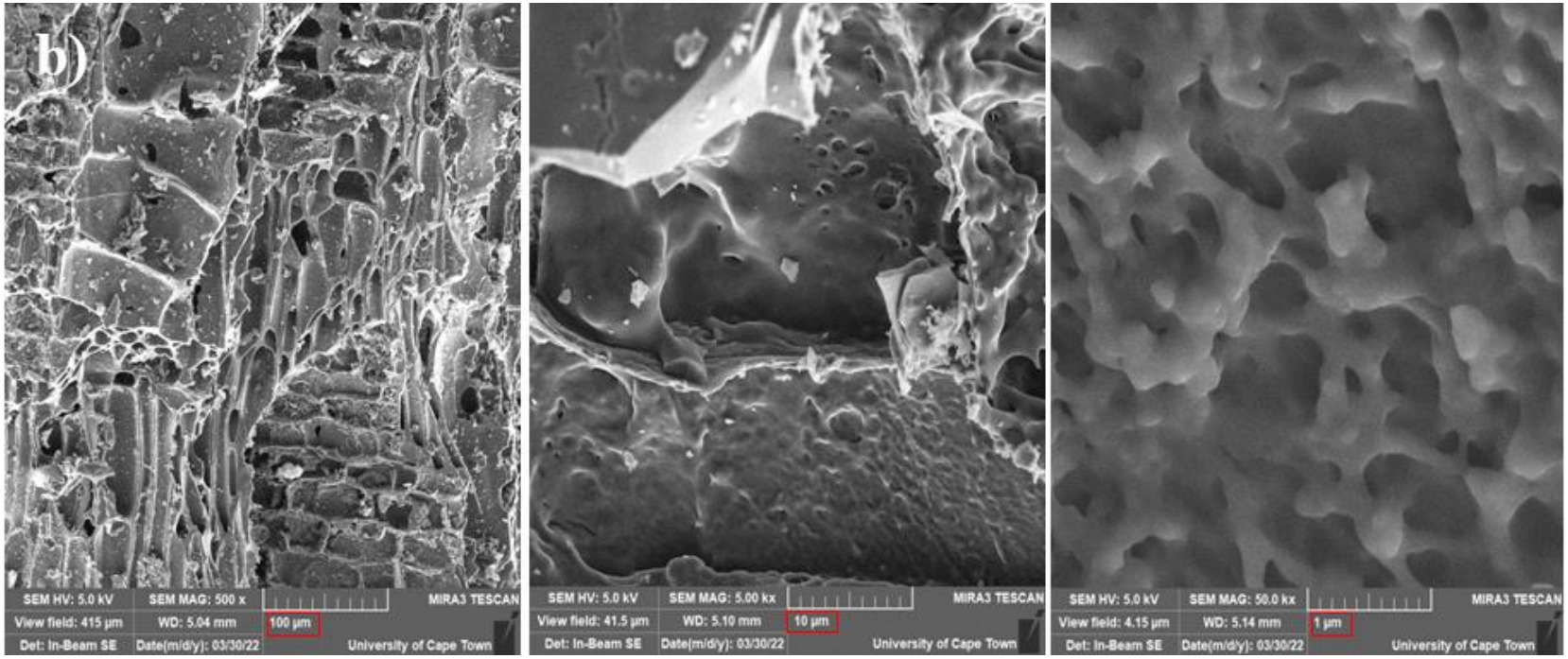
b)
SEM HV: 5.0 kV
SEM MAG: 500 x
MIRA3 TESCAN
View field: 415 µm
WD: 5.04 mm
100 µm
Det: In-Beam SE
Date(m/d/y): 03/30/22
University of Cape Town
SEM HV: 5.0 kV
SEM MAG: 5.00 kx
MIRA3 TESCAN
View field: 41.5 µm
WD: 5.10 mm
10 µm
Det: In-Beam SE
Date(m/d/y): 03/30/22
University of Cape Town
SEM HV: 5.0 kV
SEM MAG: 50.0 kx
MIRA3 TESCAN
View field: 4.15 µm
WD: 5.14 mm
1 µm
Det: In-Beam SE
Date(m/d/y): 03/30/22
University of Cape Town

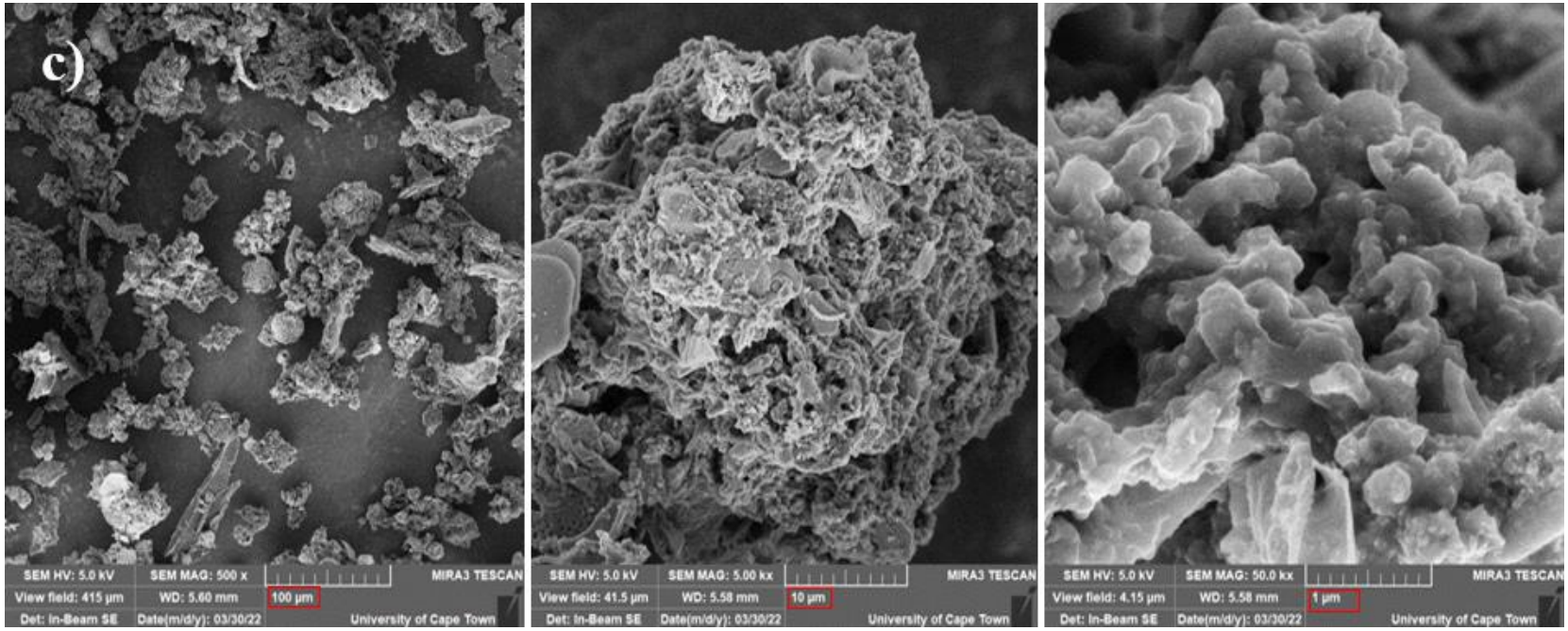

Figure 4.3 Scanning electron micrographs of a) GAC, b)AW-AC, and c) HC-AC

4.3.9 Raman Spectroscopy

The Raman spectra was recorded over a range of 10-3000 cm^{-1}. Three distinct peaks were observed on all the carbon samples as can be seen in

Figure 4.4. The Raman spectra of the three carbon samples GAC, AW-AC, and HC-AC have bands present at 1336, 1340, and 1368 cm-^{1}, respectively. Bands in this range are referred to as the D band peaks which highlight defects and disorder in the crystalline structure of the carbon (Chia *et al.*, 2012; Liu *et al.*, 2017; Medhat *et al.*, 2021). Sharp peaks are observed around 1586, 1590, and 1597 cm^{-1} for the samples GAC, AW-AC, and HC-AC, respectively. Peaks in this range are distinctive of the graphitic arrangement known as the G-band which is the primary signature for sp^2 carbon in Raman spectra. The G-band indicates that pairings of sp^2 atoms in both rings and chains are stretched by a c-c link (Chia *et al.*, 2012; Medhat *et al.*, 2021). Ill-defined second order Raman peaks were observed around 2879, 2910, and 2948 cm^{-1} for GAC, AW-AC, and HC-AC respectively. Peaks within this range identify these carbons as materials with low order in aromatic domains but rich in sp^3 (Giorcelli *et al.*, 2021). The combination of D and G bands found is proof that the carbons are polyaromatic and graphitic (Chia *et al.*, 2012). In GAC, the D band is more intense than the G band which is indicative of the disorder of a large number of carbon atoms. For AW-AC and HC-AC the D band is less intense than the G band inferring just a slight disorder of the carbon atoms. The measure of the extent of disorder in the carbon materials is expressed by the intensity ratio between the D and G band (R= ID/IG) (Medhat *et al.*, 2021). The intensity ratio of the activated carbons, GAC, AW-AC, and HC-AC are 0.84, 0.84, and 0.86, respectively. The similarity

of the three numbers suggests that the carbons have similar graphitic structures (Kristianto *et al.*, 2016).

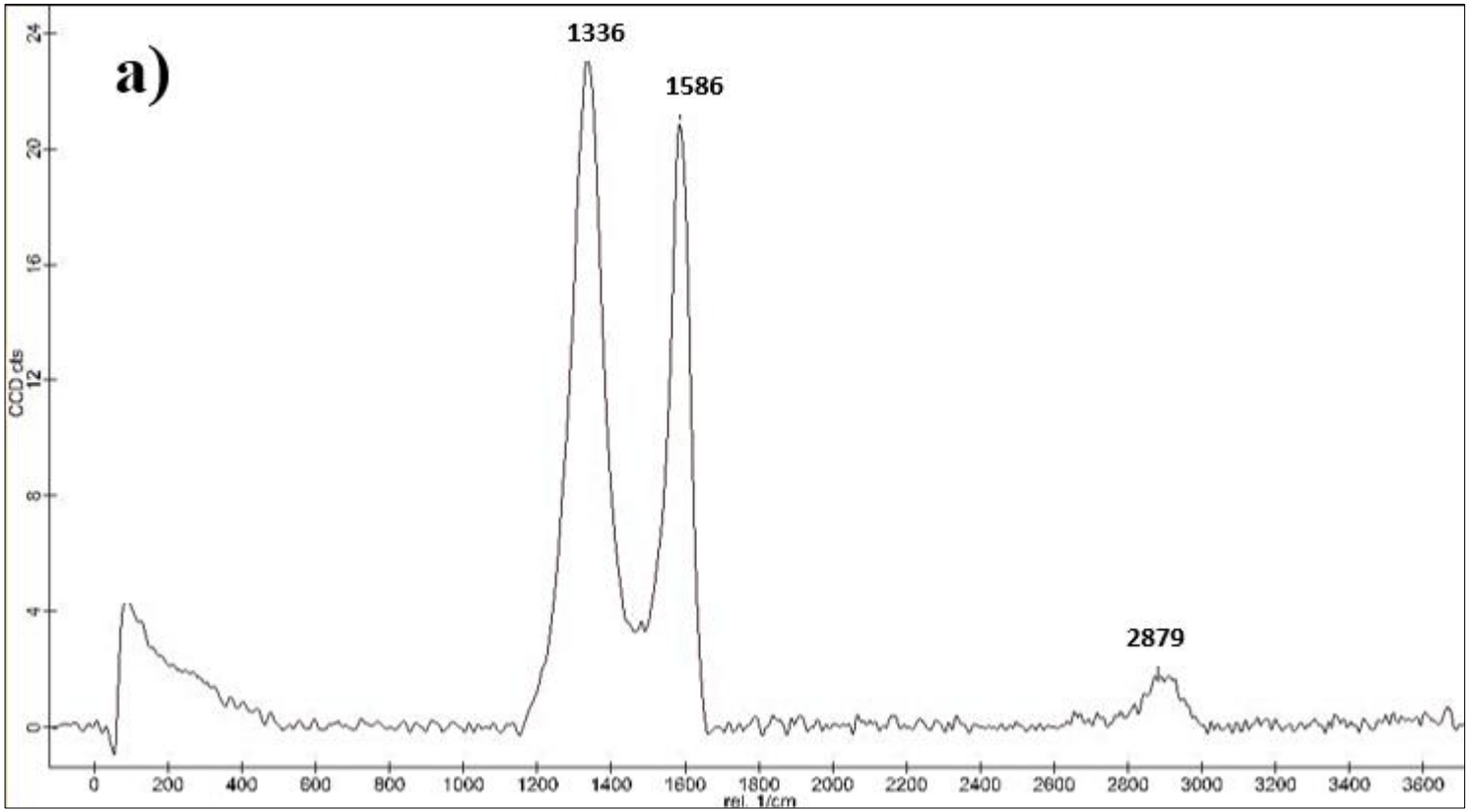
a)
1336
1586
2879
CCD cts
rel. 1/cm

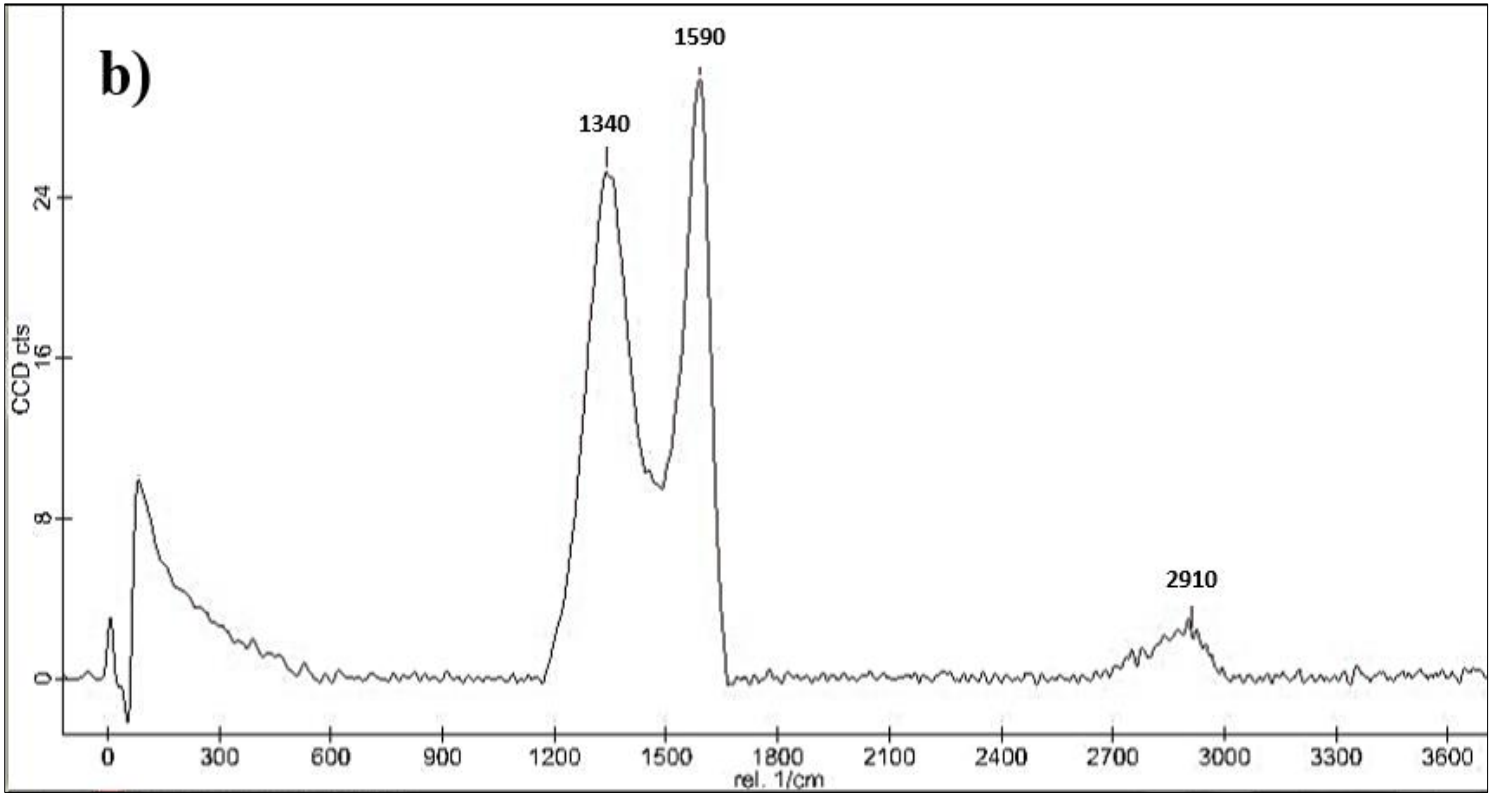
b)
1590
1340
2910
CCD cts
0
8
16
24
0
300
600
900
1200
1500
1800
2100
2400
2700
3000
3300
3600
rel. 1/cm

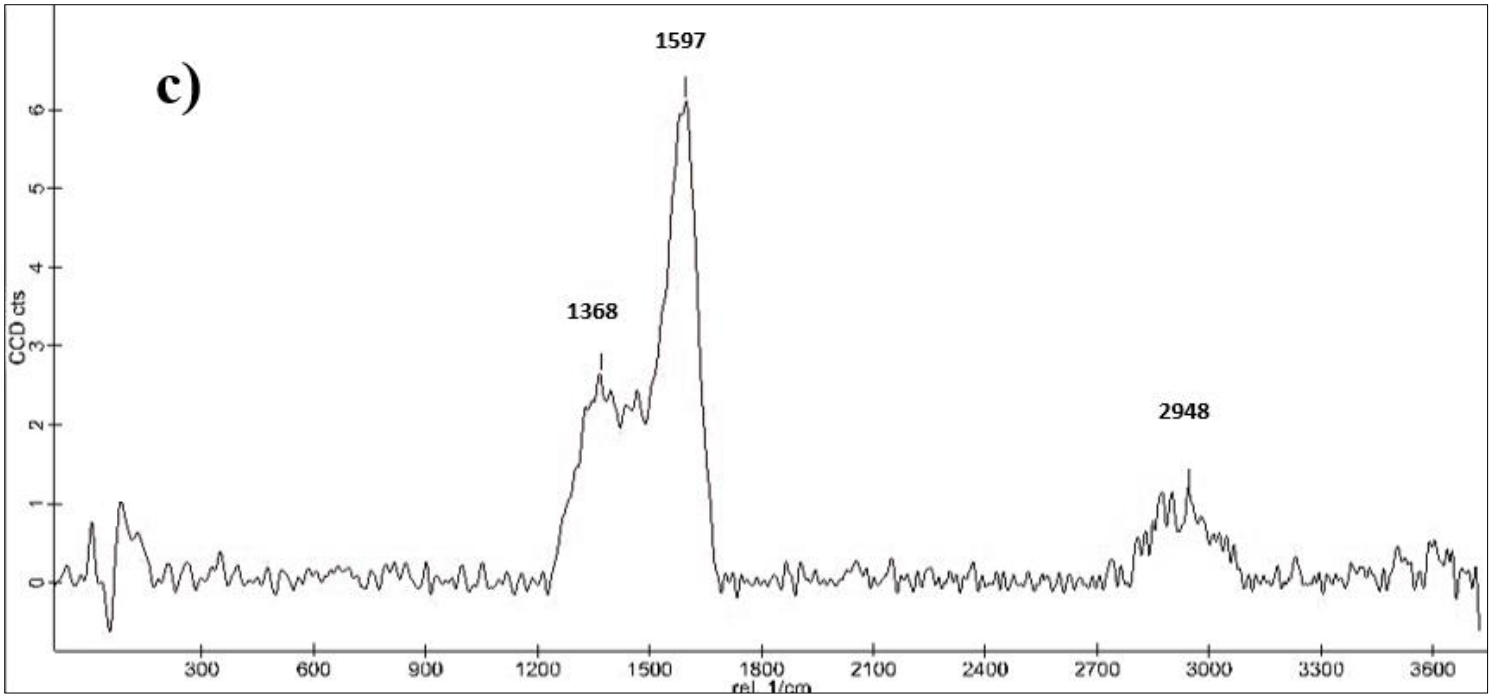

Figure 4.4 Raman spectra of (a) GAC, (b) AW-AC, and (c) HC-AC

4.3.10 Energy Dispersive Spectroscopy (EDS) Mapping

Five spectra were marked on each activated carbon. A single spectrum was chosen on each carbon sample and its elemental results were displayed and discussed. For GAC spectrum 2 was chosen, for AW-AC and HC-AC spectrum 5 was chosen. The main elements obsereved for the three adsorbents are carbon and oxygen as can be seen in Figure 4.5 . There was a greater ratio of carbon compared to oxygen in the GAC and AW-AC samples while the ratio observed in HC-AC was almost 1:1. The alien wood based activated carbon (AW-AC) only contained carbon and oxygen which was similar to another study carried out on a wood-based adsorbent (Danish *et al.*, 2020). Of the three carbons AW-AC contained the most carbon (91.8 %), followed by GAC (78.8 %), and lasty HC-AC (43.4%). Though HC-AC contained the least carbon of the three it contained the most oxygen (40.5 %) which was almost thrice the amount of oxygen in GAC (13.5 %) and 5 times more than AW-AC (8.2 %).

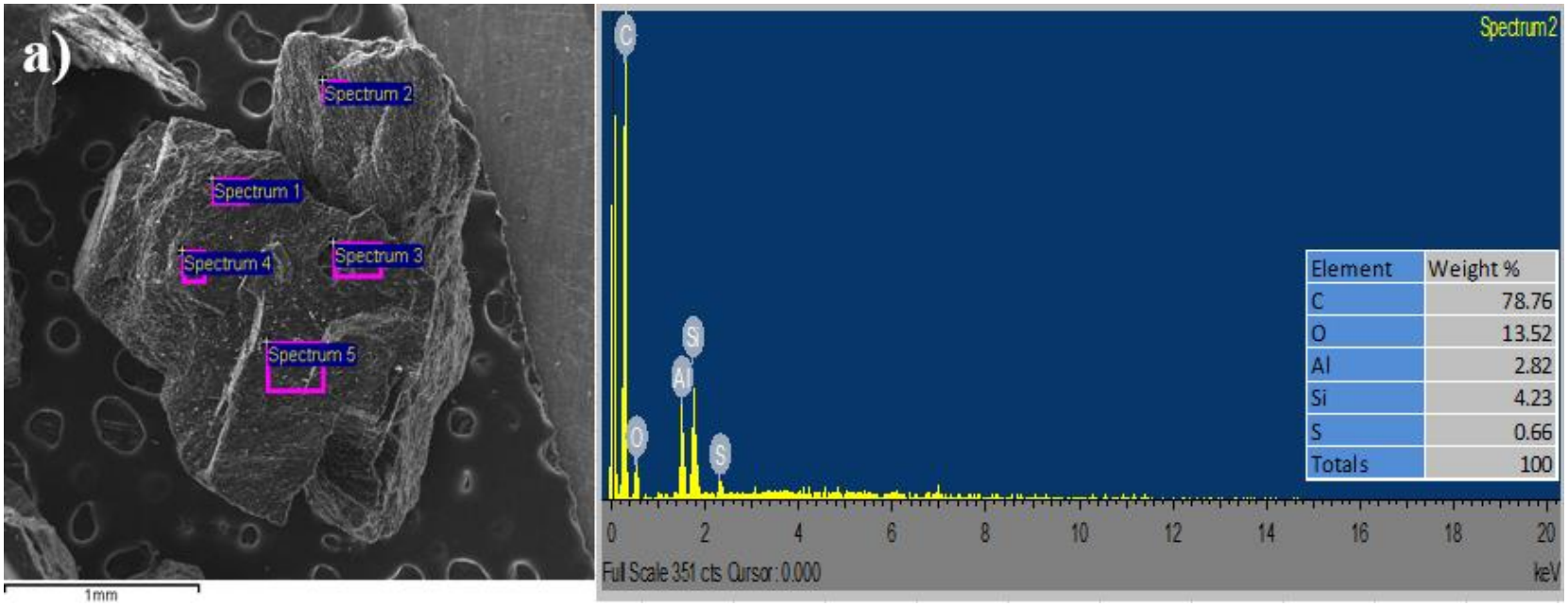
a)
Spectrum 2
Spectrum 1
Spectrum 4
Spectrum 3
Spectrum 5
1mm
Spectrum2
C
O
Al
Si
S
Element | Weight %
C | 78.76
O | 13.52
Al | 2.82
Si | 4.23
S | 0.66
Totals | 100
0 2 4 6 8 10 12 14 16 18 20
Full Scale 351 cts Cursor: 0.000
keV

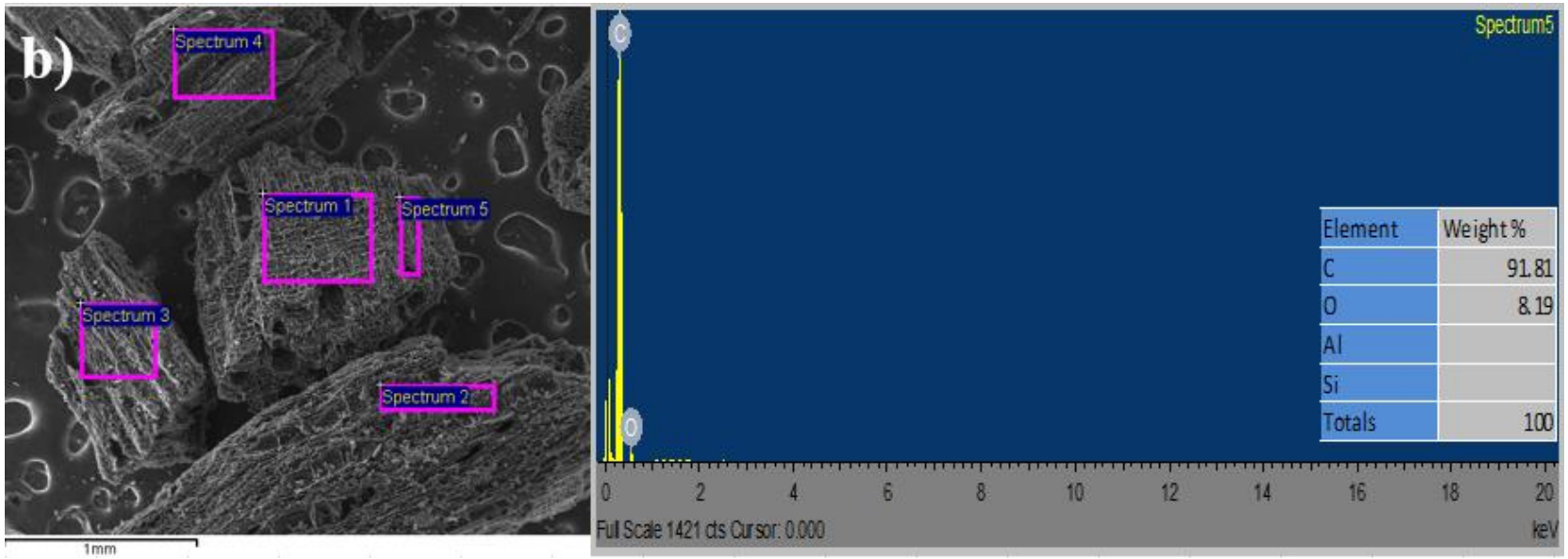
b)
Spectrum 4
Spectrum 1
Spectrum 5
Spectrum 3
Spectrum 2
1mm
Spectrum5
C
O
Element
Weight %
C
91.81
O
8.19
Al
Si
Totals
100
0
2
4
6
8
10
12
14
16
18
20
Full Scale 1421 cts Cursor: 0.000
keV

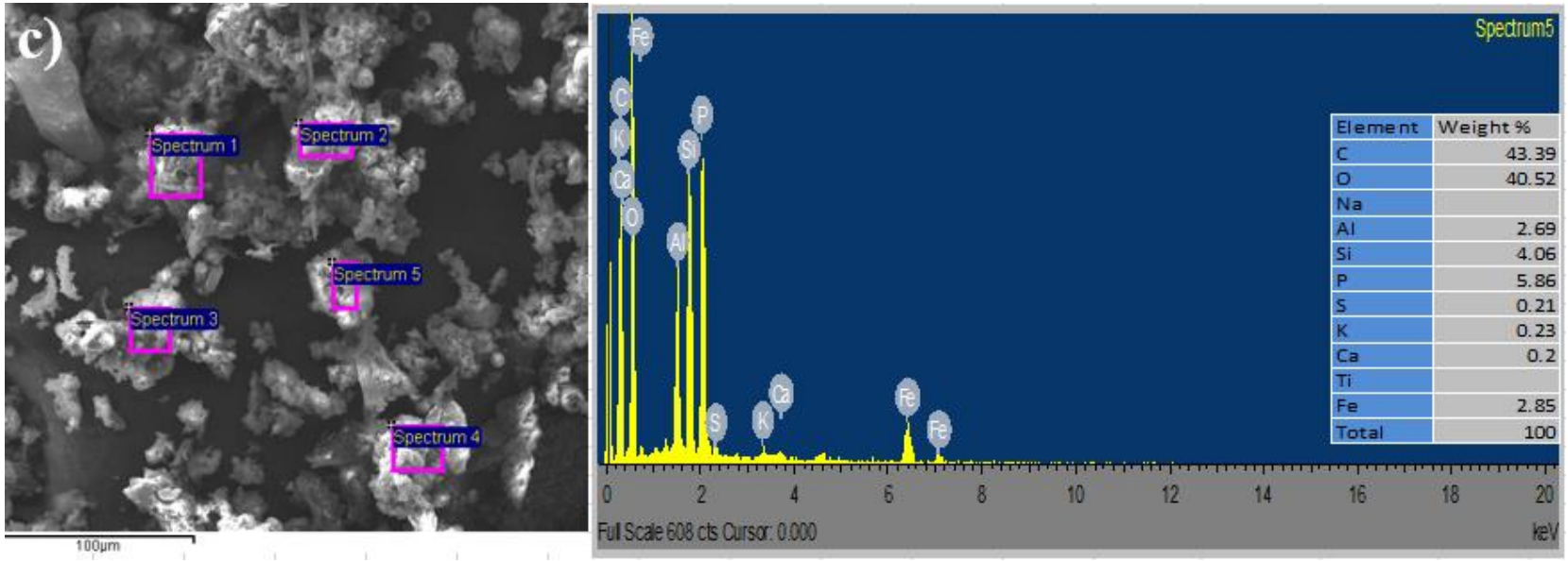

Figure 4.5 EDS spectrum of a) GAC, b) AW-AC, and c) HC-AC

4.3.11 Fourier Transform Infrared (FT-IR) Spectroscopy

The FT-IR spectra of the three carbons are displayed in Figure 4.6. The presence or absence of surface functional groups based on the assignments given in Table 3.11 in the methods section are presented in Table 4.3. The presence of surface functional groups is an important characteristic of adsorbents as it has been known to influence their adsorptive capacity (Onundi *et al.*, 2010; Yagub, Sen and Ang, 2014; Tomczyk, 2020) by complexation, electrostatic attraction and ion exchange between the surface groups on the adsorbent and the adsorbate in solution (Ullah *et al.*, 2020; Dutta *et al.*, 2021). In some cases the presence of functional groups has been reported as being more important to the removal process than the surface area (Saleem *et al.*, 2019). The presence of oxygen containing functional groups on the surface of adsorbents such as the carboxyl and hydroxyl groups has been identified as having a strong influence on their adsorptive performance (Gupta and Suhas, 2009; Badawi, Abd Elkodous and Ali, 2021). From Figure 4.6, it is clear that HC-AC contained both the hydroxyl and carboxyl peaks as indicated by the sharp peaks at 3406 cm^{-1} and 1102 cm^{-1}. The carbons GAC, and AW-AC also contained peaks within the ranges of 1000-1200 cm^{-1} and 3200-3500 cm^{-1} like HC-AC, but these peaks were shorter and less pronounced.

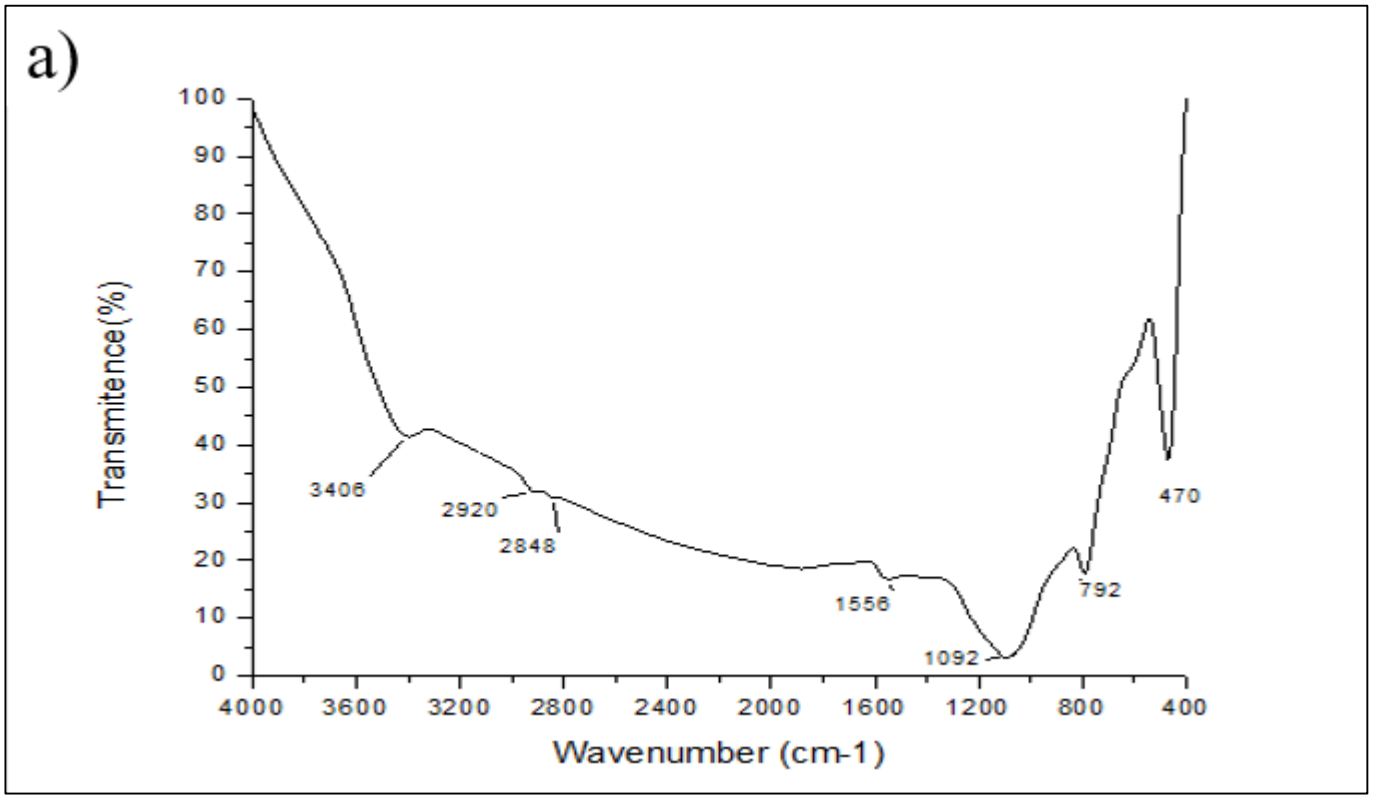
a)
Transmitence(%)
100
90
80
70
60
50
40
30
20
10
0
4000
3600
3200
2800
2400
2000
1600
1200
800
400
Wavenumber (cm-1)
3406
2920
2848
1556
1092
792
470

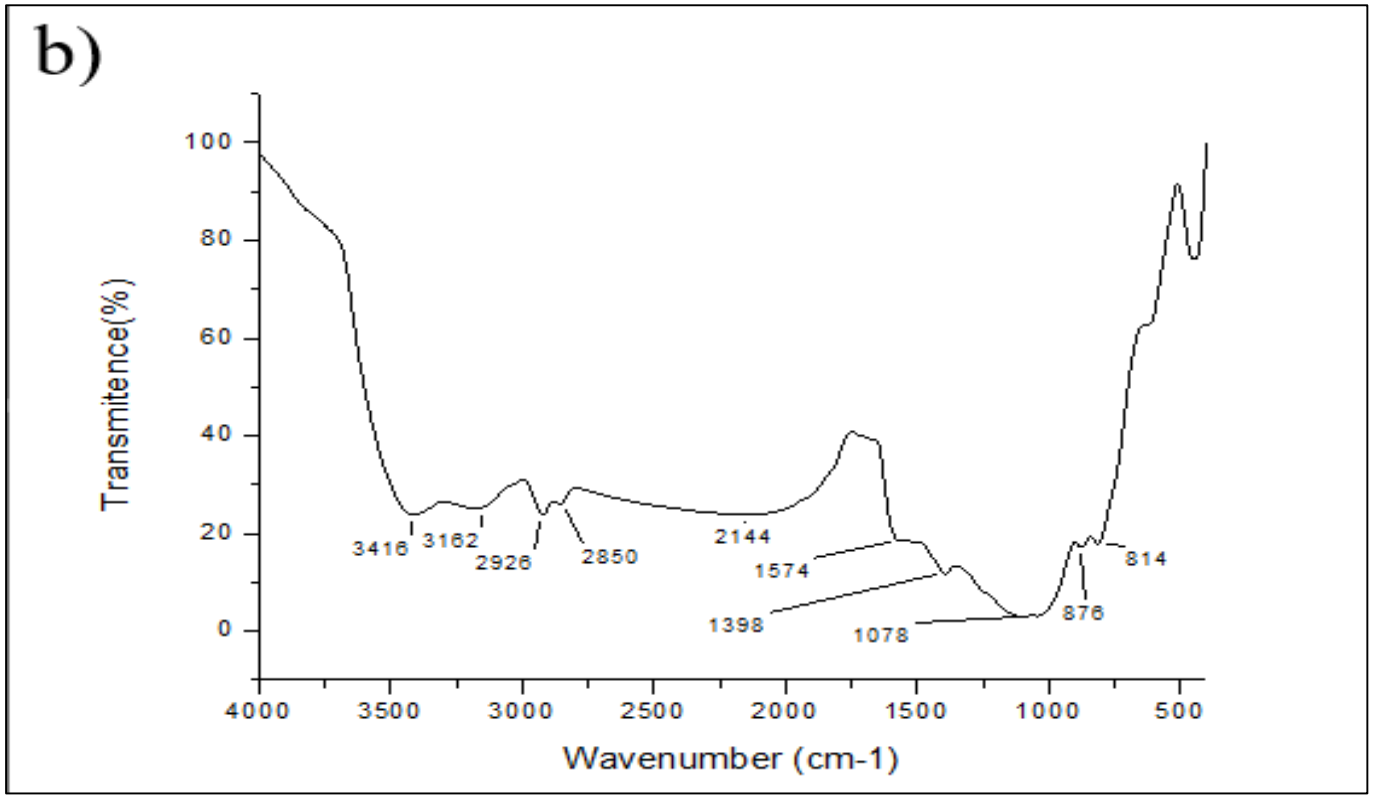
b)
Transmitence(%)
100
80
60
40
20
0
3416
3162
2926
2850
2144
1574
1398
1078
876
814
4000
3500
3000
2500
2000
1500
1000
500
Wavenumber (cm-1)

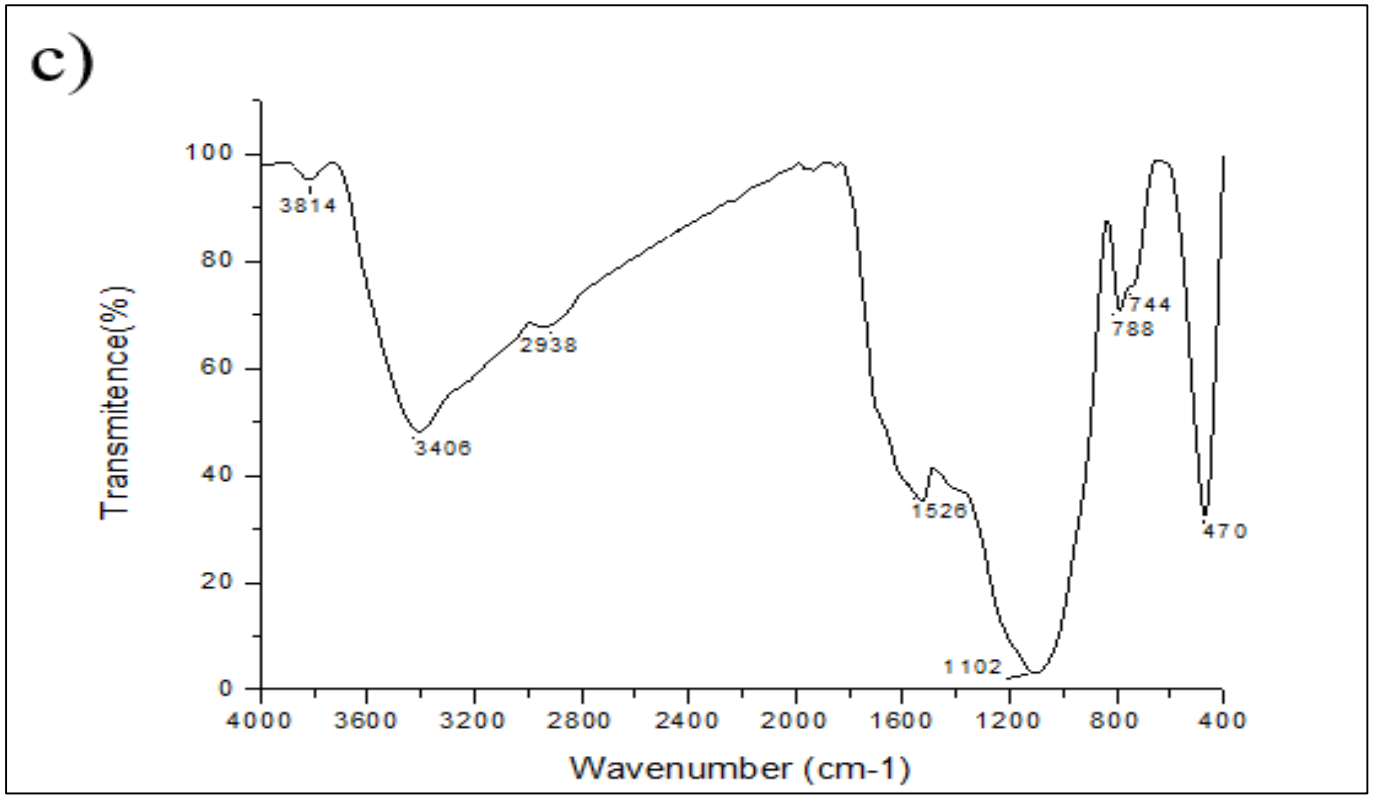

Figure 4.6 FT-IR spectra of (a) GAC, (b) AW-AC, (c) HC-AC

Table 4.3 Summary of the presence and absence of functional groups on GAC, AW-AC, and HC-AC.

	GAC	AW-AC	HC-AC
Group or functionality			
C-O in ethers (stretching)	✓	✓	✓
Alcohols	✓	✓	✓
–C-OH (stretching)	✓	✓	✓
Quinones	✓	✓	×
C-H (stretching)	✓	✓	✓
N-H, C=N	×	✓	×
N-O-	✓	✓	✓
✓ present ; × absent			

4.4 Optimization of Adsorption Experiments for Methylene Blue (MB) and Lead (Pb (II)) Ions

4.4.1 Methylene Blue (MB) Adsorption

Preliminary tests were carried out to determine the optimum concentration for methylene blue adsorption and the wavelength at which the absorbance of the dye would be measured. Three concentrations (2.5, 5, and 7.5 mg/L) were investigated. Of the three 7.5 mg/L showed the highest removal and it was therefore chosen as the working concentration at which the subsequent experiments would be carried out. The wavelength of methylene blue was measured between the range of 350-700 nm, and the wavelength of 663 nm was found as having the highest absorbance peak. Hence, 663 nm was chosen as the wavelength at which all methylene blue absorbance readings would be taken at in this study.

4.4.1.1 The Calibration Curve

Figure 4.7 depicts a 5-point calibration curve for methylene blue (MB) in the range of 1-10 mg/L. The graph was used to determine the relationship between the concentration of methylene blue dye in mg/L and its absorbance measured in nm. Calculations to determine the concentration of unknown dye samples were obtained by substituting the attained absorbance values into the equation displayed on the graph in Figure 4.7.

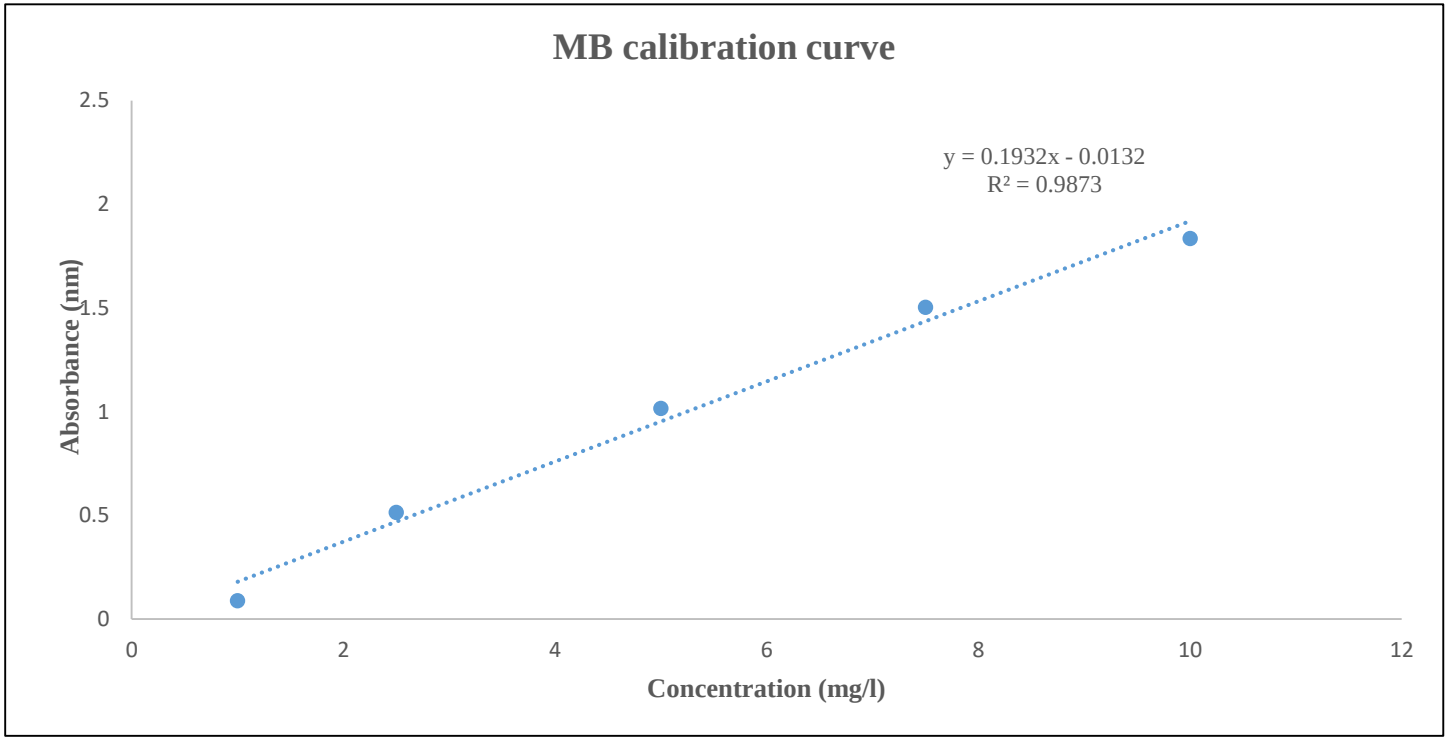

Figure 4.7 Calibration curve of methylene blue

4.4.1.2 Effect of Contact Time on Adsorption of Methylene Blue

The effect of contact time on the removal of methylene blue dye (MB) is shown in Figure 4.8. The general trend displayed by the three curves representing adsorption by the three adsorbents (GAC, AW-AC, and HC-AC), indicates an increase in dye removal with time, until a certain point in time after which the removal becomes constant. This point is referred to as the equilibrium time and it is described in literature as a state at which the amount of dye being absorbed onto the activated carbon is equal to the amount being desorbed from the adsorbent (Bello *et al.*, 2008). The adsorbents maximum capacity for adsorption under the employed operating conditions is taken as the quantity of dye absorbed at the equilibrium time (Hameed, Din and Ahmad, 2007). The rapid rate of MB adsorption during the initial stages might be due to the high solute concentration gradient and the availability of vacant active sites on the adsorbent (Pathania, Sharma and Singh, 2017). Gradually, the number of vacant sites on the adsorbent surface decreases leading to a reduction in the rate of adsorption and constant removal values indicating that the system has reached equilibrium (Singh, Sidhu and Singh, 2019). The percentage removal was observed as stabilizing around 130, 160, and 280 minutes for GAC, AW-AC, and HC-AC, respectively. These times were taken as the equilibrium times and subsequent optimization experiments were conducted at the above-mentioned times for each adsorbent.

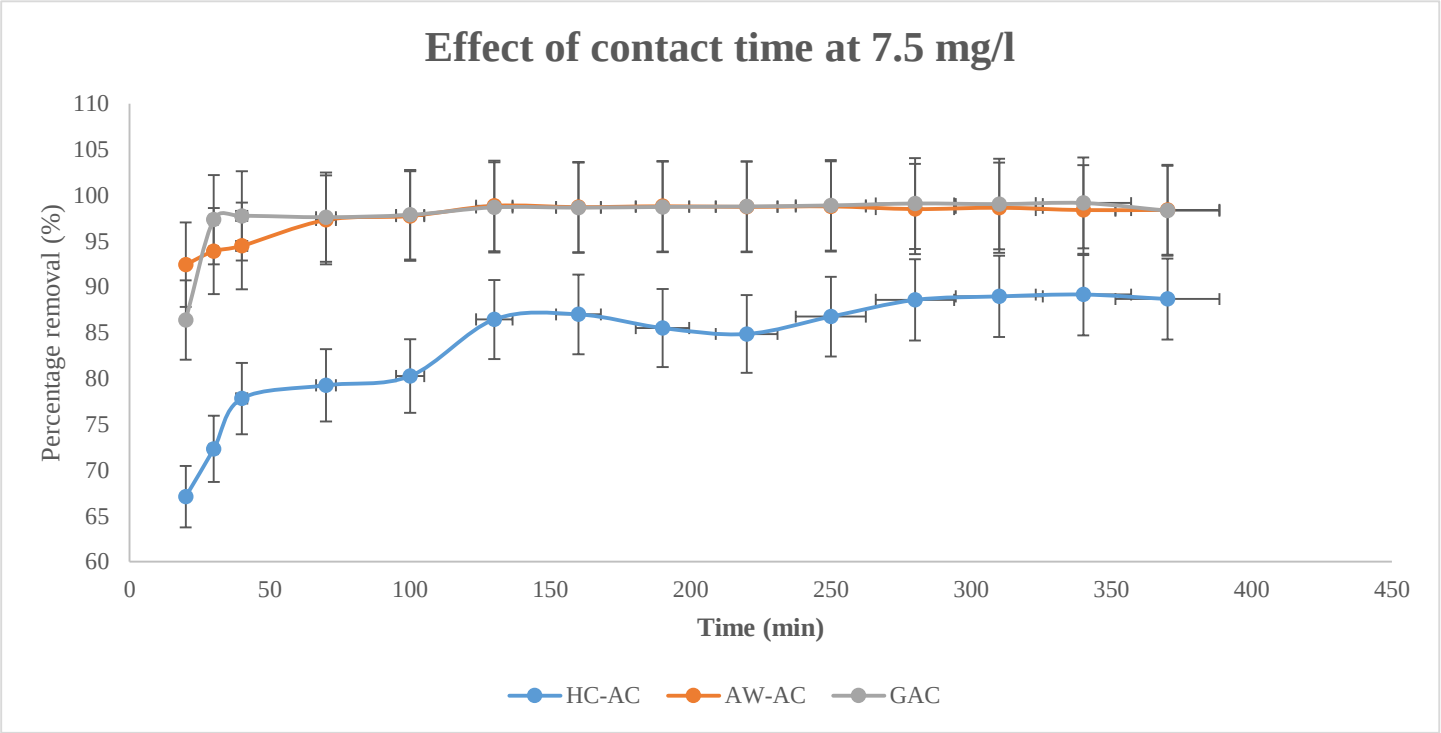

Figure 4.8 Effect of contact time and initial concentration on adsorption of MB - initial concentration: 7.5 mg/L, solution volume: 100 mL, contact time: 370 min, adsorbent dose: 0.2 g/100 mL, and pH: 6.5.

4.4.1.3 Effect of pH of Solution on Adsorption of Methylene Blue

The effect of pH on methylene blue adsorption was investigated for values between the pH ranges of 2 – 11. The percentage removal of MB by GAC increased from 97.68 % at pH 2 to attain maximum removal of 99.08 % at pH 8. This slight increment over the pH range indicates that the adsorbent performed reasonably effectively across the whole pH range studied. For AW-AC, the percentage removal increased significantly from 62.63 % at pH 2 to achieve a maximum removal of 98.89 % at a pH of 8. (Pathania, Sharma and Singh, 2017) and (Alam *et al.*, 2021) also reported having attained maximum removal at a pH of 8. However, the hydrochar derived carbon, HC-AC, attained its maximum removal of 99.25 % at pH of 11 which was similar to the optimum pH for MB removal reported by (Fan *et al.*, 2017). Observation of the trends displayed in Figure 4.9 clearly show that the adsorption of methylene blue is favorable in alkaline conditions. This could be as a result of the net negative charge that the adsorbent surface develops due to its deprotonation at high pH values (Patawat *et al.*, 2020) as a result of the presence of negatively charged functional groups such as the carboxyls and hydroxyls (Ebrahimian Pirbazari, Saberikhah and Habibzadeh Kozani, 2014; Singh, Sidhu and Singh, 2019) which then enhance the electrostatic attraction between the MB dye and the adsorbent (Pathania, Sharma and Singh, 2017). The reason for the low removal of the cationic dye in the lower pH range, has been attributed to the abundant presence of hydrogen ions which then compete with the dye molecules for vacant active sites (Yagub, Sen and Ang, 2012; Ebrahimian Pirbazari, Saberikhah and Habibzadeh Kozani, 2014; Singh, Sidhu and Singh, 2019). Another reason for this observation in the lower pH range has been ascribed to the release of positively charged ions by the cationic dye when it is dissolved in water, leading to electrostatic repulsion

between the ions and the positively charged adsorbent, thus lowering removal (Ebrahimian Pirbazari, Saberikhah and Habibzadeh Kozani, 2014; Pathania, Sharma and Singh, 2017; Patawat *et al.*, 2020). The increased percentage removal observed at higher pH ranges has been ascribed to the electrostatic attraction between the positively charged ions released by the dye when it dissolves in water and the surface of the adsorbents that become negatively charged due to deprotonation at increased pH levels (Ebrahimian Pirbazari, Saberikhah and Habibzadeh Kozani, 2014; Pathania, Sharma and Singh, 2017; Patawat *et al.*, 2020). The presence of numerous functional groups on the surface of the activated carbons as displayed on the FTIR spectra in Figure 4.6 above confirms that the functional groups on the surface of the adsorbent play a large role in the adsorption of MB as they undergo protonation or deprotonation depending on the pH of solution (Ebrahimian Pirbazari, Saberikhah and Habibzadeh Kozani, 2014). These results also confirm that pH is an important parameter for MB adsorption as it can be seen that the removal of HC-AC was greater than that of GAC and AW-AC when its optimum pH of 11 was reached. The dosage experiments were conducted at the contact times and pH values obtained in Sections 4.4.1.2 and 4.4.1.3.

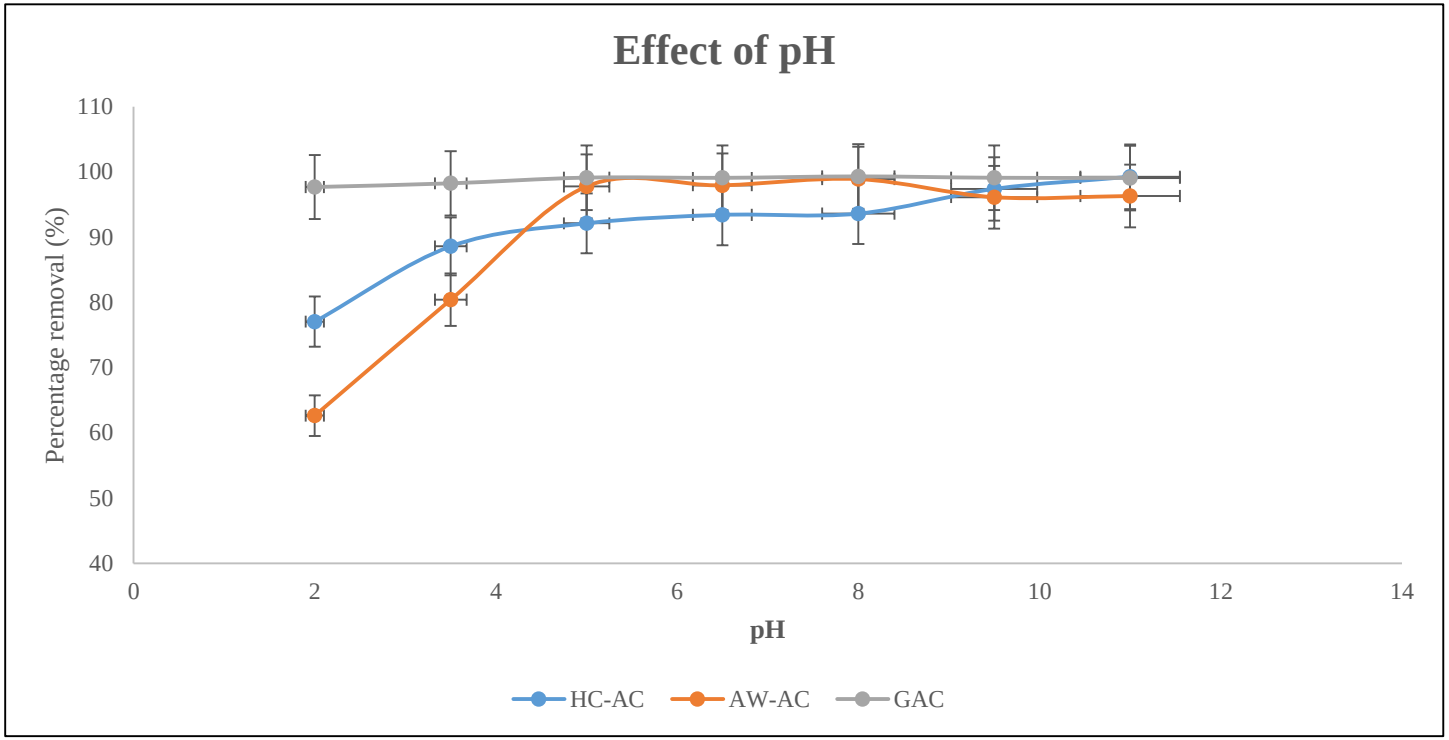

Figure 4.9 Effect of pH on adsorption of MB - initial concentration: 7.5 mg/L, solution volume: 100 mL , contact time: 130 min for GAC, 160 min AW-AC, and 280 min for HC-AC, adsorbent dose: 0.2 g/100 mL) , and pH: 2-11.

4.4.1.4 Effect of Adsorbent Dosage on Adsorption of Methylene Blue

The dosage of adsorbent used during the adsorption experiments is important. It not only aids in determining the removal efficiency of a particular adsorbent under set conditions, but it can be used to estimate the cost of the adsorbent to be used for each unit of the solution to be treated (Alam *et al.*, 2021). The dose for each adsorbent was varied between 0.1 to 1 g /100 ml as can be seen in Figure 4.10. The removal of MB by HC-AC appeared to be almost constant and approach 100 % removal over the dosage range. Its highest removal was observed at 0.6g at 99.28 %. It can be said that removal of MB by HC-AC was more pH dependent than it was dosage dependent as it achieved high removal even at low dosage. Of the three adsorbents HC-AC showed the highest removal. The removal of GAC showed a slight increase from 98.41 % at 0.1g to 99.13 % at 0.4 g. The optimal dose for GAC was taken as 0.4 g as no significant change in removal was observed beyond 0.4 g. The AW-AC showed a sharp increase in removal from 83.14 % at 0.1 g to 98.73 % at 0.8 g. Thereafter, no significant change in removal was observed. Therefore, 0.8 g was chosen as the optimum dosage for AW-AC. Of the three adsorbents it showed the lowest percentage removal. The increase in removal as the dosage increased could be attributed to the availability of sufficient adsorption sites as well as that of specific surface area (Fan *et al.*, 2017; Pathania, Sharma and Singh, 2017). However, the lack of significant change in percentage removal past a certain dosage increment has been reported as being the result of adsorbent particle aggregation (Pathania, Sharma and Singh, 2017) or the saturation of adsorbent sites by the dye (Fan *et al.*, 2017). The percentage removal of the dye at the optimum conditions was in the following order: HC-AC (99.28 %) > GAC (99.13 %) > AW-AC (98.73 %).

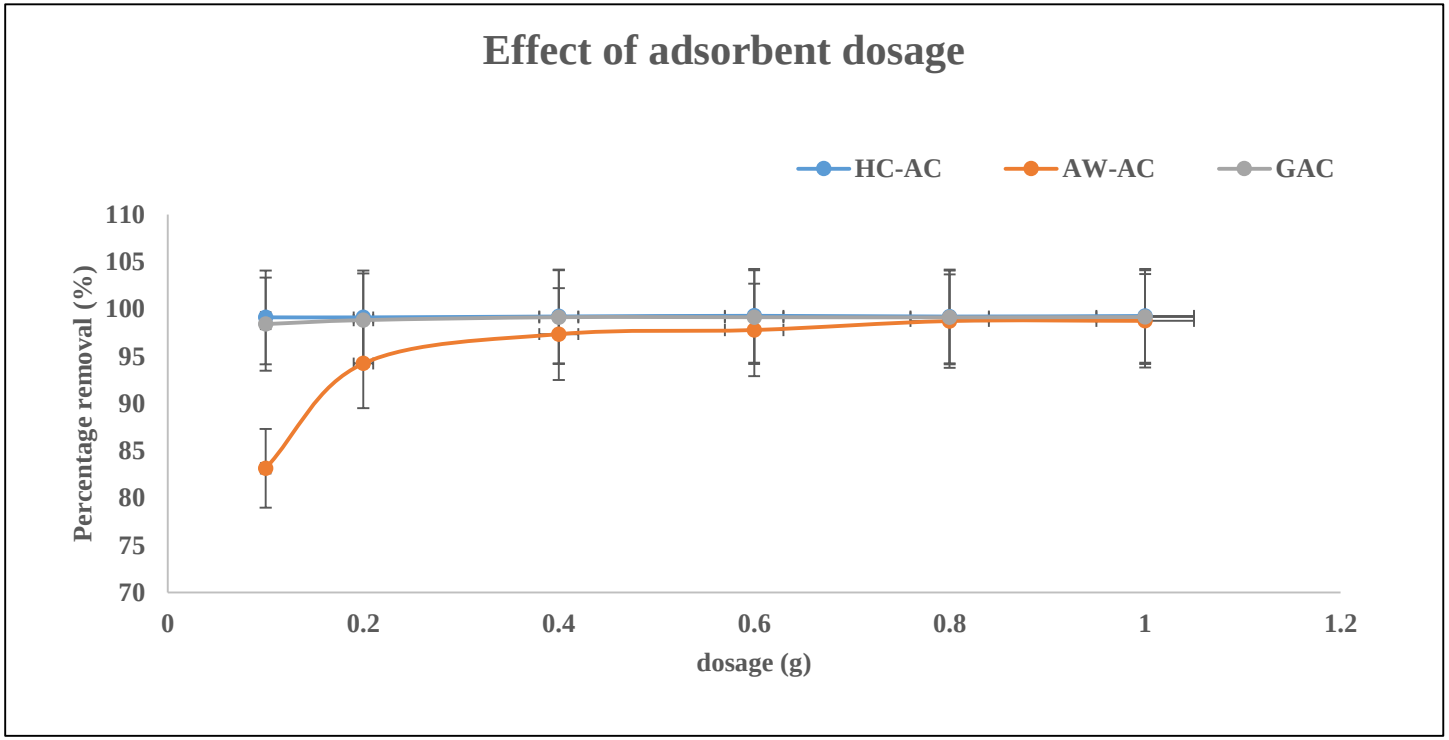

Figure 4.10 Effect of adsorbent dosage on adsorption of MB - initial concentration: 7.5 mg/L , solution volume: 100 mL, contact time: 130 min for GAC, 160 min for AW-AC, and 280 min for HC-AC , adsorbent dose: 0.1-1(g/100 mL), pH: 8 for GAC and AW-AC, and pH: 11 for HC-A.

4.4.2 Kinetic Studies for Methylene Blue Adsorption

The kinetics for the three adsorbents were investigated for a contact time of 370 minutes using the pseudo-first-order and pseudo-second-order model equations found in Table 2.2. The parameters obtained using these equations are listed in Table 4.4. The pseudo-second-order kinetic model best fit the kinetic data for GAC, AW-AC, and HC-AC with R^2 values of 0.999, 1.00, and 0.9994, respectively. The experimental adsorption capacity values, for GAC, AW-AC, and HC-AC (3.8892, 3.8633, and 3.4340 mg/g, respectively) were close to the calculated q_e values, 3.8890, 3.8772, and 3.4957 mg/g (see Table 4.4). According to (Ho and McKay, 1999a), The results suggest that the sorption system is second-order and that the rate limiting step is chemisorption as the R^2 values are greater than 0.996.

Table 4.4 Kinetic parameters of MB adsorption onto GAC, AW-AC and HC-AC

			GAC	AW-AC	HC-AC
Kinetic model	**Parameters**	**Unit**	**Obtained value**		
Pseudo-first-order	q_e	(mg/g)	0.9917	0.9979	0.9893
	K_1	min^{-1}	0.0076	0.0062	0.0035
	R^2		0.3628	0.0187	0.3793
Pseudo-second-order	q_e	(mg/g)	3.8890	3.8772	3.5202
	q_e^2	(mg/g)	15.1246	15.0329	12.3919
	K_2	min^{-1}	0.2244	0.3046	0.0317
	R^2		0.9999	1	0.9994

4.4.3 Isotherm Studies for Methylene Blue Adsorption

The experimental data of the three adsorbents were analyzed using the Langmuir and Freundlich isotherm model equations found in Table 2.3. The parameters obtained are listed in Table 4.5. The parameters obtained from analysis showed that the data for GAC and AW-AC was best fitted to the Langmuir 2 equation with R^2 values of 0.9993 and 0.9764, respectively. The data for HC-AC showed high correlation with the Langmuir 1 isotherm equation with an R^2 value of 0.9877. The maximum adsorption capacity q_{max} of GAC and HC-AC were similar (7.500 and 7,467 mg/g, respectively), while AW-AC had the highest q_{max} with a value of 8.183 mg/g. The results suggest that sorption onto the three adsorbents was a monolayer operation and that the isotherm was favorable as the R_L values were within the range of $0 < R_L < 1$ (Hameed, Din and Ahmad, 2007).

Table 4.5 Isotherm parameters of MB adsorption onto GAC, AW-AC and HC-AC

Adsorption isotherm	Parameters	Unit	GAC	AW-AC	HC-AC
			Obtained value		
Langmuir 1	q_{max}	(mg/g)	8.4965	5.4881	7.4667
	K_L	min^{-1}	72.1903	30.1190	55.7512
	R_L		0.0018	0.0044	0.0024
	R^2		0.9982	0.2058	0.9877
Langmuir 2	q_{max}	(mg/g)	7.50013114	8.18295019	-1.3224935
	K_L	min^{-1}	56.2519671	66.9606739	1.74898917
	R_L		0.00236468	0.00198726	0.07083448
	R^2		0.9993	0.9764	0.8094
Langmuir 3	q_{max}	(mg/g)	0.13342698	0.12515904	-0.9341945
	K_L	min^{-1}	0.01780276	0.01566479	0.87271936
	R_L		0.8822071	0.89486588	0.13253116
	R^2		0.9993	0.9764	0.8094
Langmuir 4	q_{max}	(mg/g)	-1.1394272	-0.7158755	6.61102768
	K_L	min^{-1}	1.29829444	0.51247772	43.705687
	R_L		0.09313408	0.20645873	0.00304143
	R^2		0.9942	0.1695	0.9503
Freundlich	n	(mg/g)	0.3473	0.2298	1.4748
	K_f	(mg/g)	2494.0651	35943.8512	3.9533
	R^2		0.9813	0.3318	0.9594

4.4.4 Lead (Pb (II)) Adsorption

4.4.4.1 Effect of Solution pH on Adsorption of Lead (II) Ions

The solution pH is a crucial parameter in adsorption as it not only facilitates the removal of lead by adsorption by influencing the properties of the metal ion, but also plays a significant role by influencing the surface charge of the adsorbent (Alghamdi *et al.*, 2019; Onwordi *et al.*, 2019; Kavand, Eslami and Razeh, 2020; Mandal *et al.*, 2021). The effect of pH on the removal of lead by the three activated carbons is shown in Figure 4.11. The removal of lead was the lowest in the low pH range (pH 2-4). This has been widely discussed in literature and is attributed to the competition for active sites by the Pb^{2+} ions and the H^{+} ions which are highly concentrated in acidic environments (Mohan *et al.*, 2007, 2020; Onundi *et al.*, 2010; Boontham, 2016; Kavand, Eslami and Razeh, 2020). The gradual increase in pH saw an increase in adsorption of lead, owing to the negative charge of functional groups present on the surface of the adsorbents which made them readily available for lead adsorption (Guyo and Moyo, 2017). A pH of 7 was taken as the optimal value to attain maximum lead removal by true adsorption for all three adsorbents, as it is believed that pH values greater than 7 facilitate the precipitation of lead ions into hydroxide species (Alghamdi *et al.*, 2019; Kavand, Eslami and Razeh, 2020; Mohan *et al.*, 2020; Mandal *et al.*, 2021). (Boontham, 2016) reported high lead removal (above 90 %) at neutral pH, and highlighted the preferred treatment of wastewater at a neutral pH due to the possibility that the utility of using excessive pH values for lead removal will result in greater post treatment expenses.

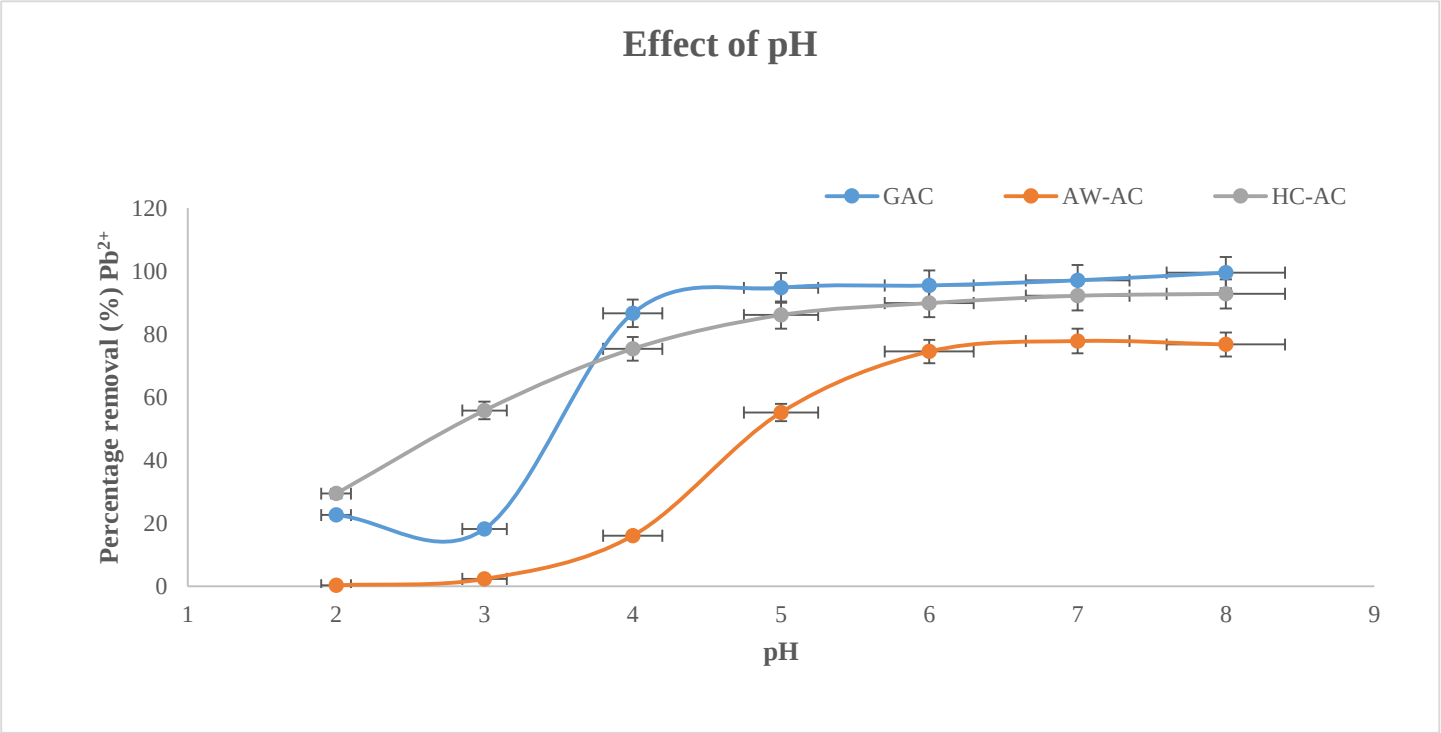

Figure 4.11 Effect of pH on the adsorption of Pb (II) ions - initial concentration: 5.3 mg/L, solution volume : 100 mL, contact time: 120 min, adsorbent dose: 0.2 g/100 mL), and solution pH: 2-8.

4.4.4.2 Effect of Dosage on Adsorption of Lead (II) Ions

The use of the optimum dosage of the adsorbent during the adsorption process, is crucial for the effective uptake of the lead ions as it ensures the availability of active sites that the ions have access to (Wahi, Ngaini and Jok, 2009; Tejada-Tovar *et al.*, 2022). The results displayed in Figure 4.12 show that GAC and HC-AC showed greater efficiency in the removal of lead ions when compared to AW-AC. As the adsorbent dosage increased from 0.1 to 0.6 g/100 mL, the percentage removal of the lead ions increased from 89.28 to 95.92 % for GAC, and 89.27 to 95.47 % for HC-AC. As the adsorbent dosage increased from 0.1 to 0.8 g, the percentage removal of AW-AC increased from 28.96 to 94.21 %. This shows that the removal rate increased as the dosage of adsorbent increased. This phenomenon can be attributed to the increased availability of active sites or surface area, for the same quantity of adsorbate molecules, which facilitates better access for the Pb(II) ions onto the activated carbons adsorption sites (Moyo *et al.*, 2013; Onwordi *et al.*, 2019; Mandal *et al.*, 2021). Subsequent increases in adsorbent dosage after 0.6 g for GAC and HC-AC, and 0.8 g for AW-AC, did not result in significant increases in the percentage removal of the Pb (II) ions. This could be attributed to the overcrowding of adsorbent particles present in the solution, causing the adsorption sites to overlap (Bernard, Jimoh and Odigure, 2013; Onwordi *et al.*, 2019).

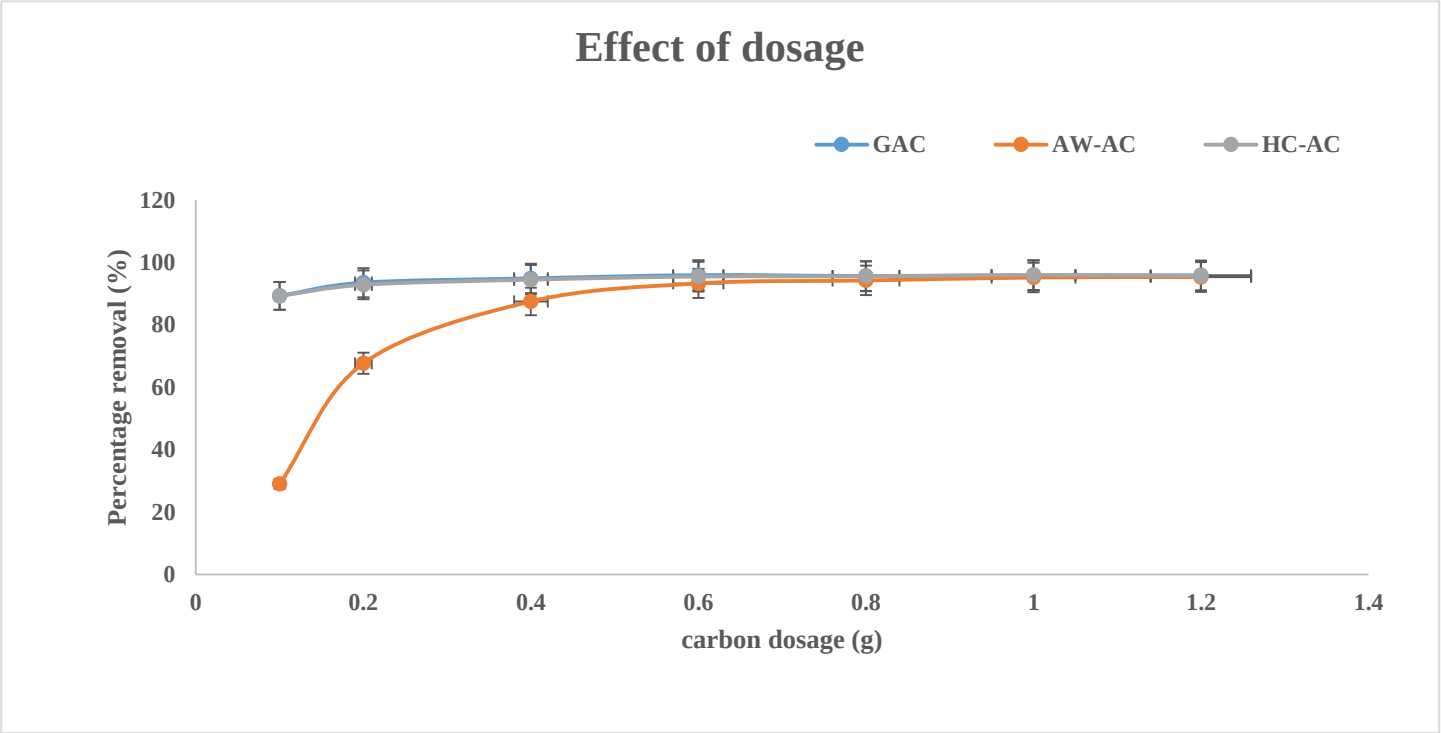

Figure 4.12 Effect of adsorbent dosage on the adsorption of Pb (II) ions - initial concentration: 5.3 mg/L , solution volume: 100 mL, contact time: 120min, adsorbent dose: 0.1-1g/100 mL, and solution pH: 7.

4.4.4.3 Effect of Initial Concentration on Adsorption of Lead (II) Ions

The starting concentration of the adsorbate serves as a crucial driving factor to overcome all Pb(II) mass transfer resistances between the solid and aqueous phases (Guyo and Moyo, 2017). It also governs the rate of the adsorption process, therefore, making it an important component to take into account for efficient adsorption. The effect of concentration on the adsorption process was tested for a concentration range of 1.9 to 14.3 mg/L. It can be observed from Figure 4.13 that the percentage removal of the lead ions initially increased with an increase in concentration of lead ions for all adsorbents up until a concentration of 9.10 mg/L was reached. The percentage removal of the Pb (II) ions at 9.10 mg/L was 97.64 %, 97.56 %, and 96.05 % for GAC, HC-AC, and AW-AC, respectively. A further increment in concentration by 5 mg/L saw a decrease in metal ion uptake across the three adsorbents. The observed phenomena can be linked to the strong interaction between the adsorbate and the numerous active sites of the adsorbent available for adsorption at lower adsorbate concentrations, hence the higher removal (Guyo and Moyo, 2017). The decrease in removal at higher concentrations can be attributed to the saturation of active sites as the amount of lead ions increases while the number of active sites on the activated carbon remains unchanged, resulting in a remnant of ions in solution after the adsorption process is complete (Moyo *et al.*, 2013; Musumba *et al.*, 2020). This decrease in removal at higher concentrations could also be explained by the involvement of active sites that are energetically less favorable to adsorption as the favorable sites will already be at capacity. Additionally, the increase in ion concentrations ,results in high ion collision rates and high diffusion rates which lead to decreased removal (Musumba *et al.*, 2020).

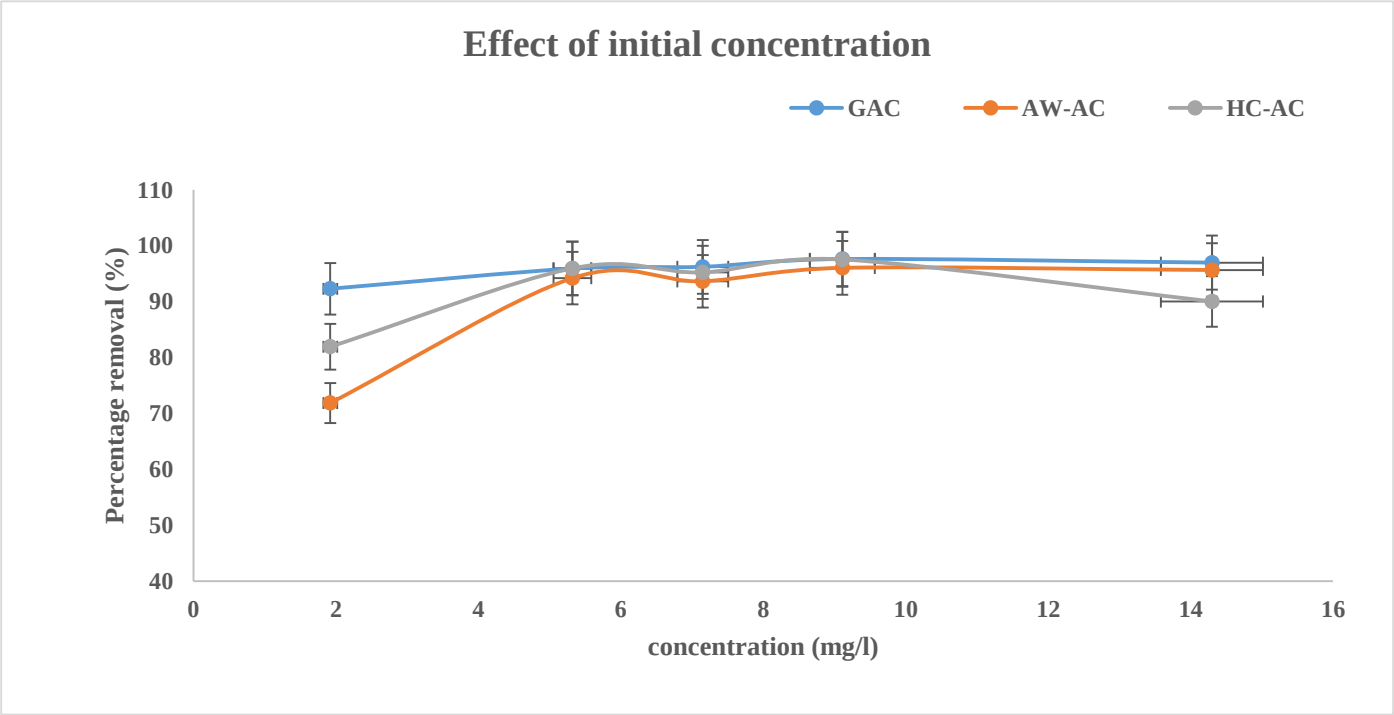

Figure 4.13 Effect of initial concentration on the adsorption of Pb (II) ions - initial concentration: 1.9-14.3 mg/L, solution volume: 100 mL, contact time: 120 min, adsorbent dose: 0.6 g for GAC and HC-AC, 0.8 g for AW-AC, and solution pH: 7.

4.4.4.4 Effect of Contact Time on Adsorption of Lead (II) Ions

The effect of contact time experiment was conducted at a contact time ranging from 10-150 minutes using the optimum conditions (pH 7, adsorbent dosage of 0.6 g for GAC and HC-AC, and 0.8 g for AW-AC, and initial concentration of 9.10 mg/L) found when varying the parameters in Sections 4.4.4.1-4.4.4.3. The effect of the contact time on the percentage removal of lead is displayed in Figure 4.14 . The adsorption was rapid in the initial stages. In the first 30 minutes GAC achieved a removal of 94.70 %, HC-AC achieved 98.01 %, and AW-AC achieved 93.11 %. This observed trend showing rapid removal in the initial rate of adsorption may have been accelerated by the presence of a sufficient number of active functional groups and vacant active sites on the activated carbons exterior surface (Moyo *et al.*, 2013; Guyo and Moyo, 2017; Mandal *et al.*, 2021). It could also be explained as being a result of the concentration gradient between the adsorbate in solution and the quantity of vacant sites on the surface of the adsorbent (Acharya *et al.*, 2009; Onundi *et al.*, 2010). Granular activated carbon (GAC) reached equilibrium faster than the other two adsorbents (HC-AC and AW-AC). From 40 minutes to 150 minutes the change in removal percentage was almost constant with a slight inflection at 150 minutes, indicating that equilibrium had been achieved. The HC-AC showed a slight decrease in uptake after 90 minutes which could be as a result of the saturation of the active sites after equilibrium had been reached (Guyo and Moyo, 2017). The increment of contact time after this point has been linked to a decrease in percentage removal due to reduction in available Pb (II) ions to bind to the remaining active sites (Mandal *et al.*, 2021). For AW-AC, the trend showed a gradual increase from 93.11 % at 30 minutes to 96.92 % at 120 minutes where equilibrium was

reached. The change in the rate of uptake after this was negligible. It can be noted that at the optimum conditions for each adsorbent HC-AC (99.33 %) showed the highest percentage removal followed by GAC (97.24 %) and lastly AW-AC (96.92 %).

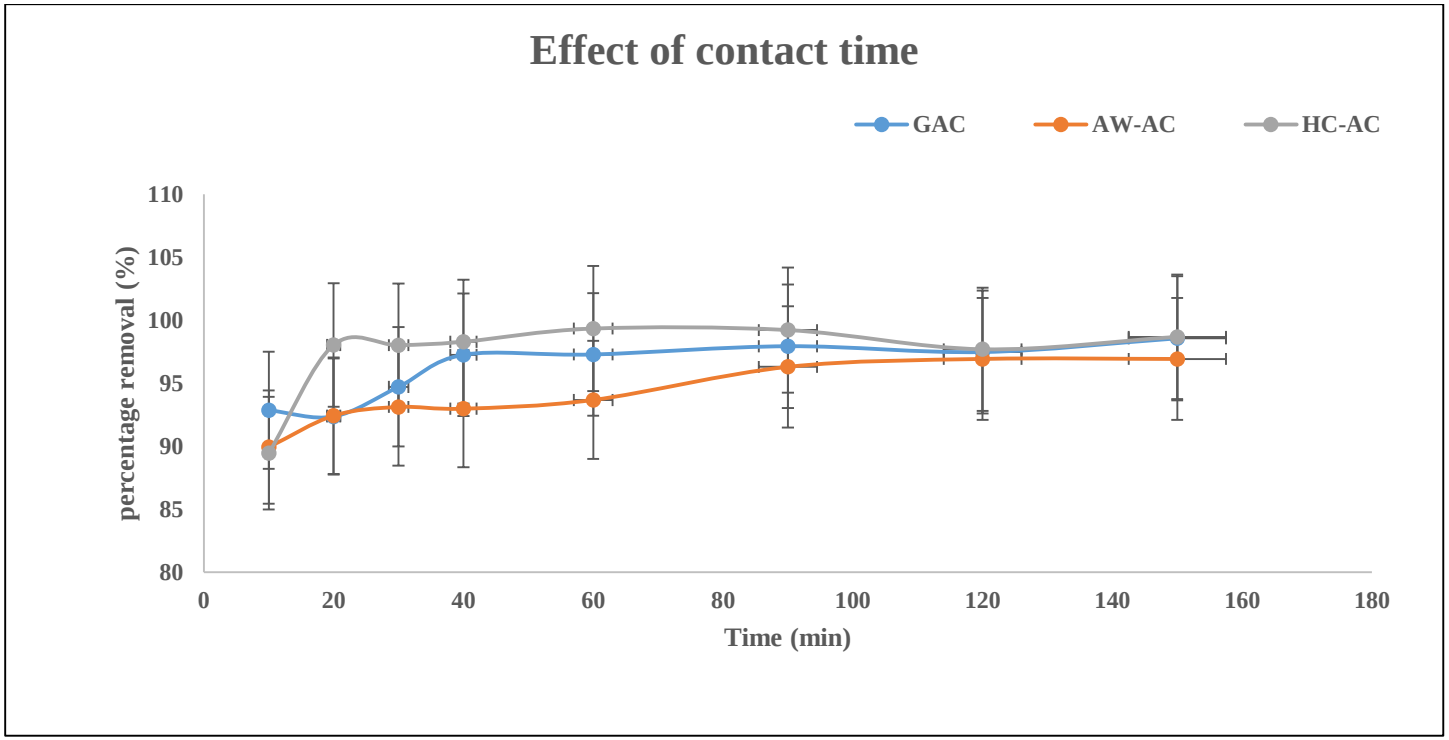

Figure 4.14 Effect of contact time on the adsorption of Pb (II) ions - initial concentration: 9.10 mg/L , solution volume: 100 mL, contact time: 150 min, adsorbent dose: 0.6 g for GAC and HC-AC, 0.8 g for AW-AC, and solution pH: 7.

4.4.5 Kinetic Studies for Pb (II) ions

The kinetics for the three adsorbents were investigated for a contact time of 150 minutes using the pseudo-first-order and pseudo-second-order model equations in Table 2.2. The parameters obtained from the plots of the equations are listed in Table 4.6.

The parameters of the two models presented in Table 4.6 were compared and it was found that the kinetic data was best suited to the Pseudo-second-order model for all the three adsorbents. The R^2 value for all the adsorbents was 0.9999 and the calculated adsorption capacity values for GAC, AW-AC, and HC-AC (1.501, 1.114 and 1.499 mg/g, respectively) were close to the experimental values, 1.495, 1.103 and 1.507 mg/g, respectively. This indicates that the correspondence between the PSO and the adsorption of the Pb (II) ions onto the adsorbents is high. According to (Ho and McKay, 1999a), an R^2 value greater than 0.996 is suggestive of chemisorption, which involves the exchange of electrons between the adsorbent and the adsorbate being the rate limiting step of the adsorption process.

Table 4.6 Kinetic parameters of Pb (II) ions adsorption onto GAC, AW-AC and HC-AC.

Kinetic model	Parameters	Unit	GAC	AW-AC	HC-AC
			Obtained value		
Pseudo-first-order	q_e	(mg/g)	0.3413	0.9761	0.9949
	K_1	min^{-1}	0.0111	0.0083	0.0167
	R^2		0.683	0.886	0.2443
Pseudo-second-order	q_e	(mg/g)	1.501	1.114	1.499
	q_e^2	(mg/g)	2.254	1.240	2.247
	K_2	min^{-1}	0.635	0.581	2.262
	R^2		0.9999	0.9999	0.9999

4.4.6 Isotherm Studies for the Adsorption of Lead (II) Ions

The experimental data of the three adsorbents was analyzed using the Langmuir and Freundlich isotherm model equations found in Table 2.3. The results obtained from the analysis were modelled and the parameters are listed in Table 4.7.

Table 4.7 Isotherm parameters of the adsorption of Pb (II) ions onto GAC, AW-AC and HC-AC

Adsorption isotherm	Parameters	Unit	GAC	AW-AC	HC-AC
			Obtained value		
Langmuir 1	q_{max}	(mg/g)	1.5360	-1.5364	24.0693
	K_L	min^{-1}	2.3592	-2.3607	579.3293
	R_L		0.0407	-0.0442	0.0002
	R^2		0.7835	0.0743	0.0023
Langmuir 2	q_{max}	(mg/g)	3.18264812	2.20561191	15.5527862
	K_L	min^{-1}	10.129249	4.86472392	241.889157
	R_L		0.00977589	0.02014211	0.00041324
	R^2		0.5713	0.7084	0.0446
Langmuir 3	q_{max}	(mg/g)	0.55001213	0.64003647	1.44200374
	K_L	min^{-1}	0.30251335	0.40964669	2.07937478
	R_L		0.24843897	0.19621436	0.04588472
	R^2		0.5713	0.7084	0.0446
Langmuir 4	q_{max}	(mg/g)	-1.3357346	0.40111218	4.76354432
	K_L	min^{-1}	1.78418695	0.16089098	22.6913545
	R_L		0.05307329	0.38330187	0.00438763
	R^2		0.3339	0.1235	0.0512
Freundlich	n	(mg/g)	0.5725	-12.2629	2.3823
	K_f	(mg/g)	12.0749	0.8755	1.4372
	R^2		0.7824	0.0007	0.1643

The analysis of the experimental results using the Langmuir and Freundlich isotherms shows that the data for GAC had a similar fit for both the Langmuir 1 and Freundlich isotherms (R^2 = 0.7835 and 0.7824, respectively), with the best fit being with the Langmuir 1 isotherm. The R^2 values for AW-AC showed that Langmuir 2 was the best with a value of 0.708. Langmuir 2 was chosen over Langmuir 3 as it had the higher adsorption capacity ($q_{max)}$ of 2.206 mg/g, while that of Langmuir 3 was 0.640 mg/g. The R^2 value for HC-AC was generally low for both isotherms with the R^2 value for the Freundlich being the higher value at 0.164. These results suggest that there was monolayer coverage of the adsorbate on the adsorbents GAC and AW-AC, while the coverage on HC-AC was multilayer in nature.

4.5 Closure

The characteristics and adsorption capacity of the prepared activated carbon (HC-AC) were ascertained and compared to those of the commercially activated carbon (GAC) and a green activated carbon (AW-AC) according to the objectives set out in Chapter 1. The results show that activated carbon was successfully derived from hydrochar and that the hydrochar derived activated carbon (HC-AC) was efficient in removing both methylene blue and lead ions from aqueous solution. At the optimum conditions, (pH, adsorbent dosage, initial solute concentration, and equilibrium time) HC-AC performed better than GAC and AW-AC.

Chapter 5 Conclusions and Recommendations

5.1 Conclusions

The key findings on the characterization and adsorption studies of the three carbons (mainly the hydrochar derived activated carbon) in line with the objectives set out in Chapter 1 are summarized as follows:

- Activated carbon was successfully produced by the pyrolysis of hydrochar derived from a combination of primary sludge and waste activated sludge at a temperature of 425 °C under an N_2 atmosphere with no further activation.
- Of the three activated carbons, HC-AC exhibited the lowest microporocity as determined by its low iodine number (110.66mg/g), however it showed an abundance of oxygen and sufficient oxygen functional groups which were attributed for its high removal of the dye and metal ions in solution.
- The results showed that removal of the dye and metal ions was largely dependent on the pH of the solution. The highest percentage removal for both pollutants was achieved at alkaline conditions. The optimum pH for MB adsorption was 8 for GAC and AW-AC, and 11 for HC-AC. The optimum pH for the adsorption of Pb (II) ions was 7.
- In reflection of the hypothesis in Chapter 1, the removal of methylene blue by HC-AC and GAC was similar (at 99.28 ± 0.004 % and 99.13 ± 0.04 %, respectively). For the lead adsorption tests HC-AC performed slightly better than GAC, achieving a removal of 99.33 ± 0.09 % and 97.24 ± 0.48 %, respectively.

- The results for the kinetic studies for the three adsorbents and the two adsorbates show a high correlation with the pseudo-second-order equation. All had an R^2 value greater than 0.999.
- The results of the isotherm studies for the adsorption of methylene blue onto the three adsorbents indicated that the equilibrium data of the three adsorbents was best suited to the linear forms of the Langmuir Isotherm. The R^2 values for GAC, AW-AC, and HC-AC were 0.9993, 0.9764, and 0.9877, respectively.
- The results of the isotherm studies for the adsorption of lead onto the three adsorbents indicated that the equilibrium data of GAC and AW-AC was best suited to the linear forms of the Langmuir Isotherm. The R^2 values for GAC and AW-AC were 0.7835 and 0.708 respectively. The data for HC-AC showed low correlation with both the Langmuir and Freundlich equations but the higher R^2 of the two was found to be that of the Freundlich isotherm at 0.164.

5.2 Recommendations

- The HC-AC could be further activated by chemical or physical means to improve its surface area.
- The HC-AC could be employed in a multiple-metal system to investigate if it exhibits high removal efficiencies as it has in the single-metal system used in this study.
- The regeneration and reuse of HC-AC in adsorption could be investigated to find out if it is a single use product.
- The temperature of adsorption experiments could be conducted to see if it has a significant effect on the adsorption process.
- The cost of production of the HC-AC could be investigated to inform production at a larger scale.

References

Abdul Halim Abdullah, Anuar Kassim, Zulkarnain Zainal, Mohd Zobir Hussien, Dzulkefly Kuang, F. A. and O. S. W. (2001) 'Preparation and Characterization of Activated Carbon from Gelam Wood Bark (Melaleuca cajuputi)', *Malaysian Journal of Analytical Sciences*, Vol. 7(No. 1), pp. 65–68.

Acharya, J. *et al.* (2009) 'Removal of lead(II) from wastewater by activated carbon developed from Tamarind wood by zinc chloride activation', *Chemical Engineering Journal*, 149(1–3), pp. 249–262. doi: 10.1016/j.cej.2008.10.029.

Ahmad, M. A. *et al.* (2021) 'Optimization and batch studies on adsorption of Methylene blue dye using pomegranate fruit peel based adsorbent', *Chemical Data Collections*, 32, p. 100676. doi: 10.1016/j.cdc.2021.100676.

Alam, S. *et al.* (2021) 'Preparation of activated carbon from the wood of paulownia tomentosa as an efficient adsorbent for the removal of acid red 4 and methylene blue present in wastewater', *Water (Switzerland)*, 13(11). doi: 10.3390/w13111453.

Alghamdi, A. A. *et al.* (2019) 'Efficient adsorption of lead (II) from aqueous phase solutions using polypyrrole-based activated carbon', *Materials*, 12(12). doi: 10.3390/ma12122020.

Ali, I. (2012) 'New generation adsorbents for water treatment', *Chemical Reviews*, 112(10), pp. 5073–5091. doi: 10.1021/cr300133d.

Aljamali, N. M., Khdur, R. A. and Alfatlawi, I. O. (2021) 'Physical and Chemical Adsorption and its Applications', (December). doi: 10.37628/IJTCK.

Almahbashi, N. M. Y. *et al.* (2021) 'Optimization of Preparation Conditions of Sewage sludge based Activated Carbon', *Ain Shams Engineering Journal*, 12(2), pp. 1175–1182. doi: 10.1016/j.asej.2020.07.026.

ASTM D2854 - 96 (2000) 'Standard Test Method for Apparent Density of Activated Carbon', 96, pp. 1–3.

ASTM D4607-94 (2006) 'Standard Test Method for Determination of Iodine Number of Activated Carbon', 94, pp. 1–5.

Asuquo, E. *et al.* (2017) 'Adsorption of Cd(II) and Pb(II) ions from aqueous solutions using mesoporous activated carbon adsorbent: Equilibrium, kinetics and characterisation studies', *Journal of Environmental Chemical Engineering*, 5(1), pp. 679–698. doi: 10.1016/j.jece.2016.12.043.

Badawi, A. K., Abd Elkodous, M. and Ali, G. A. M. (2021) 'Recent advances in dye and metal ion removal using efficient adsorbents and novel nano-based materials: An overview', *RSC Advances*, 11(58), pp. 36528–36553. doi: 10.1039/d1ra06892j.

Batool, F. *et al.* (2018) 'Study of Isothermal, Kinetic, and Thermodynamic Parameters for Adsorption of Cadmium: An Overview of Linear and Nonlinear Approach and Error Analysis', *Bioinorganic Chemistry and Applications*, 2018. doi: 10.1155/2018/3463724.

Bello, O. S. *et al.* (2008) 'Adsorption of methylene blue onto activated carbon derived from periwinkle shells: Kinetics and equilibrium studies', *Chemistry and Ecology*, 24(4), pp. 285–295. doi: 10.1080/02757540802238341.

Bergström, J. (2015) *Experimental Characterization Techniques*, *Mechanics of Solid Polymers*. doi: 10.1016/b978-0-323-31150-2.00002-9.

Bernard, E., Jimoh, a and Odigure, J. O. (2013) 'Heavy Metals Removal from Industrial Wastewater by Activated Carbon Prepared from Coconut Shell', *Research Journal of Chemical Sciences*, 3(8), pp. 3–9.

Bernardo, M. *et al.* (2020) 'Porous carbons derived from hydrothermally treated biogas digestate', *Waste Management*, 105, pp. 170–179. doi: 10.1016/j.wasman.2020.02.011.

Berthomieu, C. and Hienerwadel, R. (2009) 'Fourier transform infrared (FTIR) spectroscopy', *Photosynthesis Research*, 101(2–3), pp. 157–170. doi: 10.1007/s11120-009-9439-x.

Bestani, B. *et al.* (2008) 'Methylene blue and iodine adsorption onto an activated desert plant', *Bioresource Technology*, 99(17), pp. 8441–8444. doi: 10.1016/j.biortech.2008.02.053.

Bhatnagar, A. *et al.* (2013) 'An overview of the modification methods of activated carbon for its water treatment applications', *Chemical Engineering Journal*, 219, pp. 499–511. doi: 10.1016/j.cej.2012.12.038.

Boonpoke, A. *et al.* (2013) 'Synthesis of activated carbon and MCM-41 from bagasse and rice husk and their carbon dioxide adsorption capacity', *Journal of Sustainable & Environment*, 2(October 2014), pp. 77–81. Available at: http://antispam.kmutt.ac.th/index.php/JSEE/article/view/9188.

Boontham, W. (2016) 'Removal of lead from solution by using low cost adsorbents from aplaceae family'.

Bottom, R. (2008) 'Thermogravimetric Analysis', *Principles and Applications of Thermal Analysis*, 1(906), pp. 87–118. doi: 10.1002/9780470697702.ch3.

Brunauer, S., Emmett, P. H. and Teller, E. (1938) 'Adsorption of Gases in Multimolecular Layers', *J. Am.Chem.Soc.*, 60(2), pp. 309–319.

CEFIC, E. (1986) 'Test Methods for Activated Carbon', *European Council Of Chemical Manufacturers Federation/European Chemical Industry Council*, pp. 9–43.

Chan, L. S. *et al.* (2012) 'Error analysis of adsorption isotherm models for acid

dyes onto bamboo derived activated carbon', *Chinese Journal of Chemical Engineering*, 20(3), pp. 535–542. doi: 10.1016/S1004-9541(11)60216-4.

Chen, X., Jeyaseelan, S. and Graham, N. (2002) 'Physical and chemical properties study of the activated carbon made from sewage sludge', *Waste Management*, 22(7), pp. 755–760. doi: 10.1016/S0956-053X(02)00057-0.

Chia, C. H. *et al.* (2012) 'Imaging of mineral-enriched biochar by FTIR, Raman and SEM-EDX', *Vibrational Spectroscopy*, 62, pp. 248–257. doi: 10.1016/j.vibspec.2012.06.006.

Chowdhury, I. R. *et al.* (2022) *Removal of lead ions (Pb2+) from water and wastewater: a review on the low-cost adsorbents*, *Applied Water Science*. Springer International Publishing. doi: 10.1007/s13201-022-01703-6.

Chowdhury, Z. Z. (2013) 'Preparation , Characterization and Adsorption Studies of Heavy Metals Onto Activated Adsorbent Materials Derived From Agricultural Residues Thesis Submitted in Fulfilment of the Requirements for the Degree of Doctor of Philosophy Department of Chemistry F', pp. 23–24.

Chung, H. K. *et al.* (2015) 'Application of Langmuir and Freundlich isotherms to predict adsorbate removal efficiency or required amount of adsorbent', *Journal of Industrial and Engineering Chemistry*, 28, pp. 241–246. doi: 10.1016/j.jiec.2015.02.021.

Comm Rep (1974) 'Awwa Standard for Granular Activated Carbon.', *Journal / American Water Works Association*, 66(11), pp. 672–681. doi: 10.1002/j.1551-8833.1974.tb02114.x.

Crini, G. *et al.* (2019) 'Conventional and non-conventional adsorbents for wastewater treatment', *Environmental Chemistry Letters*, 17(1), pp. 195–213. doi: 10.1007/s10311-018-0786-8.

Crini, G. and Lichtfouse, E. (2019) 'Advantages and disadvantages of techniques used for wastewater treatment', *Environmental Chemistry Letters*, 17(1), pp. 145–155. doi: 10.1007/s10311-018-0785-9.

Cuhadaroglu, D. and Uygun, O. A. (2008) 'Production and characterization of activated carbon from a bituminous coal by chemical activation', *African Journal of Biotechnology*, 7(20), pp. 3706–3713.

Dąbrowski, A. (2001) 'Adsorption - From theory to practice', *Advances in Colloid and Interface Science*, 93(1–3), pp. 135–224. doi: 10.1016/S0001-8686(00)00082-8.

Danish, M. *et al.* (2020) 'Analysis using image segmentation for the elemental composition of activated carbon', *MethodsX*, 7, pp. 1–9. doi: 10.1016/j.mex.2020.100983.

Danish, M. and Ahmad, T. (2018) 'A review on utilization of wood biomass

as a sustainable precursor for activated carbon production and application', *Renewable and Sustainable Energy Reviews*, 87(February), pp. 1–21. doi: 10.1016/j.rser.2018.02.003.

Dichiara, A. B., Weinstein, S. J. and Rogers, R. E. (2015) 'On the Choice of Batch or Fixed Bed Adsorption Processes for Wastewater Treatment'. doi: 10.1021/acs.iecr.5b02350.

Du, M. *et al.* (2019) 'Study on Preparation of Activated Carbon from Sludge', *IOP Conference Series: Materials Science and Engineering*, 484(1), pp. 8–13. doi: 10.1088/1757-899X/484/1/012013.

Dutta, S. *et al.* (2021) 'Recent advances on the removal of dyes from wastewater using various adsorbents: A critical review', *Materials Advances*, 2(14), pp. 4497–4531. doi: 10.1039/d1ma00354b.

Ebrahimian Pirbazari, A. *et al.* (2014) 'Alkali treated Foumanat tea waste as an efficient adsorbent for methylene blue adsorption from aqueous solution', *Water Resources and Industry*, 6, pp. 64–80. doi: 10.1016/j.wri.2014.07.003.

Ebrahimian Pirbazari, A., Saberikhah, E. and Habibzadeh Kozani, S. S. (2014) 'Fe3O4-wheat straw: Preparation, characterization and its application for methylene blue adsorption', *Water Resources and Industry*, 7–8, pp. 23–37. doi: 10.1016/j.wri.2014.09.001.

El-Dairi, M. *et al.* (2014) 'Introduction', *Alliances : Re/envisioning Indigenous-non-indigenous Relationships*, 25(Ii), pp. 11–28.

Fan, S. *et al.* (2017) 'Removal of methylene blue from aqueous solution by sewage sludge-derived biochar: Adsorption kinetics, equilibrium, thermodynamics and mechanism', *Journal of Environmental Chemical Engineering*, 5(1), pp. 601–611. doi: 10.1016/j.jece.2016.12.019.

Filho, A. V. *et al.* (2020) 'Preparation and characterization of activated carbon obtained from water treatment plant sludge for removal of cationic dye from wastewater', *Processes*, 8(12), pp. 1–13. doi: 10.3390/pr8121549.

De Filippis, P. *et al.* (2013) 'Production and characterization of adsorbent materials from sewage sludge by pyrolysis', *Chemical Engineering Transactions*, 32, pp. 205–210. doi: 10.3303/CET1332035.

Fu, F. and Wang, Q. (2011) 'Removal of heavy metal ions from wastewaters: A review', *Journal of Environmental Management*, 92(3), pp. 407–418. doi: 10.1016/j.jenvman.2010.11.011.

Gad, H. M. H., El-Mouhty, N. R. A. and Aly, H. F. (2009) 'Applicability of activated carbon to treatment of waste containing iodine-labeled compounds', *Separation Science and Technology*, 44(3), pp. 681–711. doi: 10.1080/01496390802437172.

Giorcelli, M. *et al.* (2021) 'High-Temperature Annealed Biochar as a Conductive Filler for the Production of Piezoresistive Materials for Energy Conversion Application', *ACS Applied Electronic Materials*, 3(2), pp. 838–844. doi: 10.1021/acsaelm.0c00971.

Gude, V. G. (2017) 'Desalination and water reuse to address global water scarcity', *Reviews in Environmental Science and Biotechnology*, 16(4), pp. 591–609. doi: 10.1007/s11157-017-9449-7.

Gupta, V. K. *et al.* (2009) 'Low-Cost adsorbents: Growing approach to wastewater treatmenta review', *Critical Reviews in Environmental Science and Technology*, 39(10), pp. 783–842. doi: 10.1080/10643380801977610.

Gupta, V. K. and Suhas (2009) 'Application of low-cost adsorbents for dye removal - A review', *Journal of Environmental Management*, 90(8), pp. 2313–2342. doi: 10.1016/j.jenvman.2008.11.017.

Guyo, U. and Moyo, M. (2017) 'Cowpea pod (Vigna unguiculata) biomass as a low-cost biosorbent for removal of Pb(II) ions from aqueous solution', *Environmental Monitoring and Assessment*, 189(2). doi: 10.1007/s10661-016-5728-y.

Hadi, P. *et al.* (2015) 'A critical review on preparation, characterization and utilization of sludge-derived activated carbons for wastewater treatment', *Chemical Engineering Journal*, 260, pp. 895–906. doi: 10.1016/j.cej.2014.08.088.

Hameed, B. H., Din, A. T. M. and Ahmad, A. L. (2007) 'Adsorption of methylene blue onto bamboo-based activated carbon: Kinetics and equilibrium studies', *Journal of Hazardous Materials*, 141(3), pp. 819–825. doi: 10.1016/j.jhazmat.2006.07.049.

Heidarinejad, Z. *et al.* (2020) 'Methods for preparation and activation of activated carbon: a review', *Environmental Chemistry Letters*, 18(2), pp. 393–415. doi: 10.1007/s10311-019-00955-0.

Herschy, R. W. (2012) 'Water quality for drinking: WHO guidelines', *Encyclopedia of Earth Sciences Series*, pp. 876–883. doi: 10.1007/978-1-4020-4410-6_184.

Ho, Y. S. and McKay, G. (1999a) 'Pseudo-second order model for sorption processes', *Process Biochemistry*, 34(5), pp. 451–465. doi: 10.1016/S0032-9592(98)00112-5.

Ho, Y. S. and McKay, G. (1999b) 'The sorption of lead(II) ions on peat', *Water Research*, 33(2), pp. 578–584. doi: 10.1016/S0043-1354(98)00207-3.

Hoon, Q. and Cheok, N. (2013) 'Activated Carbon Manufacture: An opportunity for sustainable management of problematic waste biomass',

(January). Available at: https://spiral.imperial.ac.uk/bitstream/10044/1/17796/1/Cheok-QHN-2013-PhD-Thesis.pdf.

Hubbe, M. A., Azizian, S. and Douven, S. (2019) 'Implications of Apparent Pseudo-Second-Order Adsorption Kinetics onto Cellulosic Materials : A Review', 14, pp. 7582–7626.

Hwang, N. and Barron, A. R. (2011) 'BET Surface Area Analysis of Nanoparticles', *The connexions project*, pp. 1–11.

Jawing, D. *et al.* (2021) 'Palm Kernel Shell Activated Carbon for Lead and Methylene Blue Removal', *Transactions on Science and Technology*, 8(3–2), pp. 290–304.

Jeyakumar, R. P. S. and Chandrasekaran, V. (2014) 'Preparation and characterization of activated carbons derived from marine green algae ulva fasciata sp.', *Asian Journal of Chemistry*, 26(9), pp. 2545–2549. doi: 10.14233/ajchem.2014.15723.

Jjagwe, J. *et al.* (2021) 'Synthesis and Application of Granular Activated Carbon from Biomass Waste Materials for Water Treatment: A Review', *Journal of Bioresources and Bioproducts*, 6(4), pp. 292–322. doi: 10.1016/j.jobab.2021.03.003.

K D Vernon-Parry (2000) 'Microscopy : an introduction', 13(4), pp. 40–44.

Kavand, M., Eslami, P. and Razeh, L. (2020) 'The adsorption of cadmium and lead ions from the synthesis wastewater with the activated carbon: Optimization of the single and binary systems', *Journal of Water Process Engineering*, 34(August 2019), p. 101151. doi: 10.1016/j.jwpe.2020.101151.

Khan, Idrees *et al.* (2022) 'Review on Methylene Blue: Its Properties, Uses, Toxicity and Photodegradation', *Water (Switzerland)*, 14(2). doi: 10.3390/w14020242.

Kristianto, H. *et al.* (2016) 'The effect of activated carbon support surface modification on characteristics of carbon nanospheres prepared by deposition precipitation of Fe-catalyst', *IOP Conference Series: Materials Science and Engineering*, 162(1). doi: 10.1088/1757-899X/162/1/012034.

Kudelski, A. (2008) 'Analytical applications of Raman spectroscopy', *Talanta*, 76(1), pp. 1–8. doi: 10.1016/j.talanta.2008.02.042.

Li, S. *et al.* (2020) 'Engineered Biochar Production and Its Potential Benefits in a Closed-Loop Water-Reuse Agriculture System', (3).

Li, W. H., Yue, Q. Y., Gao, B. Y., Ma, Z. H., *et al.* (2011) 'Preparation and utilization of sludge-based activated carbon for the adsorption of dyes from aqueous solutions', *Chemical Engineering Journal*, 171(1), pp. 320–327. doi:

10.1016/j.cej.2011.04.012.

Li, W. H., Yue, Q. Y., Gao, B. Y., Wang, X. J., *et al.* (2011) 'Preparation of sludge-based activated carbon made from paper mill sewage sludge by steam activation for dye wastewater treatment', *Desalination*, 278(1–3), pp. 179–185. doi: 10.1016/j.desal.2011.05.020.

Li, Y.-H. *et al.* (2002) 'Lead adsorption on carbon nanotubes', *Chemical physics letters*, 357, pp. 236–266. doi: 10.1016/b978-008044464-2.50020-1.

Li, Yili *et al.* (2016) 'Preparation and analysis of activated carbon from sewage sludge and corn stalk', *Advanced Powder Technology*, 27(2), pp. 684–691. doi: 10.1016/j.apt.2016.02.029.

Lin, K. H. *et al.* (2021) 'Product characteristics of sludge pyrolysis and adsorption performance of metals by char', *Sustainability (Switzerland)*, 13(21), pp. 1–16. doi: 10.3390/su132112125.

Liu, T. *et al.* (2017) 'Heteroatoms doped porous carbon derived from hydrothermally treated sewage sludge: Structural characterization and environmental application', *Journal of Environmental Management*, 197, pp. 151–158. doi: 10.1016/j.jenvman.2017.03.082.

Lyon, L. A. *et al.* (1998) 'Ra m a n Spe c t rosc opy', 2700(98), pp. 341–362.

Mandal, S. *et al.* (2021) 'Mesoporous activated carbon as a green adsorbent for the removal of heavy metals and Congo red: Characterization, adsorption kinetics, and isotherm studies', *Journal of Contaminant Hydrology*, 243(August), p. 103869. doi: 10.1016/j.jconhyd.2021.103869.

Mariana, M. *et al.* (2021) 'Recent advances in activated carbon modification techniques for enhanced heavy metal adsorption', *Journal of Water Process Engineering*, 43(June), p. 102221. doi: 10.1016/j.jwpe.2021.102221.

Medhat, A. *et al.* (2021) 'Efficiently activated carbons from corn cob for methylene blue adsorption', *Applied Surface Science Advances*, 3(August 2020), p. 100037. doi: 10.1016/j.apsadv.2020.100037.

Mkungunugwa, T. *et al.* (2021) 'Synthesis and Characterisation of Activated Carbon Obtained from Marula (Sclerocarya birrea) Nutshell', *Journal of Chemistry*, 2021. doi: 10.1155/2021/5552224.

Mohan, D. *et al.* (2007) 'Sorption of arsenic, cadmium, and lead by chars produced from fast pyrolysis of wood and bark during bio-oil production', *Journal of Colloid and Interface Science*, 310(1), pp. 57–73. doi: 10.1016/j.jcis.2007.01.020.

Mohan, D. *et al.* (2020) 'Batch and continuous fixed-bed lead removal using himalayan pine needle biochar: Isotherm and kinetic studies', *ACS Omega*, 5(27), pp. 16366–16378. doi: 10.1021/acsomega.0c00216.

Mokhena, T. *et al.* (2016) 'We are IntechOpen , the world ' s leading publisher of Open Access books Built by scientists , for scientists TOP 1 %', *Intech*, pp. 225–240. Available at: https://www.intechopen.com/books/advanced-biometric-technologies/liveness-detection-in-biometrics.

Moyo, M. *et al.* (2013) 'Adsorption batch studies on the removal of Pb(II) using maize tassel based activated carbon', *Journal of Chemistry*, 2013. doi: 10.1155/2013/508934.

Musah, M. *et al.* (2022) 'Adsorption Kinetics and Isotherm Models: A Review', *Caliphate Journal of Science and Technology*, 4(1), pp. 20–26. doi: 10.4314/cajost.v4i1.3.

Musumba, G. *et al.* (2020) 'Adsorption of Lead (II) and Copper (II) Ions from Mono Synthetic Aqueous Solutions Using Bio-Char from <i>Ficus natalensis</i> Fruits', *Journal of Encapsulation and Adsorption Sciences*, 10(04), pp. 71–84. doi: 10.4236/jeas.2020.104004.

Musvoto, E. *et al.* (2018) *"Energy Recovery from Wastewater Sludge – A Review of Appropriate Emerging and Established Technologies for the South African Industry".* PWater Research Commission. Available at: www.wrc.org.za%0AThe.

Ntuli, V. and Hapazari, I. (2013) 'Sustainable waste management by production of activated carbon from agroforestry residues', *South African Journal of Science*, 109(1–2), pp. 1–6. doi: 10.1590/sajs.2013/1077.

Onundi, Y. B. *et al.* (2010) 'Adsorption of copper, nickel and lead ions from synthetic semiconductor industrial wastewater by palm shell activated carbon', *International Journal of Environmental Science and Technology*, 7(4), pp. 751–758. doi: 10.1007/BF03326184.

Onwordi, C. T. *et al.* (2019) 'Comparative study of the adsorption capacity of lead (II) ions onto bean husk and fish scale from aqueous solution', *Journal of Water Reuse and Desalination*, 9(3), pp. 249–262. doi: 10.2166/wrd.2019.061.

Osmari, T. A. *et al.* (2013) 'Statistical analysis of linear and non-linear regression for the estimation of adsorption isotherm parameters', *Adsorption Science and Technology*, 31(5), pp. 433–458. doi: 10.1260/0263-6174.31.5.433.

Otero, M. *et al.* (2003) 'Elimination of organic water pollutants using adsorbents obtained from sewage sludge', *Dyes and Pigments*, 57(1), pp. 55–65. doi: 10.1016/S0143-7208(03)00005-6.

Papanikolaou, N. C., Hatzidaki, E. G. and Belivanis, S. (2005) 'Lead toxicity update . A brief review', (May 2014).

Patawat, C. *et al.* (2020) 'Preparation of activated carbon fromDipterocarpus alatusfruit and its application for methylene blue adsorption', *RSC Advances*,

10(36), pp. 21082–21091. doi: 10.1039/d0ra03427d.

Pathania, D., Sharma, S. and Singh, P. (2017) 'Removal of methylene blue by adsorption onto activated carbon developed from Ficus carica bast', *Arabian Journal of Chemistry*, 10, pp. S1445–S1451. doi: 10.1016/j.arabjc.2013.04.021.

Pedroza, M. M. *et al.* (2014) 'Characterization of the products from the pyrolysis of sewage sludge in 1 kg/h rotating cylinder reactor', *Journal of Analytical and Applied Pyrolysis*, 105, pp. 108–115. doi: 10.1016/j.jaap.2013.10.009.

Piaskowski, K., Świderska-Dąbrowska, R. and Zarzycki, P. K. (2018) 'Dye removal from water and wastewater using various physical, chemical, and biological processes', *Journal of AOAC International*, 101(5), pp. 1371–1384. doi: 10.5740/jaoacint.18-0051.

Puccini, M. *et al.* (2017) 'Activated carbon from hydrochar produced by hydrothermal carbonization of wastes', *Chemical Engineering Transactions*, 57(July), pp. 169–174. doi: 10.3303/CET1757029.

El Qada, E. N., Allen, S. J. and Walker, G. M. (2006) 'Adsorption of Methylene Blue onto activated carbon produced from steam activated bituminous coal: A study of equilibrium adsorption isotherm', *Chemical Engineering Journal*, 124(1–3), pp. 103–110. doi: 10.1016/j.cej.2006.08.015.

Qiu, H. *et al.* (2009) 'Critical review in adsorption kinetic models *', 10(5), pp. 716–724. doi: 10.1631/jzus.A0820524.

Qureshi, K. *et al.* (2008) 'Physical and Chemical Analysis of Activated Carbon Prepared from Sugarcane Bagasse and Use for Sugar Decolorisation', *International Journal of Chemical and Biological Engineering*, 1(3), pp. 144–148. Available at: https://citeseerx.ist.psu.edu/viewdoc/summary?doi=10.1.1.193.5317.

Raposo, F., De La Rubia, M. A. and Borja, R. (2009) 'Methylene blue number as useful indicator to evaluate the adsorptive capacity of granular activated carbon in batch mode: Influence of adsorbate/adsorbent mass ratio and particle size', *Journal of Hazardous Materials*, 165(1–3), pp. 291–299. doi: 10.1016/j.jhazmat.2008.09.106.

Ravichandran, P. *et al.* (2018) 'Optimizing the route for production of activated carbon from Casuarina equisetifolia fruit waste', *Royal Society Open Science*, 5(7). doi: 10.1098/rsos.171578.

Rengaraj, S. *et al.* (2002) 'Agricultural solid waste for the removal of organics: Adsorption of phenol from water and wastewater by palm seed coat activated carbon', *Waste Management*, 22(5), pp. 543–548. doi: 10.1016/S0956-053X(01)00016-2.

Rozada, F. *et al.* (2003) 'Dye adsorption by sewage sludge-based activated carbons in batch and fixed-bed systems', *Bioresource Technology*, 87(3), pp. 221–230. doi: 10.1016/S0960-8524(02)00243-2.

RShashankVRaman, by (2015) 'PREPARATION AND CHARACTERIZATION OF ACTIVATED CARBON FROM WASTE FOOD PACKAGING POLYMERS Master of Technology (5 year Integrated Dual Degree Course) in Chemical Engineering'.

Saadatkhah, N. *et al.* (2020) 'Experimental methods in chemical engineering: Thermogravimetric analysis—TGA', *Canadian Journal of Chemical Engineering*, 98(1), pp. 34–43. doi: 10.1002/cjce.23673.

Sacksteder, C. and Barry, B. A. (2001) 'Fourier transform infrared spectroscopy: A molecular approach to an organismal question', *Journal of Phycology*, 37(2), pp. 197–199. doi: 10.1046/j.1529-8817.2001.037002197.x.

Saha, N. *et al.* (2019) 'Effect of Pyrolysis Temperature on Acidic Oxygen-Containing Functional Groups and Electron Storage Capacities of Pyrolyzed Hydrochars', *ACS Sustainable Chemistry and Engineering*, 7(9), pp. 8387–8396. doi: 10.1021/acssuschemeng.9b00024.

Sajjadi, B., Chen, W. Y. and Egiebor, N. O. (2019) 'A comprehensive review on physical activation of biochar for energy and environmental applications', *Reviews in Chemical Engineering*, 35(6), pp. 735–776. doi: 10.1515/revce-2017-0113.

Saka, C. (2012) 'BET, TG-DTG, FT-IR, SEM, iodine number analysis and preparation of activated carbon from acorn shell by chemical activation with ZnCl2', *Journal of Analytical and Applied Pyrolysis*, 95, pp. 21–24. doi: 10.1016/j.jaap.2011.12.020.

Saleem, J. *et al.* (2019) 'Production and applications of activated carbons as adsorbents from olive stones', *Biomass Conversion and Biorefinery*, 9(4), pp. 775–802. doi: 10.1007/s13399-019-00473-7.

SANS 241 (2015) 'DRINKING WATER SANS 241 - 1:2015'.

Saravanan, A. *et al.* (2021) 'Effective water/wastewater treatment methodologies for toxic pollutants removal: Processes and applications towards sustainable development', *Chemosphere*, 280, p. 130595. doi: 10.1016/j.chemosphere.2021.130595.

Sazali, Norsuhailizah, Harun, Z. and Sazali, Norazlianie (2020) 'A Review on Batch and Column Adsorption of Various Adsorbent Towards the Removal of Heavy Metal', 2(2), pp. 66–88.

Shen, W., Li, Z. and Liu, Y. (2012) 'Surface Chemical Functional Groups Modification of Porous Carbon', *Recent Patents on Chemical Engineeringe*,

1(1), pp. 27–40. doi: 10.2174/2211334710801010027.

Simonin, J. P. (2016) 'On the comparison of pseudo-first order and pseudo-second order rate laws in the modeling of adsorption kinetics', *Chemical Engineering Journal*, 300, pp. 254–263. doi: 10.1016/j.cej.2016.04.079.

Singh, B. *et al.* (2017) 'Biochar pH, electrical conductivity and liming potential', *Biochar: A Guide to Analytical Methods*, (June 2018), pp. 23–38.

Singh, S., Sidhu, G. K. and Singh, H. (2019) 'Removal of methylene blue dye using activated carbon prepared from biowaste precursor', *Indian Chemical Engineer*, 61(1), pp. 28–39. doi: 10.1080/00194506.2017.1408431.

Sinha, P. *et al.* (2019) 'Surface Area Determination of Porous Materials Using the Brunauer-Emmett-Teller (BET) Method: Limitations and Improvements', *Journal of Physical Chemistry C*, 123(33), pp. 20195–20209. doi: 10.1021/acs.jpcc.9b02116.

Smith, K. M. *et al.* (2009) 'Sewage sludge-based adsorbents: A review of their production, properties and use in water treatment applications', *Water Research*, 43(10), pp. 2569–2594. doi: 10.1016/j.watres.2009.02.038.

Tan, I. A. W., Ahmad, A. L. and Hameed, B. H. (2008) 'Adsorption of basic dye using activated carbon prepared from oil palm shell: batch and fixed bed studies', *Desalination*, 225(1–3), pp. 13–28. doi: 10.1016/j.desal.2007.07.005.

Tan, K. L. and Hameed, B. H. (2017) 'Insight into the adsorption kinetics models for the removal of contaminants from aqueous solutions', *Journal of the Taiwan Institute of Chemical Engineers*, 74, pp. 25–48. doi: 10.1016/j.jtice.2017.01.024.

Tejada-Tovar, C. *et al.* (2022) 'The elimination of lead(II) ions in a solution by bio-adsorption: Kinetics, equilibrium, and thermodynamics', *Journal of Water and Land Development*, 53, pp. 118–127. doi: 10.24425/jwld.2022.140787.

Toles, C. A. *et al.* (2000) 'Acid-activated carbons from almond shells: Physical, chemical and adsorptive properties and estimated cost of production', *Bioresource Technology*, 71(1), pp. 87–92. doi: 10.1016/S0960-8524(99)00029-2.

Tomczyk, A. (2020) 'Biochar physicochemical properties : pyrolysis temperature and feedstock kind effects', *Reviews in Environmental Science and Bio/Technology*, 19(1), pp. 191–215. doi: 10.1007/s11157-020-09523-3.

Tseng, R. L., Wu, F. C. and Juang, R. S. (2010) 'Characteristics and applications of the Lagergren's first-order equation for adsorption kinetics', *Journal of the Taiwan Institute of Chemical Engineers*, 41(6), pp. 661–669. doi: 10.1016/j.jtice.2010.01.014.

Ullah, M. *et al.* (2020) 'The effective removal of heavy metals from water by activated carbon adsorbents of Albizia lebbeck and Melia azedarach seed shells', 2020(1), pp. 30–37.

Undavalli, V. K., Khandelwal, B. and Fuels, A. (2021) 'Fourier Transform Infrared Spectrometer Impact of alternative fuels and properties on elastomer compatibility', *Aviation Fuels, 2021*.

Wahi, R., Ngaini, Z. and Jok, V. (2009) 'Removal of mercury, lead and copper from aqueous solution by activated carbon of palm oil empty fruit bunch', *World Applied Sciences Journal*, 5((special issue for environment)), pp. 84–91.

Waji, Y. A. (2018) 'Bamboo Based Activated Carbon for Removal of Lead From Aqueous Solution', p. 76.

Wang, J. and Guo, X. (2020) 'Adsorption kinetic models: Physical meanings, applications, and solving methods', *Journal of Hazardous Materials*, 390(November 2019), p. 122156. doi: 10.1016/j.jhazmat.2020.122156.

Wani, A. L., Ara, A. and Usmani, J. A. (2015) 'Lead toxicity : a review', 8(2), pp. 55–64. doi: 10.1515/intox-2015-0009.

Y., H. (2006) 'Isotherms for the Sorption of Lead Onto Peat: Comparison of Linear and Non-Linear Methods', *Polish Journal of Environmental Studies*, 15(1), pp. 81–86.

Yagub, M. T. *et al.* (2014) 'Dye and its removal from aqueous solution by adsorption: A review', *Advances in Colloid and Interface Science*, 209, pp. 172–184. doi: 10.1016/j.cis.2014.04.002.

Yagub, M. T., Sen, T. K. and Ang, H. M. (2012) 'Equilibrium, kinetics, and thermodynamics of methylene blue adsorption by pine tree leaves', *Water, Air, and Soil Pollution*, 223(8), pp. 5267–5282. doi: 10.1007/s11270-012-1277-3.

Yagub, M. T., Sen, T. K. and Ang, M. (2014) 'Removal of cationic dye methylene blue (MB) from aqueous solution by ground raw and base modified pine cone powder', *Environmental Earth Sciences*, 71(4), pp. 1507–1519. doi: 10.1007/s12665-013-2555-0.

Yahya, M. A., Al-Qodah, Z. and Ngah, C. W. Z. (2015) 'Agricultural bio-waste materials as potential sustainable precursors used for activated carbon production: A review', *Renewable and Sustainable Energy Reviews*, 46, pp. 218–235. doi: 10.1016/j.rser.2015.02.051.

Yakout, S. M. *et al.* (2015) 'Surface modification and characterization of a RS activated carbon: density, yield, XRD, ash, and moisture content', *Desalination and Water Treatment*, 53(3), pp. 718–726. doi: 10.1080/19443994.2013.846538.

Zhang, F. S., Nriagu, J. O. and Itoh, H. (2005) 'Mercury removal from water

using activated carbons derived from organic sewage sludge', *Water Research*, 39(2–3), pp. 389–395. doi: 10.1016/j.watres.2004.09.027.

Zhao, S. and Li, D. (2018) 'Limitations for Microplastic Quantif- ication in the Ocean and Recommen- dations for Improvement and Standard- ization Methods for the detection and compo- sition study of fluid inclusions'.

Zhou, W. *et al.* (2007) 'Fundamentals of scanning electron microscopy (SEM)', *Scanning Microscopy for Nanotechnology: Techniques and Applications*, pp. 1–40. doi: 10.1007/978-0-387-39620-0_1.

Zulkania, A., Hanum, G. F. and Sri Rezki, A. (2018) 'The potential of activated carbon derived from bio-char waste of bio-oil pyrolysis as adsorbent', *MATEC Web of Conferences*, 154, pp. 1–6. doi: 10.1051/matecconf/201815401029.